FINAL TECHNICAL REPORT

ADVANCED THERMOELECTRIC MATERIALS FOR EFFICIENT WASTE HEAT RECOVERY IN PROCESS INDUSTRIES

DOE AWARD DE-FC36-04GO14044

PROJECT PERIOD 7/2004 – 6/2008

PRINCIPAL INVESTIGATORS:

Adam Polcyn
(412)820-4918
apolcyn@ppg.com

Moe Khaleel
(509)375-2438
Moe.Khaleel@pnl.gov

RECIPIENT ORGANIZATION:

PPG Industries, Inc.
One PPG Place
Pittsburgh, PA 15272

PROJECT TEAM MEMBER ORGANIZATIONS:

Pacific Northwest National Laboratory
Dr. John Johnson
Owens-Illinois

30 September, 2008

Disclaimer: Any findings, opinions, and conclusions or recommendations expressed in this report are those of the author(s) and do not necessarily reflect the views of the Department of Energy.

Proprietary Data Notice: There is no proprietary data in this report.

Table of Contents

List of Acronyms

TEG – Thermoelectric Generator
TE – Thermoelectric
PNNL - Pacific Northwest National Laboratory
GAST - Germanium Silver Antimony Telluride thermoelectric material
GTC – Glass Technology Center
AGC – Asahi Glass Co.
HFT – Heat Flux Transducer
RUTDC – Right Uptank Downcomer
RDTDC – Right Downtank Downcomer
LDTDC – Left Downtank Downcomer

List of Figures

List of Tables

List of Appendices

Executive Summary

At the turn of the century, over 2 Quads of waste heat energy was generated in the United States by various industrial processes (glass, aluminum, steel, and chemical manufacturing to name a few). By recovering this waste heat and converting it to a more useful form of energy, e.g. electricity, industrial energy efficiency could be improved dramatically. Thermoelectric generators (TEGs), which directly convert heat to electricity using thermoelectric materials, are a promising technology platform for waste heat recovery because they are easy to operate and maintain, and can be easily modified and scaled for a wide variety of industrial applications. In the 1990's, new thin-film and bulk thermoelectric materials were discovered that held the promise of dramatically increasing the historically poor efficiency of thermoelectric devices[1]. For the first time, it became conceivable that thermoelectric technology could be an economically viable method for waste heat recovery. This insight provided the motivation for this project.

The overall objective of the project was to integrate advanced thermoelectric (TE) materials into a power generation device that can convert waste heat from an industrial process to electrical power with an efficiency approaching 20%. Our strategy was to build on the new discoveries in thin-film thermoelectric materials to develop suitable advanced TE materials, integrate these into a TEG, and demonstrate waste heat recovery with efficiency approaching 20% in an existing industrial process. To demonstrate the viability and flexibility of the technology, we also set out to design (at least on paper) a large-scale waste heat recovery system and to identify the system cost targets that would need to be met to make the technology economical for industrial use.

In order to achieve device efficiencies of 20%, the dimensionless figure-of-merit (ZT) for the thermoelectric materials needed to reach 2 or greater. Several potential high-ZT material candidates were investigated by PNNL, and the highest value of ZT achieved was around 1.5 at 275°C. In addition, it was recognized that due to the geometry of thin film samples and the relative thermal conductances of thin films and the substrates on which they are deposited, it is not trivial to integrate such materials into a practical thermoelectric device. However, PNNL developed a technique by which thin film thermoelectric materials could be deposited on 1.2m strips of 2-mil thick Kapton substrates. These strips were wound spirally into mechanically strong cylinders that resemble and potentially could be substituted for the conventional p- and n-type elements currently being built into commercially available TEGs.

In parallel with advanced TEG development, waste heat recovery was demonstrated in an existing industrial process using a commercially available TEG with efficiency of 5%. It was hoped that such a demonstration would provide insight into the challenges that would be faced in integrating advanced TEGs with an existing industrial process. The industrial process chosen was the glass melting process at PPG Industries' oxyfuel-fired furnace at Meadville, PA. The largest accessible waste heat source in this process is the furnace's combustion exhaust gas stream, so waste heat was recovered from this source.

Several preliminary investigations were performed in advance of the in-plant waste heat recovery demonstration. PNNL built a bench-scale apparatus to characterize the Global Thermoelectric Model 7120 TEG, which was the commercially available TEG chosen for the in-plant demonstration. PPG characterized the combustion exhaust gas stream of the oxyfuel-fired furnace, and found that convective heat transfer from the gas was poor due to the low gas stream velocity, leaving radiative heat transfer from the hot (3000°F) glass melt as the dominant heat transfer mechanism. This led the partners to consider alternative designs for waste heat recovery.

After considering several alternative designs, the partners decided to couple the TEG to a large sodium heat pipe. Heat pipe technology provides a very efficient means of transferring heat over long distances, and made it possible to collect radiant heat from the gas stream and transfer it to the TEG, which was connected to the heat pipe just outside the exhaust flue wall at room temperature conditions. This arrangement made it convenient to operate and maintain the TEG, and suggested a waste heat recovery strategy in which waste heat collection was performed by a number of modular units, each of which had a waste heat collection device that was customized to the waste heat source and transferred the heat to a TEG that need not be customized for each waste heat source. In addition to being easily adapted to a variety of waste heat recovery scenarios, this strategy makes it possible to quickly incorporate waste heat recovery in existing industrial processes without interrupting the operation of the process.

The heat pipe / TEG waste heat recovery module was operated in the exhaust gas stream at Meadville for 3 months. The TEG was operated near its peak electrical output at the beginning of this trial, but within a week of starting the trial electrical output dropped to about 50% of peak, and remained near this level for the balance of the trial. Some additional small, slow degradation in power output was observed, most of which could be reversed by periodic cleaning of the heat pipe surface.

At least one reason for the power degradation observed in the in-plant demonstration was the presence of solid and liquid materials ("condensates") that would condense on any surface placed in the stream. These condensates were studied and found to be typically sodium sulfate, a component of the batch material used to make glass, and (to a lesser extent) refractory material from the walls of the exhaust flue that melted and dripped down onto the surface. The thermal effects of these condensates on a surface placed in the exhaust stream were studied. It was found that the heat flux to this surface fell by 50% after 12 days' exposure to the exhaust stream environment, and then leveled off. This drop in heat flux was correlated to the buildup of condensates on the surface. The heat flux could be restored to its initial value by removing the surface from the exhaust stream and cleaning off the white solid powder buildup with a soft brush. Literature-based research was performed by Dr. John Johnson to study the properties of sodium sulfate and methods to remove it from heat transfer surfaces in the gas stream.

Finally, the economics of modular waste heat recovery were considered. Given current TEG costs and projected costs for heat pipes in high-volume production, a waste heat recovery system based on the module demonstrated at Meadville would not be

economical for adoption by industry, even if TEG efficiencies were near 100%. PNNL found some scenarios in which the system would be economical at lower efficiencies if the cost of heat collection and transfer to the TEG could be reduced to a fraction of the TEG cost, and if TEG costs per watt dropped by more than a factor of 10.

As a result of this work, we have concluded that waste heat recovery using thermoelectric technology is far from ready for widespread adoption by industry. In spite of the recent progress in material efficiency, it is not clear that these improvements in efficiency are adequate. Also, even with continued progress in materials efficiency, it is not trivial to incorporate these new thin-film materials into practical thermoelectric devices. Finally, the challenge of collecting waste heat and transferring it to the TEG is at least as important as the challenge of improving the efficiency of the TEG itself, and more work needs to be done to find economical ways of meeting both challenges.

Introduction

Table 1 below shows estimates of the quantities of waste heat generated by various industries on a yearly basis. In the table, "Harvestable Waste Heat" refers to waste heat sources that we felt could be used to supply waste heat recovery based on TEG technology. For the glass[2], steel[3], and aluminum[4,5] examples, these sources are combustion or other exhaust gas streams. For the chemicals[6] example, all processes are considered and it is assumed that only 10% are susceptible to waste heat recovery based on TEG technology.

Table 1 Estimate of waste heat that could be harvested with TE technology for various process industries.

Industry	Process	Energy Use (TBtu/yr)	Harvestable Waste Heat (TBtu/yr)
Glass	Melting	160	49
Steel	Electric Arc Furnace	225	45
Aluminum	Smelting	167	18
Chemical	All	6300	200
Total			**312**

It is estimated that over 3000 TBtu (i.e. 3 Quads) of energy (in all forms) is wasted in the U.S. manufacturing sector each year, and with a cursory examination of just a few industries we discovered that at least 10% of that could be harvested for electricity generation with TEG technology. Based on this simple analysis, it is clear that the potential benefits of TEG technology for energy savings and greenhouse gas emission reduction are substantial.

TEG technology has some advantages over more conventional technologies to produce electricity from waste heat, notably the use of waste heat to boil water, thereby generating superheated steam that can drive a turbine and produce electricity[7]. Since TEG technology involves the use of solid-state materials and devices with no moving parts, and since it converts the heat directly to electricity, it can be expected to provide lower operation and maintenance costs than a boiler, and potentially lower capital costs as well. Also, it should be more scalable than the conventional technology, allowing waste heat harvesting from large or small sources in a wide variety of industrial environments. Finally, this scalability could make it economical to harvest the waste heat with small "modules", as opposed to the large-scale system required with the conventional technology. This modularity could make it possible to harvest waste heat from industrial processes while they are in operation, and to harvest more or less waste heat depending on process needs and conditions.

As an example, one application envisioned by PPG Industries for a TEG-based waste heat recovery system is to use the electricity to power the Air Separation Unit (ASU) that

produces oxygen for use in an oxy-fuel glass furnace. The ASU requires roughly 3MW of electrical power, and the amount of power available in the form of heat in the combustion exhaust gas stream from the oxy-fuel furnace is approximately 20MW. Therefore, the method chosen to generate electricity from the exhaust gas stream must be at least 15% efficient. Note that this efficiency must consider both the efficiency of collecting and transferring the heat to the TEG, as well as the efficiency of the TEG itself. Typical efficiencies for commercially available TEGs that operate around 500°C (a relevant temperature for the oxy-fuel exhaust gas stream) are 5% or below. Also, commercial TEG costs are in the $5/W range, not considering the costs of the apparatus for collecting and transferring the heat to the TEG. Thus current TEG technology is not efficient enough to generate the amount of electricity needed for PPG's application, nor is it expected to be cost-effective.

The main challenge for improving the efficiency of TEG technology is improving the properties of the thermoelectric materials that convert the heat to electricity. TEG efficiency is directly related to the dimensionless figure-of-merit ZT, which are close to 0.5 in the temperature range of interest for commercial devices (despite intense work in the field beginning in the late 1930's)[8]. As described below, ZT of 0.5 provides theoretical efficiencies, in the ideal case, of just under 10%. Given that real devices will not reach the theoretical efficiency (indeed, commercial devices apparently have efficiencies roughly half of the theoretical value), significant enhancement of ZT in the temperature range of interest is required.

In 1993, Hicks and Dresselhaus[9] published theoretical work that suggested that ZT could be increased by more than a factor of 10 for Bi_2Te_3 by considering quantum-confinement effects in a multilayer thin film structure. In 2001, Venkatasubramanian and his collaborators[10] reported ZT of 2.4 at 300°K for Bi_2Te_3/Sb_2Te_3 superlattices. Also, Kanatzidis and his collaborators[11] reported ZT of 2.2 at 500°C for $AgPb_mSbTe_{2+m}$ bulk materials. These and other discoveries renewed interest in thermoelectric materials, and renewed hope that materials with high ZT at high temperatures could be realized.

This project was motivated by the promising new results in TE material efficiencies, the capabilities at Pacific Northwest National Laboratory to further develop these materials, and the desire of PPG and other industrial partners to improve the energy efficiency of their manufacturing processes. We set out to develop the new thin film materials needed, to integrate them into a TEG device that could produce a modest amount of power, to design a device to capture heat and transfer it to the TEG efficienctly, and to demonstrate waste heat recovery with an efficiency near 20% in the combustion exhaust gas stream of PPG's oxyfuel glass furnace.

Background

TE Technology

The basic concept of TE energy conversion is illustrated in Figure 1[12]. An n-type semiconductor material is electrically connected in series with a p-type semiconductor material, and the two are arranged so that a flow of heat through the elements will sustain a temperature gradient ($T_H - T_C$, where T_H is the hot side temperature and T_C the cold side temperature) across the elements. The temperature gradient causes electrons (in the n-type material) and holes (in the p-type material) to drift towards the heat sink, resulting in a flow of electrical current. The efficiency of the device is determined by $T_H - T_C$, and the figure of merit Z. Z is a property of the thermoelectric materials, equal to the square of the Seebeck coefficient, multiplied by the electrical conductivity, and divided by the thermal conductivity. Typically efficiency is described in terms of ZT, which is a dimensionless figure-of-merit equal to Z times the average of TH and TC. The dependence of the ideal, optimized efficiency of the TE device on temperature difference and ZT is described by the equation below and plotted in Figure 2.[12]
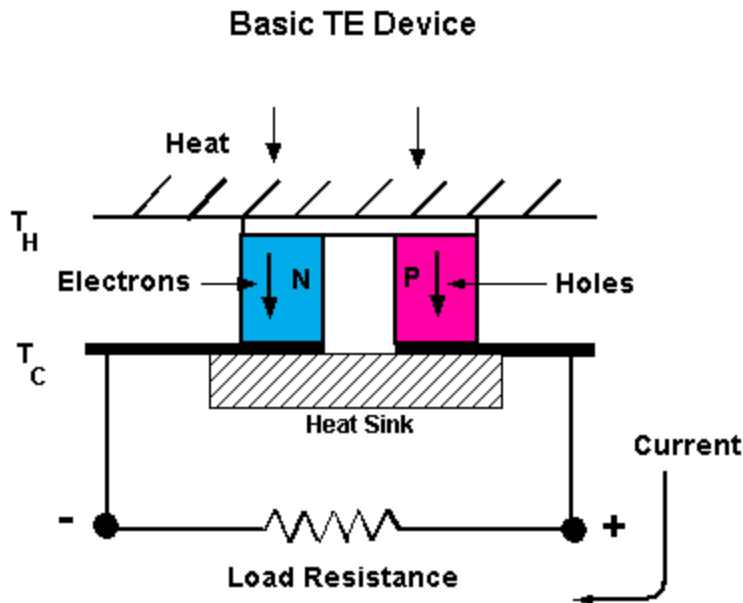
Figure 1 Schematic of basic TE device.

$$\eta = \left(\frac{T_H - T_C}{T_H}\right)\frac{\sqrt{1+ZT}-1}{\sqrt{1+ZT}+T_C/T_H}$$
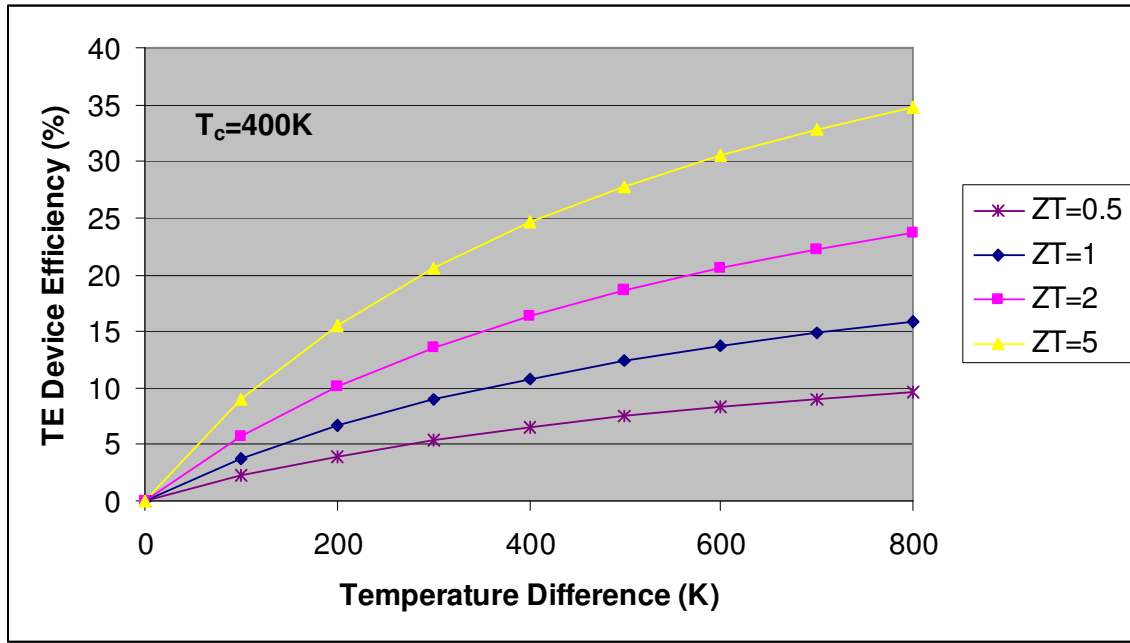
Figure 2 Ideal TE device efficiency as a function of T_H-T_C, for T_C=400K.

While there is no theoretical thermodynamic limit on ZT, typical state-of-the-art ZT values are close to 1 at temperatures relevant for industrial waste heat recovery (300C and above), which limits TEG efficiencies to less than 15%. As Hicks and Dresselhaus point out[9], for simple materials an increase in Seebeck coefficient is accompanied by a decrease in electrical conductivity. Moreover, an increase in electrical conductivity leads to an increase in the electronic component of thermal conductivity. Thus only quite unique, semiconducting materials and/or unique configurations of those materials (such as multilayer thin film structures) have found some success as thermoelectric materials.

For the waste heat recovery application considered in this project, $T_c \approx 40°C$ and $T_H \approx 500°C$. Thus the ZT value at 270°C is needed to estimate the performance of a given material in this application. A traditional material such as PbTe has ZT near 0.8 at 270°C, which (from Figure 2) gives a theoretical efficiency below 10%. In the 1990's, a new class of bulk materials known as skutterudites were investigated[13,14], with ZT's in the 0.5-1.0 range near 270°C. In 2004, Kanatzidis and his collaborators at Michigan State University reported ZT of 1.5 near 270°C for $AgPb_mSbTe_{2+m}$.[11] Chen et al.[15] then reported that the $(AgSbTe_2)_x(PbTe)_{(1-x)}$ material showed multiphase behavior over the millimeter scale, leading to large inhomogeneities in Seebeck coefficient. A related material, TAGS, has ZT just above 1 and was used successfully for TEGs for many

decades[16]. To our knowledge, the new Michigan State material has not been successfully integrated into a working device to date.

As noted in the Introduction, ZT near 2 has been reported in multilayer thin film structures near room temperature. These discoveries motivated PNNL to examine Si/SiGe and B_4C/B_9C superlattice structures for TEGs and to attempt to scale up these thin film materials in order to produce sufficient quantities of material to generate significant amounts of electrical power.

According to Figure 2, and given that current commercial devices operate at efficiencies roughly half of their theoretical values, a ZT above 5 might be required to obtain efficiencies near 20% near 270°C. While progress has been made recently on improving ZT, there are currently no substantiated claims of ZT significantly above 1 in the temperature range of interest.

Industrial Waste Heat Recovery

TEG technology is by no means the only option available for waste heat recovery in an industrial context. For the purposes of this project and this section of the Report, we will limit our discussion of industrial waste heat recovery to the glass industry, and primarily to the flat glass industry, as this is the area of expertise of the prime industrial partner involved in this project (PPG Industries).

Waste heat boilers have been studied and (in some cases) implemented for use in various glass manufacturing facilities, particularly in Europe, for many years[17,18,19]. The hot combustion exhaust gas is used to boil water to create steam, which can then be used for a number of purposes, including driving a turbine to generate electricity. Recently, an AGC flat glass furnace in the Netherlands demonstrated a system with 2.1MW electrical output capacity[20]. Also, a Heye Glas container glass furnace in Germany has operated a boiler-based system with a 1MW electrical output capacity since 1996[21]. In addition to electricity generation, boiler systems can be used to operate fans or compressors, or to provide space heating[7].

There are additional potential uses for waste heat that have been considered and implemented in the glass industry. One is to preheat the combustion gases and/or fuel used to melt the batch[22]. Indeed, one of the key ideas of the Siemens regenerative melter, the most common melter technology used in the flat glass industry, is to use combustion exhaust gases to heat refractory checker packing material. This hot refractory is then used to pre-heat combustion air drawn in from the outside before mixing it with fuel to melt the batch. Another idea is to use the waste heat to pre-heat batch material before melting it. This is particularly useful in the container glass industry, where a high proportion of cullet (which will not be carried away by an exhaust gas stream blowing over it) is used in the batch material. There are 13 glass manufacturing facilities worldwide that use this technique, 9 of them in Germany[23]. PPG also used this technique in its P-10 process for flat glass manufacturing, a unique process that was developed and used exclusively by PPG from 1979 to 1998.

As mentioned in the Introduction, our initial target for TEG technology was waste heat recovery from the combustion exhaust gas stream of a flat glass oxyfuel fired furnace operated by PPG in Meadville, Pennsylvania. Unlike conventional Siemens regenerative glass melting technology, oxyfuel-fired glass melters currently have no mechanism for capturing and using the waste heat contained in the combustion exhaust gas stream. While the efficiency of oxyfuel-fired glass melters is already superior to that of Siemens regenerative melters, with effective waste heat recovery the efficiency could be much higher.

To give the reader a better understanding of the oxyfuel process, it is important to first give an account of the Siemens regenerative process (Figure 3). In the Siemens process, ambient air is drawn into the furnace by fans. This air passes over hot refractory material, where it is preheated before being combined with natural gas and ignited to produce a high luminosity flame that extends over the surface of the molten glass, which is contained in a large tank and continuously fed with solid batch material from one end of the tank. The luminous flame heats and melts the batch material primarily via radiative heat transfer. The hot combustion gases are then exhausted through a port on the opposite side of the tank, where they flow over refractory material in order to preheat it. After ten to fifteen minutes, the direction of gas flow is reversed so that ambient air is drawn over the newly heated refractory material, and combustion gases exhausted over the (now cold) refractory on the opposite side to begin heating that refractory again in preparation for the next reversal. These refractories are known as "regenerators" (or "checkers"), and typically there are two stages of regenerator on each side of the melter. The exhaust flues in which the primary regenerators reside are known as "downcomers", since they connect the glass melter (on the first floor of the factory) with the connecting flues (in the basement). For a cross-sectional view of the process looking down the length of the melter, see Figure 4. As noted above, waste heat recovery is built into the Siemens process. However, it is relatively inefficient because a large fraction of the waste heat is used to preheat non-combustible components of air (e.g. nitrogen).

AIR FIRED

Furnace Overview and Combustion System
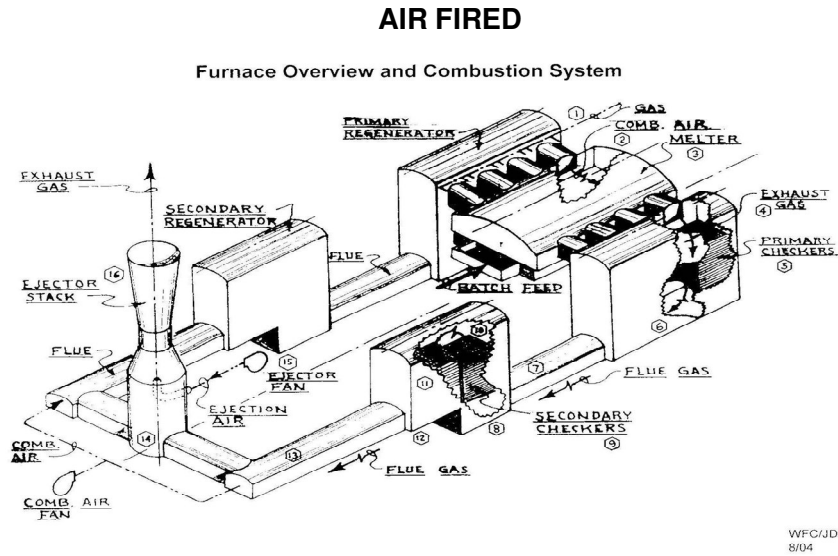
Figure 3 Schematic of Siemens regenerative glass melter.
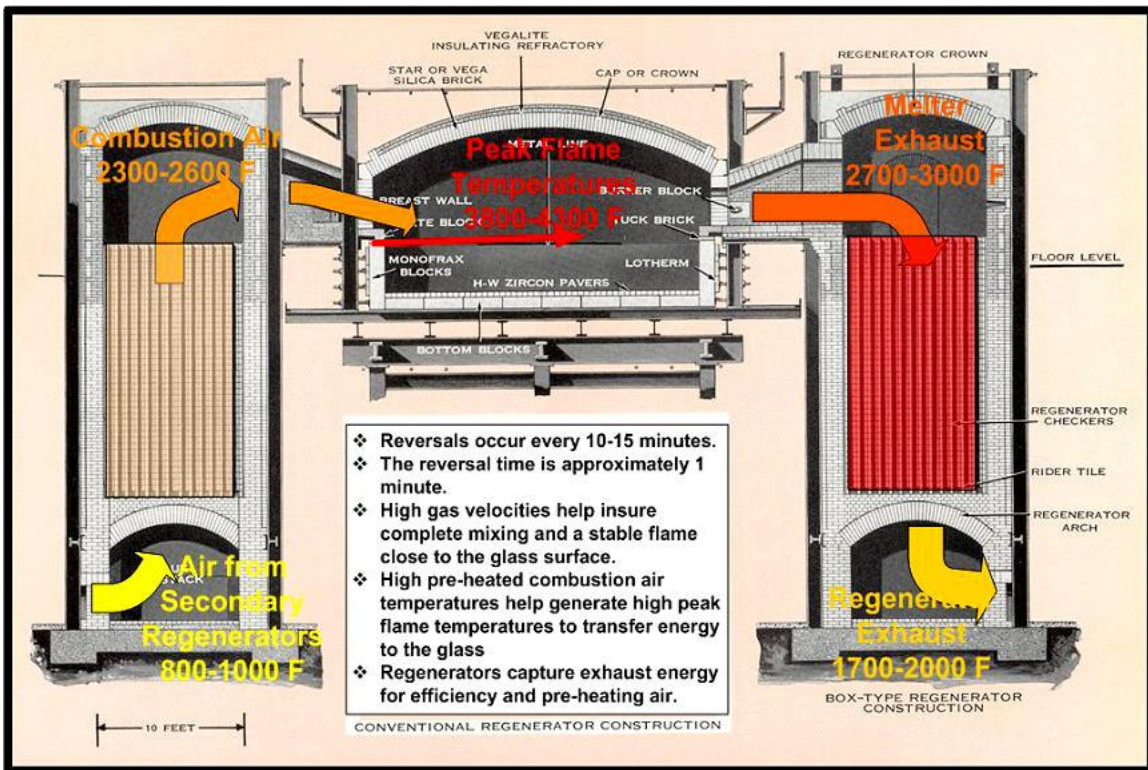
Figure 4 Cross sectional view of Siemens regenerative melter.

In the case of the oxyfuel process (Figure 5), natural gas is combined with oxygen (made at a separate facility) to produce a more efficient combustion process. The oxyfuel process does not involve reversal of the gas flow direction; rather, flames are produced continuously on both sides of the furnace, and combustion exhaust gases flow into the flues on both sides of the furnace continuously. The refractory checker material is removed from the flue regenerator areas. Because the hot combustion gases can not be exhausted directly into the atmosphere, cool ambient air is deliberately aspirated into the flues to cool the gas before ejecting it. This is achieved by introducing holes into the downcomer walls. As noted above, nearly 20MW of power are lost in this way.
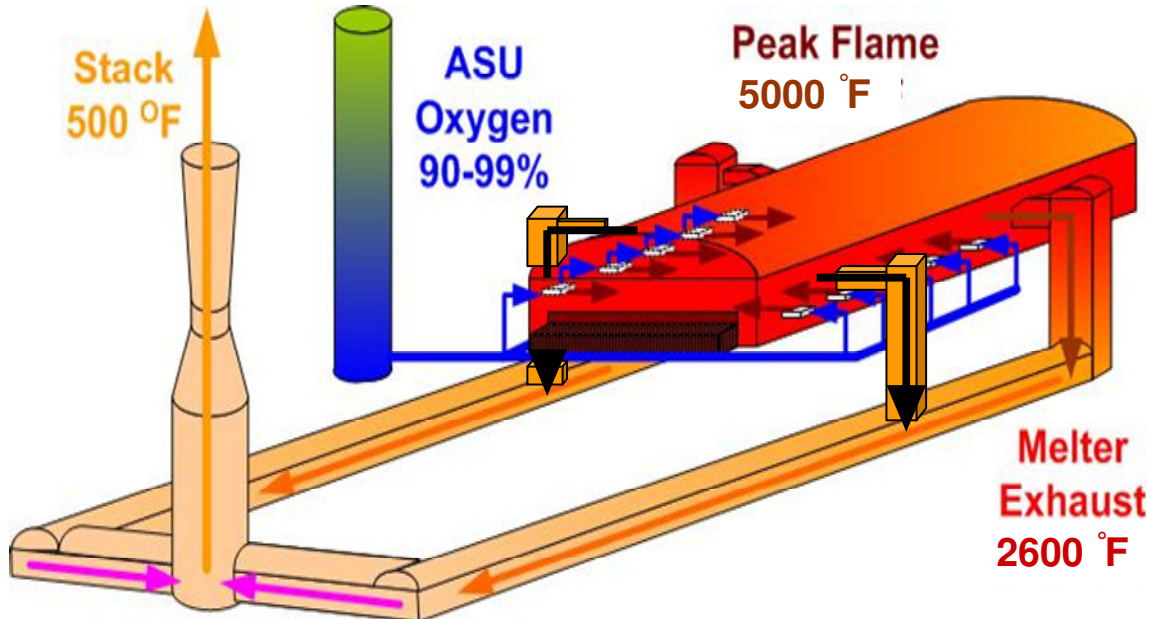
Figure 5 Schematic of oxyfuel flat glass melter.

The oxyfuel exhaust gas stream has great potential as a waste heat source. The exhaust gases continuously exit the melter at 2600°F, with an energy density of 1.8 MMBTU/ft^2/hr. In addition to the high temperature and energy density, the gas stream is quite stable. On the other hand, the gas stream velocity is quite low (a few feet per second, driven largely by the aspirated room air used to cool the gas), so convective heat transfer is likely to be poor without modifying the gas stream (for example, constricting the flue diameter to increase gas velocity). Also, the gas stream contains solid and liquid components that can collect on heat exchangers and reduce heat transfer over time.

There are other potential waste heat sources in a flat glass melter. Heat is lost through the refractory walls and crown of the melter. In addition, heat is lost further downstream in the process through the annealing lehr (which cools the glass in a controlled manner in order to optimize the stress state of the glass). We chose to focus on the exhaust gas stream for this project because (1) it is the largest concentrated source of waste heat in the process, and (2) harvesting waste heat from the exhaust gas stream could profoundly impact the efficiency of oxyfuel melting and therefore glass melting in general.

The overall objective of the project was to integrate advanced thermoelectric (TE) materials into a power generation device that can convert waste heat from an industrial process to electrical power with an efficiency approaching 20%. In order to achieve this objective, we needed to:

- develop advanced TE materials with sufficiently high ZT to enable a 20% efficient TEG device
- design a TEG device that would make efficient use of the new materials to achieve at least 20% efficiency
- produce the TE materials in sufficient quantity and build them into a TEG
- develop a method to extract heat from an industrial waste heat stream and supply the heat to the TEG
- build and validate the necessary equipment to extract the heat and supply it to the TEG
- demonstrate waste heat recovery and electricity generation at efficiency of 20% or above for a significant amount of time

In order to demonstrate efficient waste heat recovery over a significant amount of time (at least several weeks), we anticipated a need to understand the effects of gas stream condensates on heat transfer, and to develop solutions to counteract those effects. To lend practical perspective to the work and demonstrate its value, we also felt it was important to propose a design for a large-scale waste heat recovery system based on the TEG and waste heat recovery method we developed, and to evaluate the economic feasibility of the system for a real industrial application.

Given this objective and the anticipated steps required to meet the objective, the project work was organized into four major Tasks:

Task 1. Design Energy Conversion System
        Subtask 1.1. Conversion System Design
        Subtask 1.2. Economic Analysis
Task 2. Advanced Thermoelectric Materials Development
        Subtask 2.1. Advanced TE Materials Fabrication
        Subtask 2.2. Characterization of Materials
Task 3. Thermoelectric Generator Fabrication and Test
        Subtask 3.1. TEG Fabrication
        Subtask 3.2. Bench Test of Prototype TEG
        Subtask 3.3. Testing of TEG at PPG
Task 4. Combustion Emission Optimization
        Subtask 4.1. Characterization of Emission and Heat Transfer
        Subtask 4.2. Strategies to Minimize Emissions Impact

Task 1 addressed the design of a large-scale energy conversion system based on the work of Tasks 2 and 3, and the economic viability of such a system for a representative industrial user. Task 2 addressed the development of advanced TE materials with high ZT, and characterization of those materials to demonstrate the ZT and other important properties for TEG device performance. Task 3 addressed the design and assembly of a

prototype TEG with advanced materials, the testing of that prototype on a small scale in the lab, and finally the transfer of that prototype to an industrial partner (PPG) to demonstrate efficient heat-to-electricity conversion in a real industrial process. Included in Task 3 was the work to design and build an apparatus to extract heat from the industrial process and transfer it to the TEG. Finally, Task 4 addressed characterization of the chosen industrial process (in our case, the combustion exhaust gas stream of a glass furnace) to support the design of the heat extraction and transfer apparatus, as well as addressing how the negative effects of particulates and other condensates in the exhaust gas stream could be counteracted.

The impact of the project on industrial energy usage in the U.S. is driven by the efficiency and cost of the TE waste heat recovery device. This is in turn driven by the thermoelectric materials (addressed in Task 2 and Subtask 3.1) and by how heat is transferred to them (addressed in Subtasks 3.2,3.3, and 4.1). Given PNNL's expertise and capabilities for development of advanced TE materials and devices, it was natural for PNNL to focus on Task 2 and Subtask 3.1. Given PPG's expertise and capabilities for characterizing the glass furnace and testing devices in an industrial environment, it was natural for PPG to focus on Subtasks 3.3 and 4.1. PNNL also had the capability and resources to address Subtask 3.2. Both PPG and PNNL contributed to Task 1, and Subtask 4.2 was contracted to Dr. John Johnson, who brought expertise in the area of combustion emissions that was not available at either PPG or PNNL.

The initial strategy for waste heat recovery with thermoelectrics in the glass process environment was to build thermoelectric devices in the form of large area flat panels that could be inserted in the walls of the melter and the flues, and on the external surfaces of the annealing lehr (see Figure 6). Relatively small area flat panel TEGs (less than 1 square foot) are commercially available from a number of vendors (e.g. Marlow Industries, Hi-Z Technology). For example, Hi-Z's HZ-20 TEG produces 19W of power in a 3"x3"x0.2" package at 450°F hot side temperature[24]. Our initial approach was to build 10cm x 10cm "submodules" that could be connected together to produce larger "modules" that would provide higher electrical output.
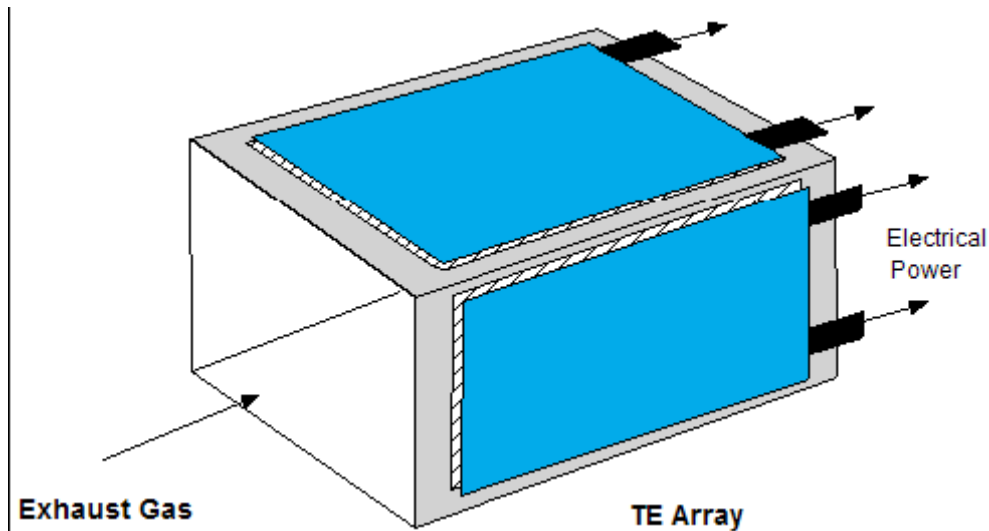
Figure 6 Proposed concept for harvesting waste heat from exhaust gas flue with TEGs.

A schematic of such a submodule is shown in Figure 7 in both side view and cross-section. The n-type and p-type film elements are 10-100 μm in thickness. Materials systems to be considered for the elements included Si/SiGe multilayers, B_4C/B_9C multilayers, and multilayers based on skutterudite materials. The films would be deposited on a coated metal substrate, with necessary masking to form n-type and p-type sections on the substrate. The coating on the substrate is designed to protect the underlying metal substrate from the high-temperature environment. Electrical interconnects are provided between n-type and p-type elements.

One important issue with this design is ensuring that the thin films have sufficiently low thermal conductance so that a significant temperature difference can be maintained across the device. For film thickness of 10 μm, thermal conductivity (typical of thermoelectrics or glassy materials) of 0.01 W/cm/K, a heat flux of 2 kW/cm^2 would be required to maintain a temperature difference of 200°C across the device. For comparison, the Hi-Z HZ-20 uses a heat flux of 10 W/cm^2 with a temperature difference of 200°C and a device thickness of 0.5cm.
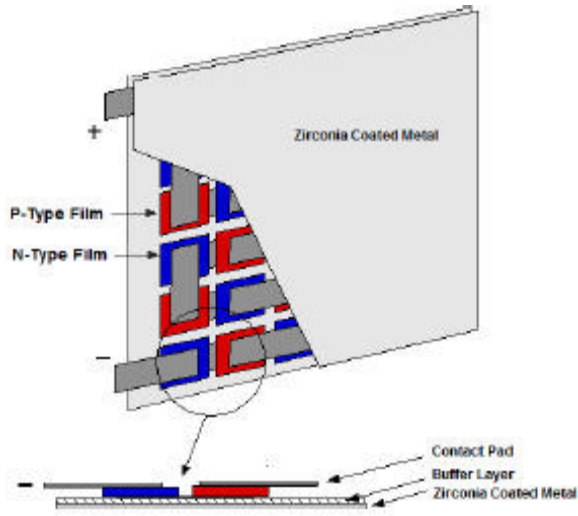
Figure 7 Concept for TEG submodule.

Results and Discussion

The results are presented in terms of the two major areas of work on this project: thermoelectric materials development, and industrial waste heat recovery with thermoelectric technology. The thermoelectric materials development work is presented first. After presentation of a novel method to fabricate thermoelements using thin-film TE material, the development of the p-type GAST material is described. This is followed by a description n-type Ag-PbTe material development, details of thermoelement fabrication using these materials, and a description of the metrology work done to characterize the thermoelectric properties of the new materials. Finally, an account of our efforts to fabricate a TEG with the new materials is given. Within the industrial waste heat recovery section, the results of an initial bench-scale test of existing TEG technology by PNNL are presented first. Next, several experiments to characterize the thermodynamics and fluid dynamics of PPG's oxyfuel glass melter exhaust flue are discussed. The bench-scale test and the flue characterization experiments drove our thinking on design options for the waste heat recovery device. These designs, and a preliminary economic analysis by PNNL based on these designs, are presented next. The culmination of the design work and characterization experiments was the in-plant test of existing TEG technology at PPG. After an account of the in-plant test, the results of experiments on condensates in the furnace exhaust are described, along with the results of the literature study on condensate formation and control in the furnace exhaust.

Advanced Thermoelectric Materials Development

In early work, several sputtered thin-films were investigated as candidates for high ZT thermoelectric materials. Multi-layer Si/SiGe and B_9C/B_4C films on thin single crystal silicon substrates were studied initially, but abandoned due to need for high-temperature heat treatment and due to substrate fragility. PNNL proceeded to study n-type Ag-doped PbTe films and p-type $AgSbTe_2$-GeTe (GAST) alloys, on Kapton substrates.

Sputter deposition of thin films of thermoelectric material has shown promise for a low cost approach to developing TE materials with ZT values approaching 2.0. Sputtered thin films produced in this task achieved electrical characteristics that suggest ZT values of 2.0 or greater can be achieved. These thin film structures are polycrystalline, multi-layered nanostructures. Whereas quantum well film structures consist of single crystal layers 1 nm to 10 nm thick, the films produced in this project are polycrystalline nanostructures. The work led to three major advances:

(1) Demonstration that TE material can be sputter deposited onto long strips of polyimide and then spooled into cylindrical thermoelements;

(2) Processes were developed for growing films of P-type thermoelectric material that exhibits very good thermoelectric properties in the temperature range of 400°K to 650°K by co-sputtering from GeTe and $AgSbTe_2$ targets;

(3) Procedures were also developed for growing films of N-type thermoelectric material that exhibits improved thermoelectric properties in the temperature range of 450°K to 650°K by co-sputtering from Ag and PbTe targets.

Further details of these advances are given in the following sections.

Thermoelement Fabrication from Sputtered Material on Polyimide

An approach was developed allowing the fabrication of thermoelements that would be capable of being substituted for the cylindrical elements found in current commercial TEGs.   This has been achieved by sputter depositing TE materials onto polyimide strips 1.2 meters long and spooling these strips into a tight, load-bearing cylindrical form. Deposition was carried out on a rotating wheel mounted in a sputtering chamber as depicted in Figure 8. The width and diameter of the wheel are 4.8 cm and 38 cm, respectively.   Thermoelement fabrication was accomplished both by cutting strips from a 4.8 cm wide Kapton sample and by depositing directly onto pre-cut tapes 1 cm wide. After material deposition and spooling each strip into a cylindrical element, the ends of the element so formed were metalized.

Sputtering Targets

Deposition of TE Material On 1 meter Strip of Kapton

Metallization

TE Film

Long Strip Removed and Wound into Cylindrical Element
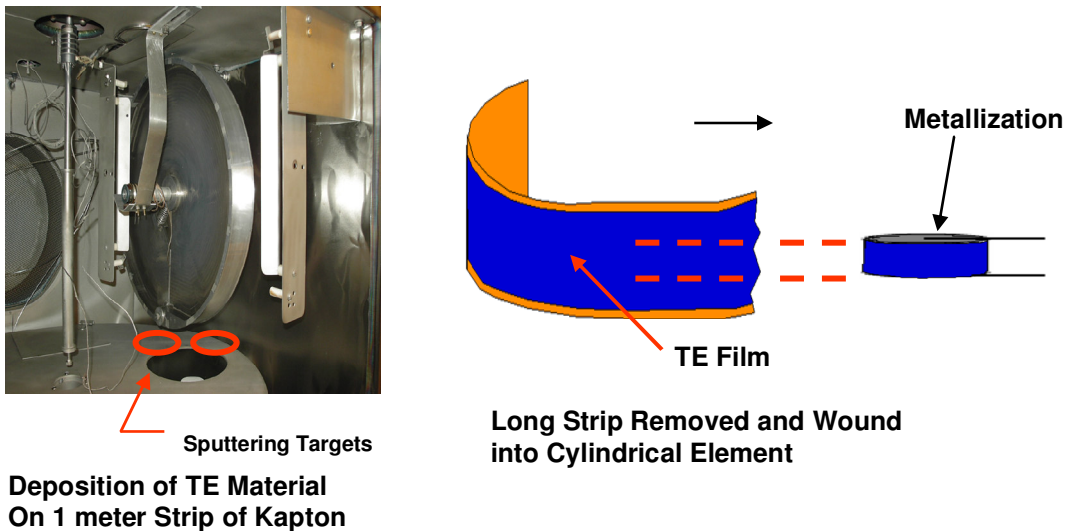
Figure 8 Approach to fabricating a thermoelement using thin films deposited on polyimide.

Arrays of n- and p-type elements fabricated in this manner could be used to assemble a functional TEG. This procedure represents a unique and practical approach to utilizing

thin films wherein the polyimide substrate acts as a scaffold to support a TE film that would not be capable of supporting itself.

Efficient thermoelectric materials are characterized by thermal conductivities in the 0.01 to 0.02 Watts/cm/K range. Because the polyimide substrate material and thermoelectric film can be approximately the same thickness (10 to 20 µm), and the thermal conductivity of polyimide is an order of magnitude less (e.g., 0.001 W/cm/K with Kapton), the thermal conductivity of the polyimide substrate can be made to have a negligible impact on conversion efficiency.   This approach was demonstrated with both n- and p-type materials.

Development of P-Type Material by Co-Sputtering AgSbTe$_2$ and GeTe

P-type materials were developed that have very good thermoelectric properties. Films of the material were grown by co-sputtering from targets of AgSbTe$_2$ and GeTe.   Figure 9 illustrates the general approach for co-sputtering from two targets on a flat substrate configuration. The major process variables that one can adjust to control properties of the deposited material are: (1) substrate temperature; (2) power supplied to the AgSbTe$_2$ target; (3) power supplied to the GeTe target; (4) and, the sputter gas pressure. Best results were achieved with process parameters set near those given in Table 2.   The composition of these films should be designated as Ge$_w$Ag$_x$Sb$_y$Te$_z$, with w, x, y, and z each ranging from 0 to 1.0. The relationship between the values of the four elements is complicated. The composition of the elements depends on the process parameters and individual element sputtering rates. Therefore, it is not appropriate to refer to these materials as 'TAGS' thermoelectric materials.   As a result, the term GAST is invoked,
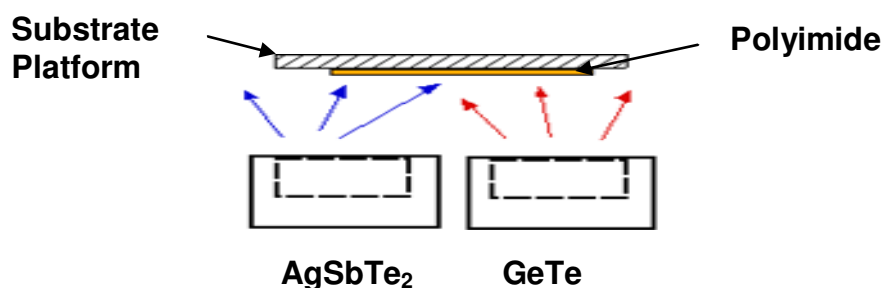
Figure 9 Approach to co-sputtering AgSbTe2 and GeTe to form a film on a substrate supported by flat substrate.

referring to the constituent elements Ge, Ag, Sb and Te.   GAST materials grown with process parameters described in Table 2 typically had a composition of the type represented in Table 3.   It should be noted that one can not define a value of 'x' in the TAGs formula, (AgSbTe$_2$)$_x$ (GeTe)$_{1-x}$ that would yield the composition values given in Table 3.   For example, the TAGs formula would always have a composition in which Ag and Sb are the same.   Thus, it would appear that work in this project has resulted in development of previously unrecognized TE material compositions with attractive properties potentially applicable to waste heat recovery.

Table 2 Typical process parameters for co-sputtering

Substrate Temperature	Sputtering Gas Pressure	Power to AgSbTe2	Power to GeTe
330 ºC	3 mTorr	1.3 W/cm^2	3.6 W/cm^2

Table 3 Typical composition of GAST TE material

Ge	13.6	Atomic %
Ag	1.5	Atomic %
Sb	5.7	Atomic %
Te	79.2	Atomic %

Evolution of Materials Development

Prior to the initiation of this project, PNNL had investigated multi-layer film structures based on thin film Si/SiGe and B_9C/B_4C multi-layer structures. These films were grown on single crystal silicon substrates. As part of the previous effort, a sputtering system had been modified to allow automated growth of multi-layer films, where individual layers were from 25 Å to 100 Å thick.   Initial studies carried out in the current project indicated that films deposited on insulating substrates are preferred over films deposited onto silicon.

Work continued with the focus of growing and measuring the performance of advanced thick-film thermoelectric materials. The conceptual embodiment of these films was sputter depositing them on suitable thin metal substrates such as aluminum, copper and molybdenum. Using this geometry, functional thermoelements would be assembled by stacking the coated substrates one on top of the other and connected in electrical series. A number of samples were prepared that achieved adherent GAST depositions with thicknesses up to 12.5 µm. The thermoelectric properties of these samples were measured and reinforced earlier findings that the GAST composition possesses superior thermoelectric properties with the potential of exhibiting ZT values considerably greater than 1.0.

Early development of GAST materials was conducted using the flat substrate configuration shown in Figure 9 which produced samples typically 25 mm wide and 75 mm long.   Later in the project and because of potential difficulties in replicating thermoelectric properties and microstructure with bulk processing techniques, the bulk thermoelement path for materials fabrication was dropped and the focus returned to thin films. With existing equipment, 6-µm/hr sputter rates were achieved and 12-µm films of AgSbTe2/GeTe alloy produced for characterization.

An important discovery applicable to industrial waste heat recovery resulted from experience gained in a different project that focuses on producing sputter-deposited TE

thin films on polyimide substrates. These films are applicable to small micro-watt level devices used as ambient energy harvesters. The films are fabricated by sputtering materials onto polyimide tapes mounted on the wheel shown in Figure 8. This wheel represents technology developed by PNNL while conducting wireless sensor studies in the DOE's Building Energy Sciences Program. Using this equipment, a much more productive and efficient laboratory-scale method was developed for achieving sputtered coatings suitable for evaluation as high power TE elements. Adherent GAST coatings of 10 μm thickness and greater were uniformly deposited on 2- and 3-mil thick Kapton tapes. Over 570 cm^2 of material deposited on tape was produced in each run. To acquire a similar amount of film deposited on 1-cm diameter metal discs would require many runs each interrupted by opening, reloaded and pumping down the deposition system.

The previously considered approach of stacking coated discs requires engineered contacts between layers. While stacked materials that should function satisfactorily with these connections, the risk was recognized that several iterations might be necessary to produce a stack assembly with adequate thermal and electrical conduction properties. In contrast, only two connections produced by metal vapor deposition are needed using the spooled tape approach. The latter is also likely to be inherently cheaper to manufacture. Thus, success in demonstrating its practicality could be expected to have a favorable impact on system level economics. The only obvious disadvantage of the rolled tape approach appears to be the Kapton substrate acting as a thermal shunt to the sputtered material it supports. However, using at most a 1-mil thick polyimide substrate coated on both sides should limit the heat shunting of the substrate to a very small and possibly negligible amount.

To achieve the same Seebeck coefficient and electrical conductivity as was obtained with small samples, it was found necessary to use an aperture with the wheel as depicted in Figure 10. If the aperture is not used, both electrical conductivity and Seebeck coefficient are reduced in value. This is apparently because deposited atoms incident at highly oblique angles apparently produce a less ordered lattice, and lower carrier mobility. Much more work would be needed to quantify this observation, but this qualitative model seems to be appropriate.
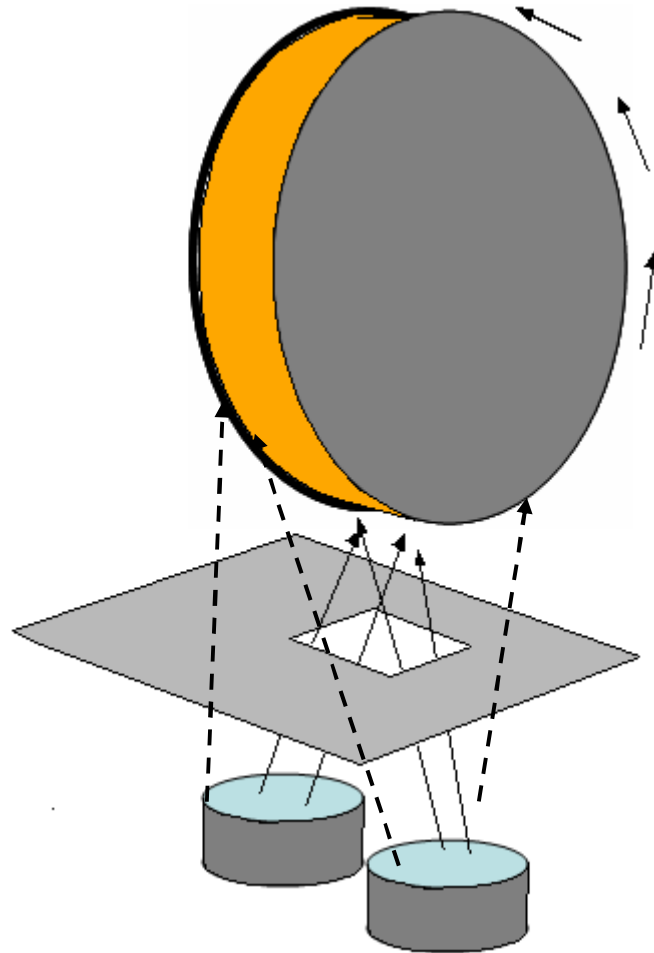
Figure 10 Modified approach to depositing thin films on long strips of polyimide. The aperature prevents deposited material from impacting the substrate at extremely oblique angles.

After considerable development, the process as described in Figure 10 was yielding TE thin-film material that could be spooled into cylindrical elements.   The material properties shown in Figure 11 were measured for samples taken from sputter-deposited Kapton strips mounted on the wheel as shown in Figure 10. The ZT values are estimated assuming a thermal conductivity of 0.01 W/cm/K. These results show a large value of electrical conductivity being achieved with reasonably high values of the Seebeck coefficient. Without the aperture, the electrical conductivity values obtained were significantly lower.
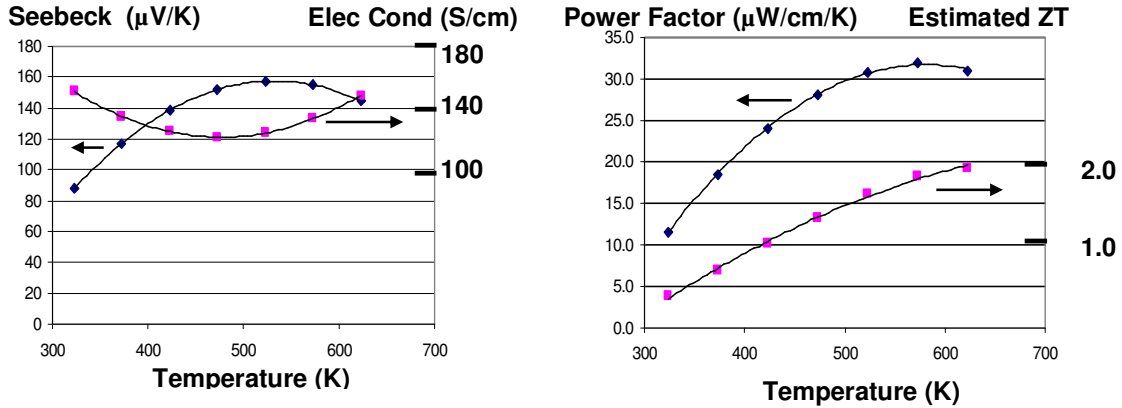
Figure 11 Electrical properties of GAST films grown with parameters tabulated in Table 2 and using the rotating wheel with an aperature.

Development of N-Type Material by Co-Sputtering Ag and PbTe

Early studies of co-sputtered Ag/PbTe films gave very good results, as shown in Figure 12. The properties plotted in Figure 12 were obtained for films deposited on polyimide mounted on a flat substrate holder. Later in the project, similar results were obtained for films grown on 1.2-m Kapton strips mounted on the wheel assembly, described above.
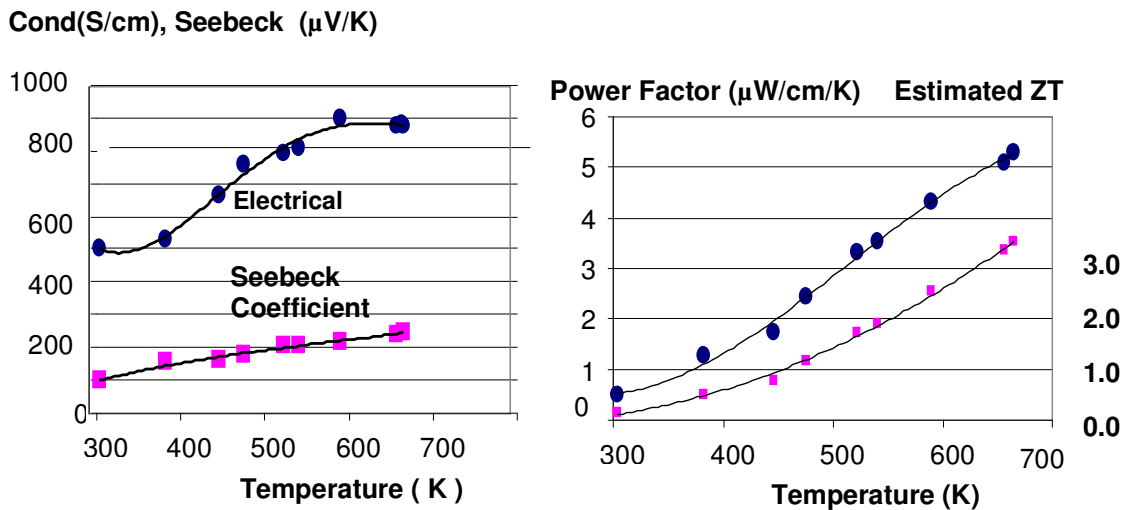
Figure 12 Results for co-sputtered Ag – PbTe films on a flat substrate platform.

Advanced TE Element Fabrication

This activity concentrated on developing an approach to thermoelement fabrication using the spooled polyimide process discussed above. This process involved the following steps:

     1. Co-sputter a 12-µm film from GeTe and $AgSbTe_2$ targets onto a 1.2-m long, 2-mil Kapton strip

     2. Wind the coated Kapton strip to form a tight spool

     3. Metalize the ends of the spool

     4. Bond copper discs to ends forming a cylindrical TE element.

The effective Seebeck coefficient and resistance of the completed thermoelectric element were measured and compared to values obtained prior to winding the film into a spooled element. Table 4 summarizes these studies.

Table 4 Characterization of GAST film and resulting TE element
Measured thermoelectric properties of the film:

     Seebeck Coefficient = 216 µV/ºC

     Electrical Conductivity = 120 $ohm^{-1}cm^{-1}$

Calculated properties of the element:

     Effective Seebeck Coefficient = 216 µV/ºC

     Resistance = 0.0506 ohms

Measured properties of element:

     Effective Seebeck Coefficient = 202 µV/ºC

     Resistance = 0.133 ohms

The film Seebeck coefficient and the effective Seebeck coefficient for the element were found to agree quite closely. The increased resistance of the element relative to the

calculated value was due to not achieving a perfect contact between the spooled film and the deposited metal on the two ends.

Depositing TE material onto polyimide tapes mounted onto a wheel and spooling a strip to form a TE element developed into an excellent approach to utilize thin film technology. However, it was found not to be a straight forward proposition to achieve TE properties as previously obtained. This is illustrated in Figure 13 that shows results for a film deposited onto a glass substrate mounted on a platform above GeTe and AgSbTe$_2$ targets. Further effort was committed to achieving performance as good as this on polyimide tape mounted on the wheel.
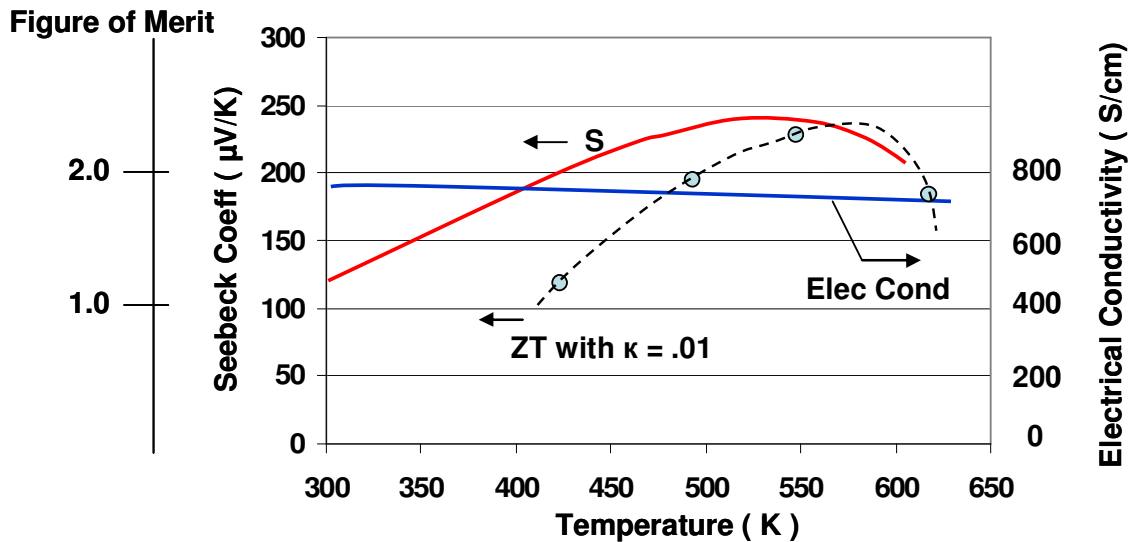
Figure 13 Seebeck coefficient and electrical conductivity vs temperature for a film deposited by co-sputtering from GeTe and AgSbTe$_2$ targets on glass.

The process of depositing TE material on a 4.8-cm wide tape that fitted the full width of the wheel and subsequently cutting strips of the desired width was found to have disadvantages. First, the cut strips tended to have slightly irregular edges that made the ends of rolled up cylinders uneven. Second, the cuts exposed bare edges of the polyimide tape. This made establishing good thermal and electrical contacts more difficult. The solution was to deposit material onto pre-cut tapes supplied by the manufacturer. Rolls of 1-cm wide, 2-mil thick polyimide tape were purchased. Sputter depositing TE materials onto precut tapes allowed the TE film to deposit around the polyimide edges (see Figure 14), which, in turn, insured that the metallization on the element faces would connect effectively to the TE film material.

Polyimide   **TE Film**

Wheel
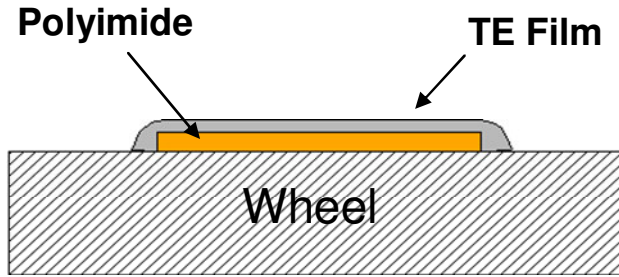
Figure 14 Illustration of TE film deposited on polyimide edges.

Characterization of Thermoelectric Properties of Materials

The figure-of-merit, ZT, of a TE material is given by the equation:

$$ZT = S^2 . \sigma . \kappa^{-1} . T$$

where:

S is the Seebeck coefficient (V/K)
σ is electrical conductivity (Siemens/cm)
κ is thermal conductivity (W/cm.K)
T is the material's temperature (K).

The above discussion reports on the ability to characterize the electrical properties (S and σ) of the TE materials developed in this project.   Up to this point, the estimation of ZT values has been based, in addition, on assuming the new materials will also exhibit reasonable values of κ expected to be about 10^{-2} W/cm.K or less. The thermal conductivity of TE samples developed in this project was measured by two methods to eliminate the uncertainty of this assumption. It should be noted that the accurate measurement of κ in thin films is extremely difficult and typically requires considerably more effort than that needed to determine electrical properties.

The first method developed was applicable to a small sample comprised of thin film TE material deposited onto a polyamide substrate and suspended as shown in Figure 15. This approach was applied to a 14-µm thick film grown on 2-mil (50.8 µm) thick Kapton.

The first step in the process involved measuring the heat loss of an uncoated sample of the polyamide tape suspended in the same fashion in a vacuum environment. The method relies on the expectation that, in a vacuum, all the heat (Q) supplied by the heater, as determined by a 4-point electrical power measurement, is conducted to the suspension structure. Knowing Q, and the physical dimensions of the suspended sample, κ may be calculated as a function of TH and TC. This step is followed by acquiring the same set of data for a sample comprised of a TE film deposited on 2-mil polyamide.

Figure 16 shows data for these two measurements for Sample 3C-S. KTotal is calculated by dividing the heat supplied to the heater by the temperature difference (TH-TC). Further refinement of the measurement would have been required before data can be obtained at higher temperatures. However, the data were fit by polynomial functions and extrapolated to higher temperatures. The thermal conductivity of the thermoelectric material is obtained by setting

$$K = (L/A) (Ktotal - Kloss)$$
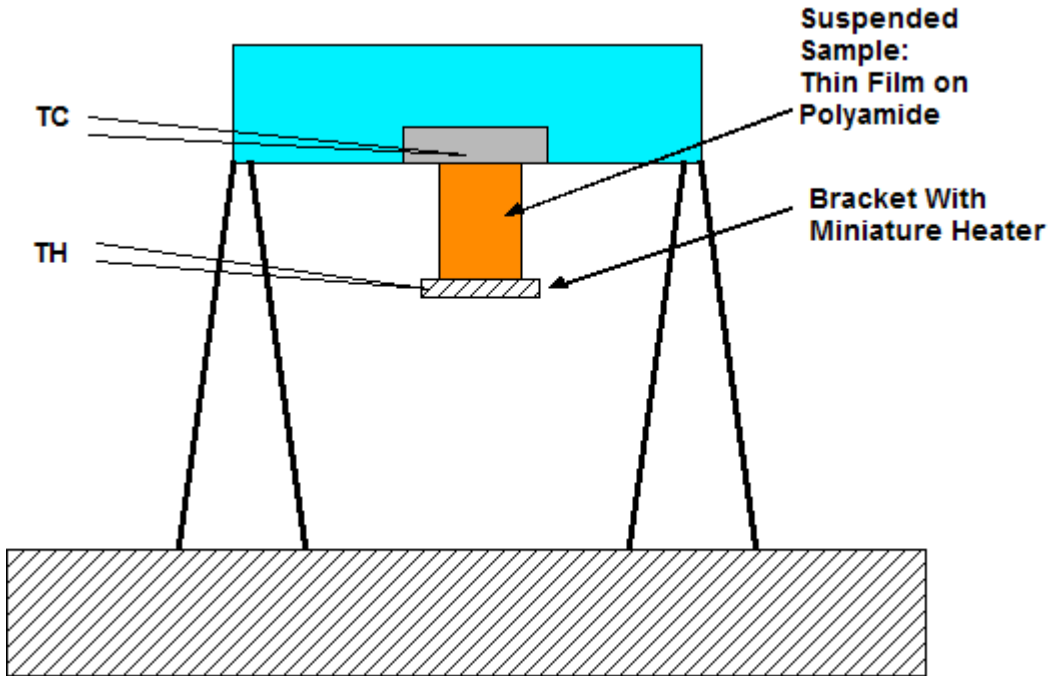
Figure 15 Approach for measuring thermal conductivity of a TE film on polyimide.

where κ is, as before, the TE material thermal conductivity, and KLoss is the total thermal conductance for Kapton only. Estimated values for κ are given in Figure 16. Note that the thermal conductivity is plotted versus TH-TC, the actual temperature difference. TC ranges between 25 ºC and 30 ºC. As with all approaches to measure thermal conductivity, this approach had its challenges. As indicated by the above equation and the plots in Figure 16, κ is calculated from a difference of two nearly equal values. Furthermore, thermal radiation from the Kapton only and TE/ Kapton films can be very different and needs to be taken into account. Thus, at this stage of the project, the thermal conductivity characteristic presented in Figure 17 of Sample 3C-S was used only as an early rough estimate.

KTotal (W/ºC)
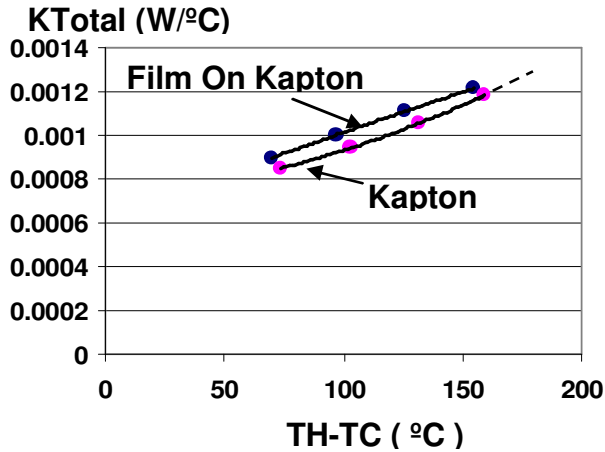
Figure 16 Measured thermal loss for a 2 mil Kapton sample and for 16 micron GAST film on Kapton.

Electrical conductivity (σ) and Seebeck coefficient (S) were also measured for TE film 3C-S versus temperature. Data are given Figure 18 and Figure 19. If values for all three parameters are combined, ZT is estimated to be 1.5 at 275 ºC to 300 ºC, and > 1.5 above 300 ºC.

These results were encouraging at the time work was proceeding to grow thick film elements that can be incorporated in a TEG. As a result, the next refinement in the measurement of thermal conductivity was to design a test rig to measure κ that utilized a disk-shaped sample. This test assembly shown schematically in Figure 20 is further illustrated in Figure 21 (showing the symmetrical sample/heater/sample subassembly with heat shield lowered) and Figure 22 (with heat shield in the normal operating position).

Thermal Conductivity
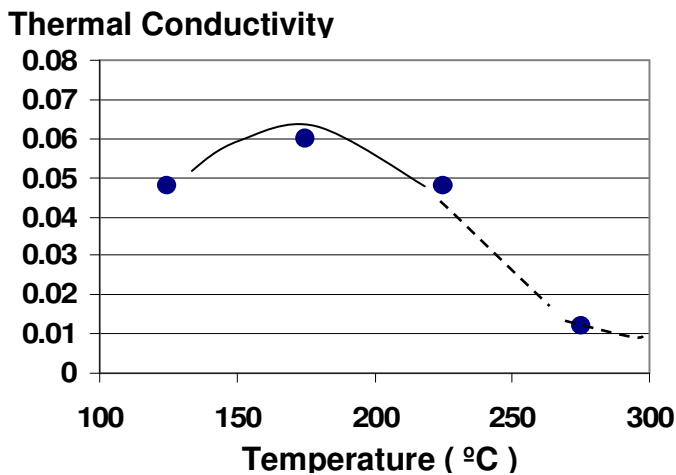
Figure 17 Estimated values of thermal conductivity for Sample 3C-S.

Electrical Conductivity
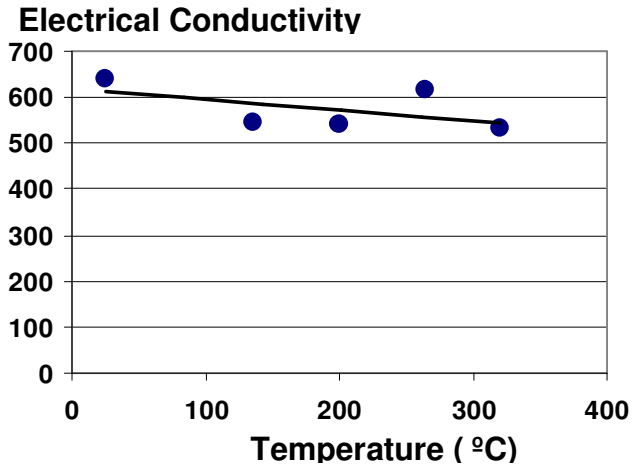
Figure 18 Electrical conductivity versus temperature for Sample 3C-S.
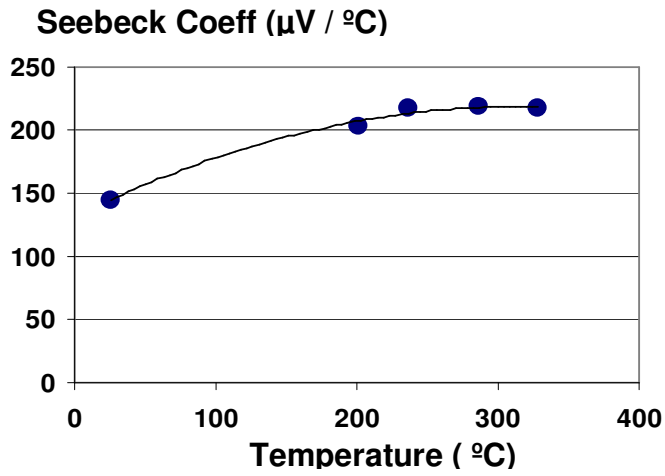
Seebeck Coeff (µV / ºC)

Figure 19 Seebeck coefficient versus temperature for Sample 3C-S.
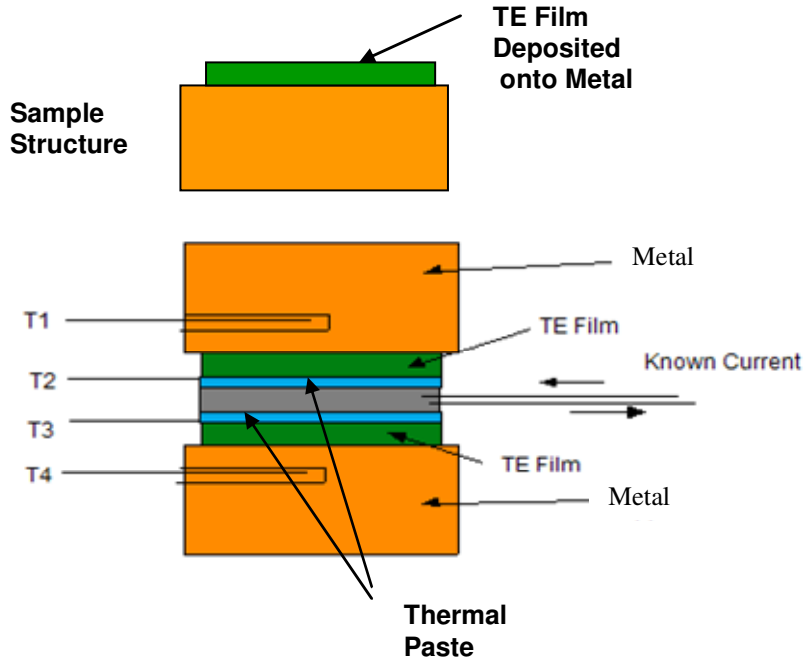
Figure 20 Schematic arrangement of samples and heater for measuring thermal conductivity of thick TE films

This equipment was used to measure the κ of three sample sets: 1) quartz discs 1 cm diameter and 1.5 mm thick; 2) GAST material deposited on 1.27 cm diameter aluminum discs to a thickness of 125 μm and 3) Type 214 fused quartz discs 1 cm diameter and 1.75 mm thick. Thermal conductivities of the first two materials were achieved under a vacuum of less than 10^{-5} torr. These experiments indicated a κ value range from 1.99 x 10^{-2} to 2.74 x 10^{-2} W/cm.K for the first quartz sample set corresponding to a temperature range 27°C to 77°C. The corresponding ranges measured for the GAST sample set was 1.89 x 10^{-3} to 2.41 x 10^{-3} W/cm.K over the temperature range 60°C to 100°C.. However, while the quartz conductivity increased with temperature as expected, the GAST thermal conductivity showed an inverse temperature relationship. This and unexpected low values of κ together with the problem of asymmetrical temperature differences across the samples made the above results quantitatively less reliable despite showing a measure of consistency. The third sample set comprising Type 214 fused quartz with a published κ value of 1.4 x 10^{-2} W/cm.K was used as a means of calibrating the overall measurement system. The encouraging result of κ = 1.35 x 10^{-2} W/cm.K at 27°C is in close agreement with the expected value. The temperature distribution across the identical samples was also symmetrical. However, performing the measurement at higher temperatures produced the unacceptable result of κ declining instead of increasing with temperature as expected. This illustrated the issue that the arrangement was exhibiting imperfect thermal conductivity between the various layers.
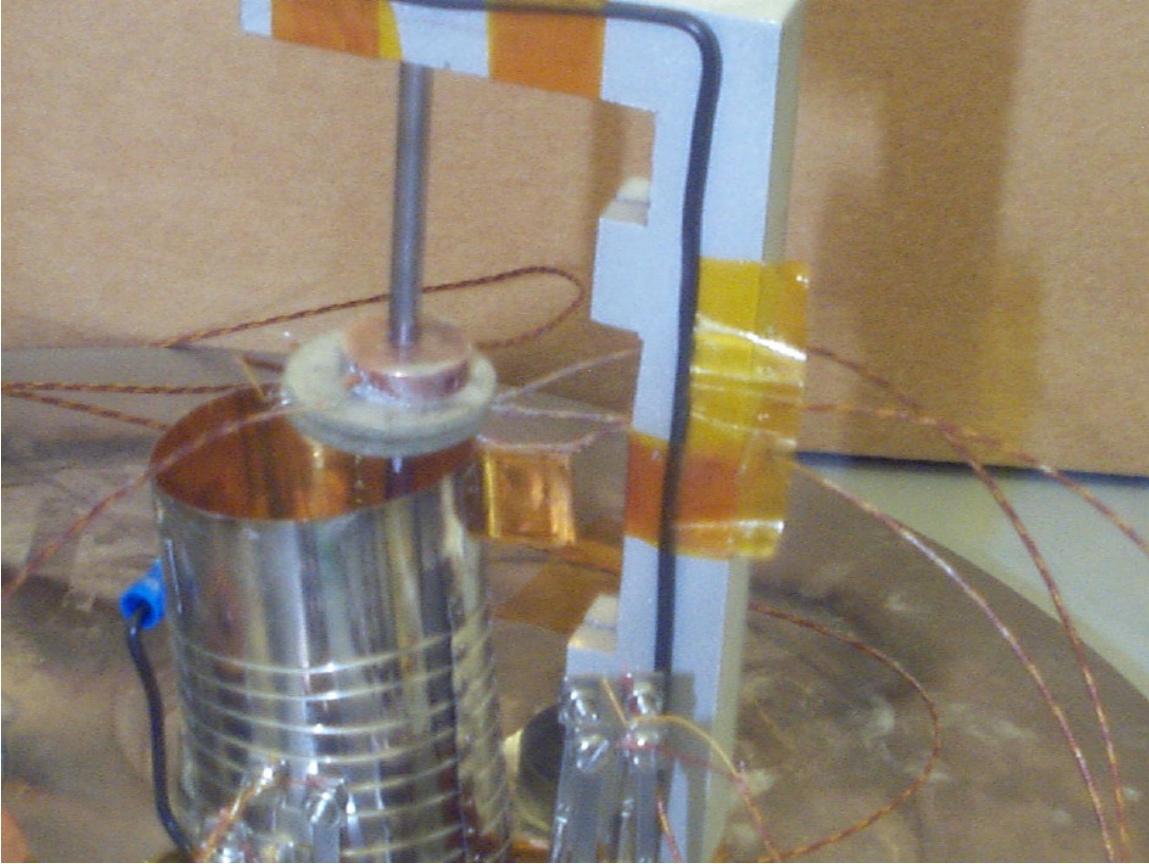
Figure 21 Apparatus for measuring thermal conductivity of disc-shaped samples (thermal shield lowered)
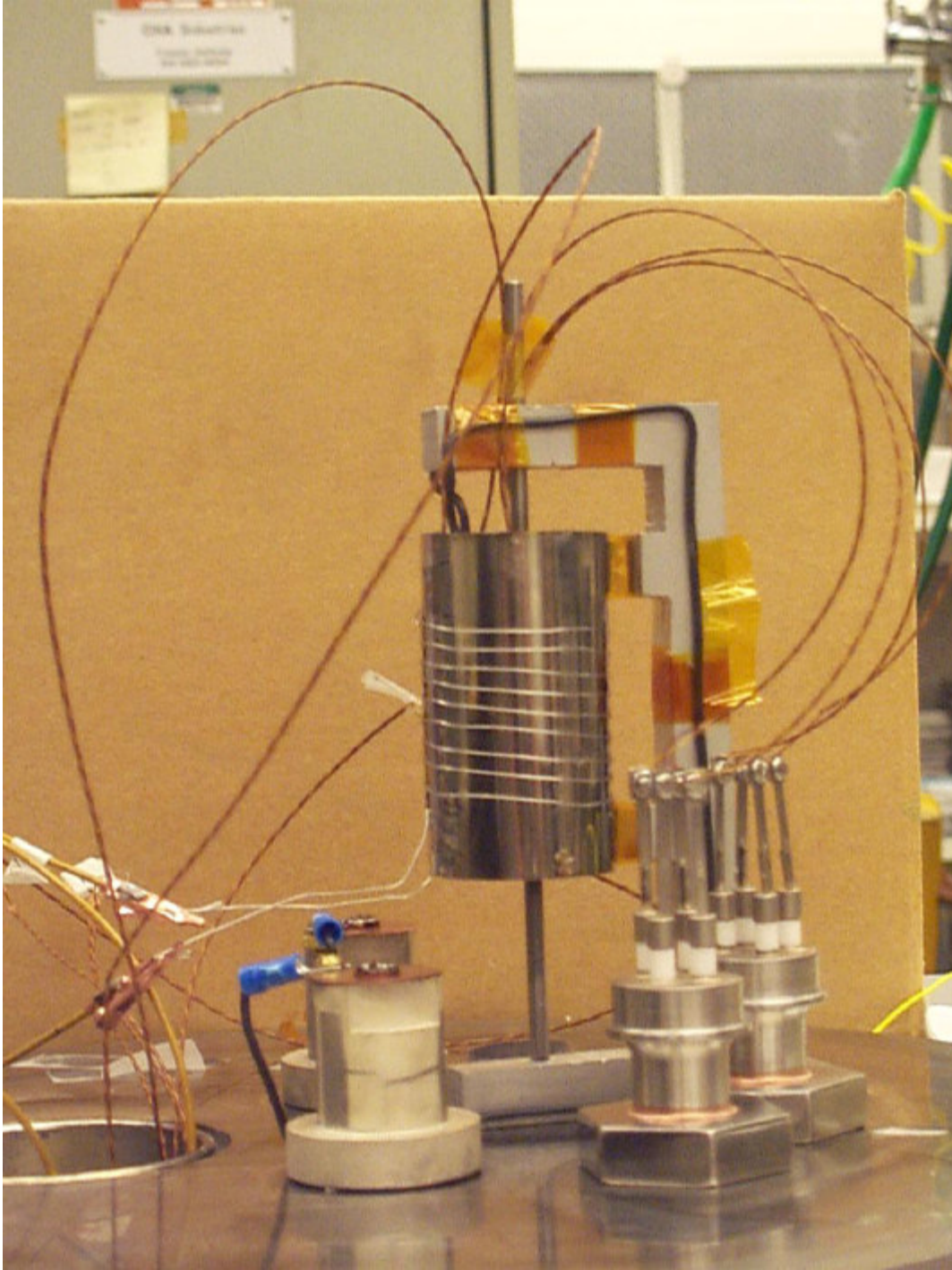
Figure 22 Apparatus for measuring thermal conductivity of disc-shaped samples (thermal shield in normal operating position).

TEG Fabrication

TEG fabrication involves: selection of n-type and p-type thermoelectric materials; development of a process to fabricate thermoelements using those materials; modeling to determine number of thermocouples, element diameters, and lengths; and finally development of TEG packaging process. PNNL selected GAST for the p-type element, and Ag-PbTe alloys for the n-type element. Thermoelement fabrication was described above.

Two basic TEG packaging geometries were considered: flat plate geometry and cylindrical geometry. In the flat plate geometry, exemplified by the design of Figure 7, heat flows normal to the surface of a flat plate at high temperature, through the thermoelectric couples, and to a second flat plate that is kept at a low temperature and serves as the heat sink. Many current thermoelectric generators (e.g. those made by High-Z or Marlow) use this geometry. These devices tend to be small and inefficient. One reason the devices are small is that the two flat plates are made of ceramic material that can withstand high temperatures and is electrically insulating, but is quite brittle and costly. This brittleness and cost makes it difficult to fabricate large (foot-size) pieces, which would be needed for large-scale waste heat recovery with TEGs. We approached several commercial TEG manufacturers in an attempt to find one who would work with us to fabricate a flat plate TEG using the spooled PNNL thermoelements, but none were interested. One manufacturer (Global Thermoelectric) did express willingness to evaluate the compatibility and performance of PNNL thermoelements with the manufacturer's existing cylindrical TEG geometry.

The cylindrical geometry is shown in cross-section in Figure 24 below. Here, the thermoelements are sandwiched between two concentric cylinders. The inner cylinder serves as the high temperature surface, and the outer cylinder is cooled and serves as the low temperature surface. The thermoelements are arranged to capture the radial heat flow and convert it to electricity. As described later, the heat transfer from the slow-moving gas stream in the PPG exhaust flue is inadequate to power directly a cylindrical TEG such as Global Thermoelectric's Model 7120. However, direct mechanical contact between the inner cylinder and a hot tube could give adequate heat transfer to power the TEG.

Given that we did not have a path to fabricate a high-temperature flat plate TEG, and the potential willingness of a TEG manufacturer to evaluate PNNL's materials in a cylindrical geometry, we focused on a cylindrical TEG for the in-plant test. PNNL had previously studied the cylindrical TEG in a bench-scale test (as described below), so this earlier work formed the basis for our study of industrial waste heat recovery with thermoelectric technology, as discussed in the next section.

Industrial Waste Heat Recovery with Thermoelectric Technology

Bench Test of Prototype TEG

PNNL built a test bed (Figure 23) for characterizing thermoelectric generators, and used it to evaluate the performance of a Global Thermoelectric Model 7120 cylindrical TEG. The test bed was built around a 2 million-BTU/hr natural gas burner that provided combustion gas temperatures up to about 1150ºC (2100ºF) to simulate temperatures in the off-gas stream of a glass furnace. Test runs were carried out over a period of several months.
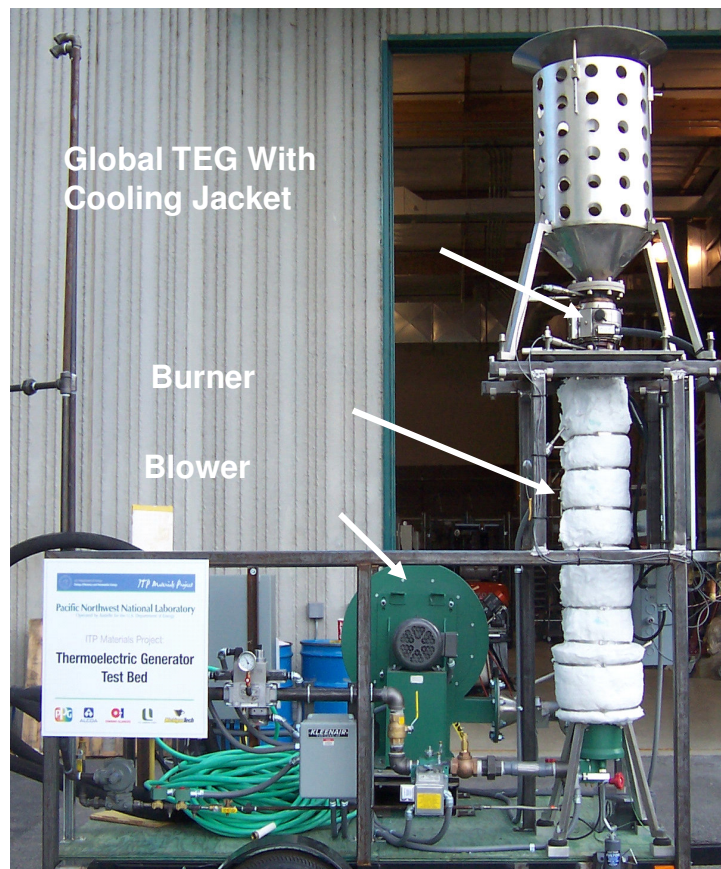
Figure 23 PNNL test bed for evaluating thermoelectric generators under waste heat flows which simulate conditions in industry.

As shown in Figure 24, the pressures and temperatures of the gas at the inlet and exit of the Global unit were utilized along with measured heat flow through the TEG to carry out fluid thermodynamic calculations. The heat transfer coefficient 'h' was calculated by comparing the values of enthalpy extracted from the gas stream to the heat flowing through the TEG as determined from a calorimetric measurement using a water jacket around the Global TEG. The gas temperature at the inlet (936ºC, 1717ºF) was higher than anticipated apparently due to the inclusion of a mantle inside the TEG to enhance heat transfer (see the cross section in Figure 24). The mantle design could be modified to achieve other desired temperatures and pressure drops.
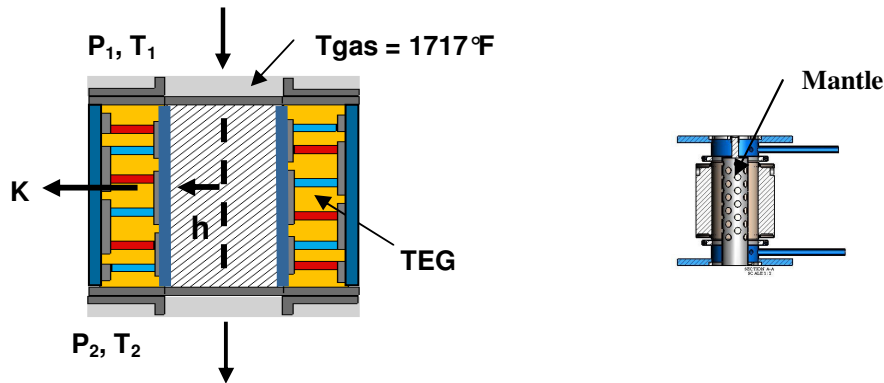
Figure 24 Cross section of converter with key parameters for determining the energy balance, and an illustration of the inserted mantle.

Testing the Model 7120 TEG was conducted to address questions affecting its operation in the planned in-plant demonstration. The focus of the investigation was 1) the function of the water jacket and 2) the pressure drop associated with the mantle placed inside the TEG to enhance heat transfer. Test runs with reduced cooling showed that the water jacket was not distributing water evenly over the cold surface of the TEG. This was evidently the cause of an asymmetrical elongation of the TEG observed at the highest heating rates in earlier runs. A subsequent discussion with the manufacturer confirmed that, if liquid cooling is desired, a new water jacket should be incorporated that delivers coolant more uniformly.

Test runs with and without the mantle in place allowed comparisons at identical gas temperatures of the pressure drop caused by the mantle. Test results showed that the mantle contributed a 4- to 6-fold increase in pressure drop along the axis of the TEG. While removal of the mantle made the converter more amenable to being powered by the natural draft of the melter exhaust, heat transfer between the gas and the hot surface of the converter was degraded when the mantle was absent. This meant that for a given hot side temperature, the gas must be correspondingly hotter by up to several hundred Celsius degrees to maintain the same heat transfer and thereby achieve the same electric output from the TEG. This finding suggests that the mantle design could be instrumental as an

independent means of optimizing the TEG's performance according to the particular temperature, pressure and flow conditions that exist in the melter exhaust stream.

After the initial test series, test bed activity was put on hold pending resolution of the choices to be considered in the design of the prototype TEG that would be built for the in-plant tests.

Glass Furnace Exhaust Flue Characterization Experiments

August 2005 Suction Pyrometry

In August 2005, concurrent with the bench test of the 7120 TEG described above, an experiment was performed at PPG's oxyfuel glass furnace in Meadville, PA to obtain gas temperature, gas composition, and pressure data at various locations in the flue. The temperature data were taken with a PPG suction pyrometer; the pressure data with a manometer; and the gas composition data with an Enerac[25] gas analysis system that measured O_2, CO, C_xH_x, NO, NO_2 and SO_x. The suction pyrometer measures only gas temperature, and not the temperature to which a surface placed in the flue would equilibrate, since such a surface would be exposed to radiant as well as convective heat transfer. Figure 25 below shows a representative sampling of the survey data.
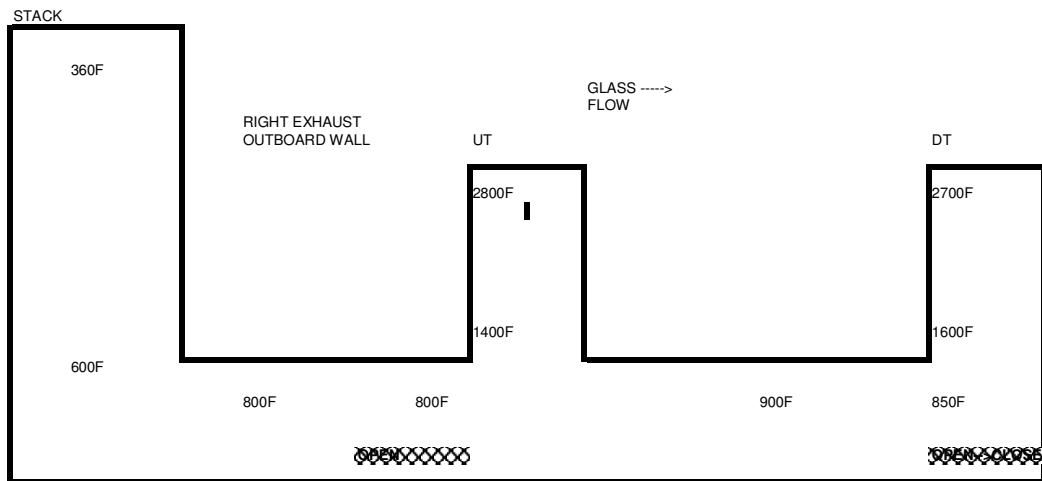
Figure 25 Flue temperature data from suction pyrometry experiments. The view is facing the outboard wall of the right exhaust flue. The section of flue labeled "UT" is the up-tank downcomer, while "DT" is the down-tank downcomer.

Based on this experiment, it was concluded that roughly 20MW of waste heat at a temperature near 2800°F was available from this source. Also, based on gas composition data, it was concluded that the dilution air aspirated into the flue from the environment effectively diluted the combustion exhaust gases by the time they reached the bottom of the downcomers. None of the holes in the flue were plugged for these measurements.

The pressure drop from the top to the bottom of the downcomer was measured to be about 0.2" WC, much lower than what was needed to drive the 7120 TEG in the bench test (there, pressure drops across the TEG were around 8" WC). Later in the project, gas velocities were measured directly with pitot tubes, and found to be less than 5 ft/sec. This led the project partners to explore alternative schemes for waste heat recovery in the glass furnace. These schemes would need to be consistent with the observation that convective heat transfer within the exhaust flue would be low, and heat transfer would need to be achieved using either large area devices or by taking advantage of other heat transfer mechanisms (e.g. radiation).

Much later in the project, another flue characterization experiment was performed to determine what area of the flue could be blocked by waste heat recovery devices without impacting the glass melting process. This experiment confirmed the low flow rates and pressure drops existing in the exhaust flue, and showed that roughly half of the area of the exhaust flue could be blocked without impacting the glass melting process. This experiment is described in detail below.

Flue Damper Experiment

A test was conducted at Meadville to quantify how much additional pressure drop could be sustained by the oxyfuel melter without disturbing the glass manufacturing process. The test results were used to determine how many heat recovery devices could potentially be installed with the existing flue design. This test (and any waste heat recovery scheme) had to consider both flues because of the furnace design. If it did not, the exhaust flow would become unbalanced. To simulate the flow resistance of a bank of waste heat recovery devices plant personnel recommended the use of flow dampers. The slots and lowering equipment for these dampers already existed but the existing dampers were made of 5/8" thick steel sheet. Plant personnel were concerned that the steel plates could warp and stick in place which had the potential of shutting down the tank. To avoid this risk Meadville personnel designed and built new dampers which consisted of a water cooled framework with sheets of high temperature fiberboard to obstruct the exhaust flow. If this became stuck the fiberboard could be easily knocked down restoring normal flow.

The test itself was carried out on May 24, 2007 with Adam Polcyn and Bill Siskos (Research), Gary Nelis and Bill Tjader (Engineering), and Dave Girvan, Mark De Young and others from Meadville participating. Several meetings and conference calls were held in preparation for this pressure drop test as well as preparatory work being done to set-up for the test. The preparatory work included installing and wiring instrumentation for the test. The instrumentation (equipment and location supplied by Research) included installation of static pressure taps before and after flue dampers on both the left and right exhaust flues and a, Research modified, S-type pitot tube (Dwyer[26] Series 160S "S" type pitot tube) located in the center but protruding six inches below the bottom edge of each damper and oriented to measure velocity pressure due to flow in a direction parallel to the flue centerline. Each pitot tube had a type K thermocouple attached at its end. The four static pressure taps and each pitot tube were connected by hoses to pressure transducers

(Setra[27] Model 260 Series Differential Pressure Transducer) each of which output a DC signal which connected to a computer data acquisition system. The two thermocouples were attached directly to the computer data acquisition system. Per Research recommendations this equipment was installed by plant personnel.

We needed to be sure that the test was in no way disruptive of actual line operation, since the line was still in production. It was determined that we would take pressure, flow and temperature readings in both flues during the test. The test involved the lowering the exhaust flue dampers (in both flues) incrementally and monitoring and recording temperature and pressure at each step. It was agreed that as soon as there was any indication that the process was being disrupted we would terminate the test. This would indicate the limit of blockage the process could tolerate before a process disruption occurred. The test was first tried on May 22, 2007 but the dampers jammed. Meadville hot works personnel worked on freeing the flue dampers and clearing any interference on May 23, 2007. The test was successfully completed on May 24, 2007.

The results are as follows:
It was found that the dampers could be lowered up to four feet from the top of the flue on each side without impacting the operation of the furnace. With the dampers lowered four feet from the top of the flue, the pressure drop across the dampers was about 0.5" water column. Also, using the pitot tube and thermocouple data, the velocities were computed to be roughly 20 ft/sec on the right flue and 35 ft per sec on the left flue (see Figure 26) with the dampers lowered four feet.

Flue Velocity vs. time
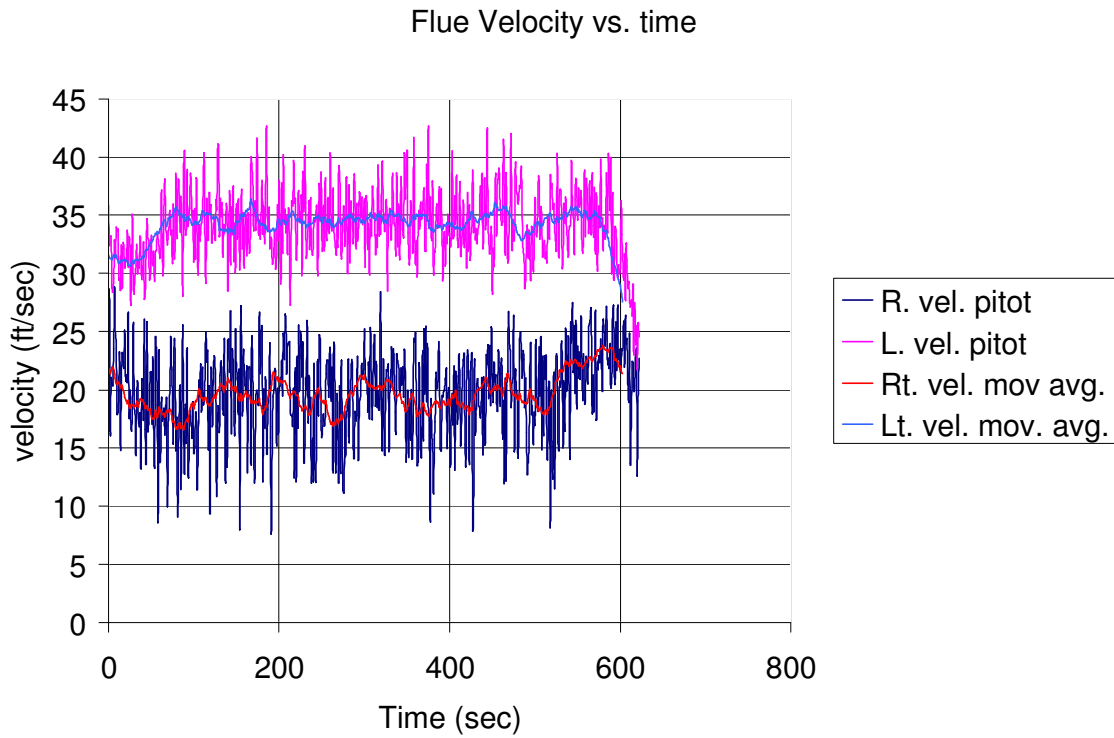
Figure 26 Flue velocity with the damper in place, blocking roughly half of the flue cross-section.

Using the velocity data it was possible to compute the total flow with time (see Figure 27).

tot. flow ft**3/sec
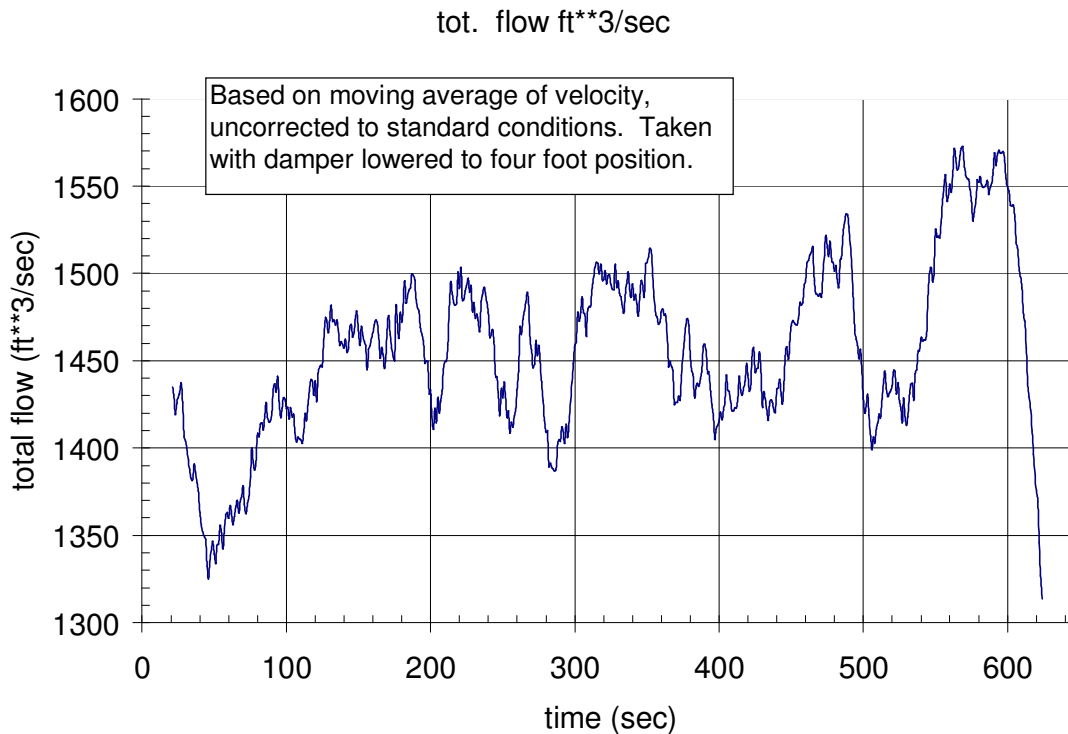
Figure 27 Gas flow in the exhaust flue with damper in place.

The flow measurements taken at the plant indicate a total exhaust gas flow of roughly 1450 ft^3/sec (see figure 2) at a temperature of about 710°F. At 710°F the gases due to combustion amount to about 200 ft^3/sec thus about 1250 ft^3/sec of air had to be sucked in from the surroundings through holes in the flue. The ambient was about 110 °F during the experiment thus the heat up is estimated at 600 °F. For this to occur 6266 Btu/sec of heat had to be added to the ambient air from the exhaust gases. As a reality check it would be desirable to compute what the temperature of the combustion gases were before they were mixed with ambient air. This was done using an approximate single value estimate of the specific heats of the constituents rather than integrating up the curve. The temperature change that is needed is computed to be 2686 °F. The gas temperature leaving the furnace would thus be computed to be 3400 °F. This is a few hundred degrees higher that actually measured but not bad considering the approximations. From the North American Combustion Handbook flame temperatures near 3400 °F is what one would expect in the combustion of natural gas or methane. This computation does not include gases given off by the batch during the melting/dissolving process in the tank.

The measurement in this experiment of a maximum flow velocity of 35 ft/sec with 0.5" WC pressure drop confirmed the earlier conclusion that the 7120 TEG could not be operated directly by the unmodified exhaust gas stream.

Conversion Device and System Design

As described in the Introduction, we pursued "modular waste heat recovery" for this project, in which many similar or identical waste heat recovery and power generation units are placed in the flue at appropriate locations to generate electricity. Such a modular approach provides for a system that is easily adaptable for various industries with various flue sizes and geometries; that can be maintained without shutting down production or stopping all waste heat recovery; and that can be "tried out" without incurring substantial risks in the form of large capital investments or significant modifications to the existing production facility. This is a natural approach for TEG technology, in which many units that individually generate a relatively small amount of electricity can be distributed in a waste heat source to yield a significant electrical output.

After the initial results in the PNNL test bed, and recognizing that the conditions in the unmodified exhaust flue would not support adequate heat transfer from the gas to a Model 7120 TEG, the team proposed building a slipstream taken from the main exhaust gas stream of the glass furnace, and accelerating the gas in that slipstream to generate the gas velocities and pressure drop required to operate the Global 7120 as designed (Figure 28).
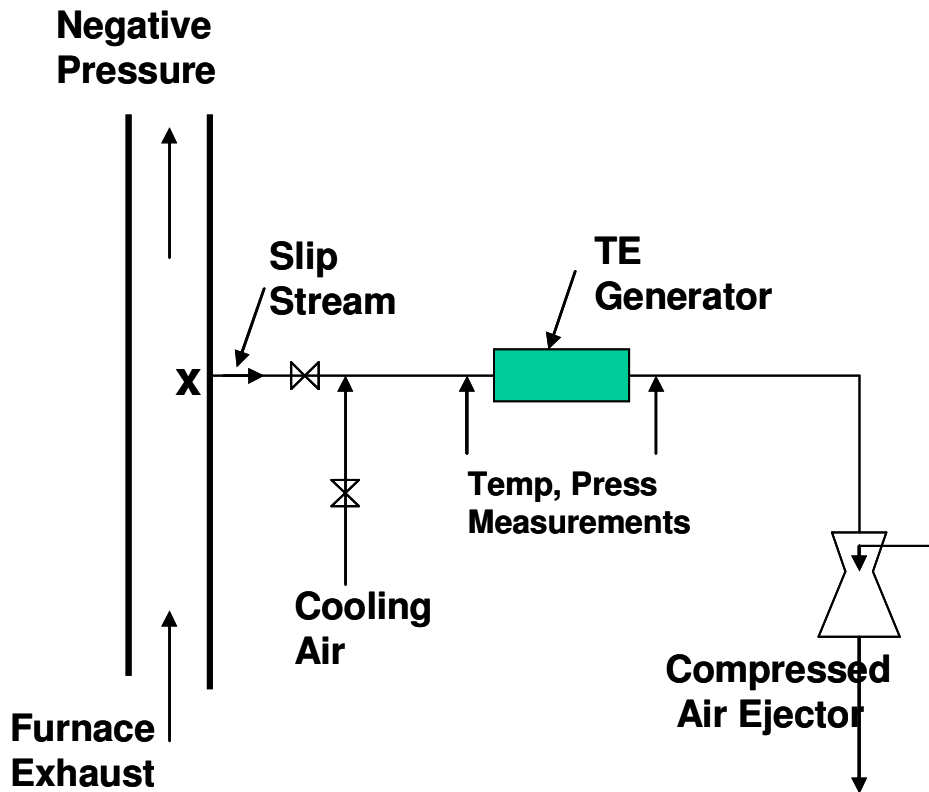
Figure 28 Proposed slipstream design for in-plant test.

However, a number of objections arose to this module design. First, it was not clear how much the energy required to accelerate the gas stream through the generator would offset the energy produced by the TEG itself, making this a potentially unrealistic (or at least inefficient) method to integrate TE technology with the gas stream. Second, this design could obviate the low operation and maintenance costs expected for TE technology. Third, the slipstream would not be a good approximation of conditions inside the flue itself, making it difficult to use slipstream results to predict behavior in the actual exhaust flue. Finally, PNNL considered TEG operation with a slipstream that did not include a compressed air ejector, i.e. a TEG driven by the natural gas flow available in the flue. It was found that the heat transfer coefficient in such a case was an order of magnitude lower than with the ejector, requiring temperature differences between the gas and the TEG of considerably greater than 2000°F. The materials required to build a slipstream that would withstand such temperatures was enough to reject this design as impractical.

After abandoning the slipstream approach, the team decided to look for module designs that would harvest waste heat from the exhaust gas stream without substantially modifying the existing properties of the gas stream. The primary challenges here are to obtain excellent heat transfer from the exhaust stream to the TEG hot face and to be compatible with the flue environment (i.e. address presence of condensates, as well as high temperatures).

PNNL performed some preliminary conceptual design work to evaluate a flat plate converter exposed to the flue gas as illustrated in Figure 29. A pancake-shaped converter (using Global Thermoelectric's 5120 unit as an example) is mounted on an insert that fits existing windows in the flue. A flow diverter is supported above the hot shoe to direct flue gasses onto the TEG. The diverter is in the form of a scoop that causes partial stagnation of the hot gas in the space it encloses. At 1450°F, a one foot square scoop opening above each TEG will intercept about 1.3 MMBTU/hr (384 kW$_t$). The 5120 TEG produces 120 W$_e$ at 7 V and 5% efficiency. Thus, it must receive about 2400 W$_t$ of heat to operate at its design point. This can be achieved by designing the rear of the scoop to leak the appropriate amount of gas consistent with 2400 W$_t$ out of the potential 384 kW$_t$ being transferred into the hot shoe. The tail end of the scoop acts as a "waste gate" that "leaks" gas back into the main stream at a rate that is controlled by the longitudinal pressure drop in the flue and eddy entrainment motion that occurs at its mouth. Also included in the design of this module is the concept of applying fins to the cold face of the TEG, and opening holes in the flue wall downstream of the module. In this way, it was hypothesized that room air would be aspirated into the flue, passing over the fins and providing cooling to the cold face of the TEG. This "natural draft cooling" concept was used for the economic analysis described below.
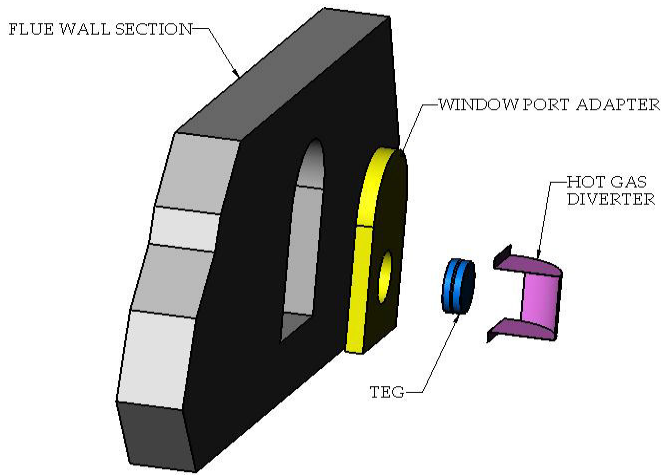
Figure 29 Exploded Schematic of Flat Plate TEG, Diverter and Window Port Adapter.

In addition to this "diverter" module described above, a "boom" module geometry was considered. In the boom geometry, a flat-plate TEG is hung from a boom extended directly into the gas stream, and exhaust gas heat is transferred to the TEG via direct gas impingement. This design has the advantages of allowing the operator to adjust the convective heat transfer by adjusting the angle of the flat-plate TEG relative to the gas flow direction, and the possibility that the gas flowing over the surface could minimize build up of particulate on the surface. Also, such a geometry could take advantage of radiant heat transfer from the furnace. On the other hand, since the entire TEG is submerged in the hot gas stream, cooling of the cold face of the TEG (the face opposite the face on which hot gas impinges) would be relatively inefficient.
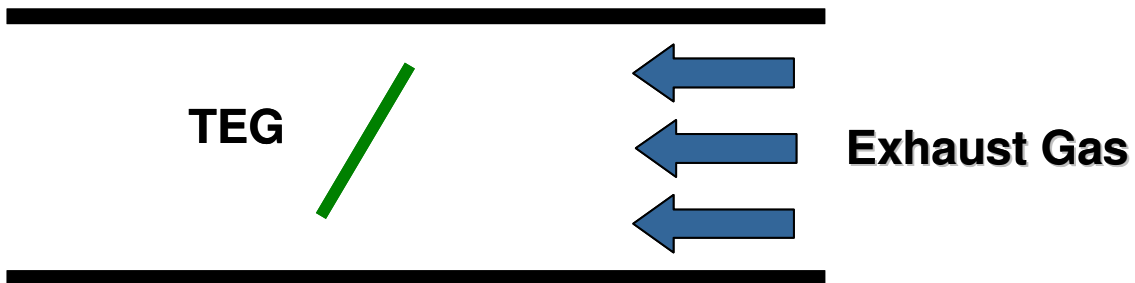
Figure 30 Boom module geometry, looking across the flue cross-section.
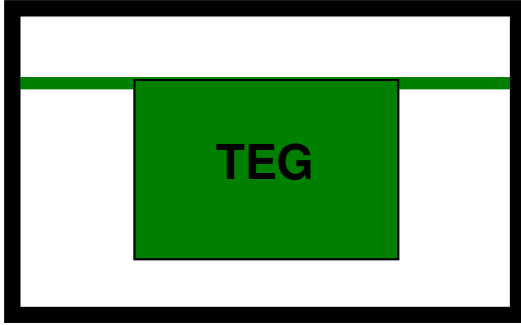
Figure 31 Boom module geometry, looking down the length of the flue.

In addition to these diverter and boom modules, the heat pipe module was proposed (Figure 32). The concept is to insert a heat pipe into the exhaust flue, and attach a cylindrical TEG (such as the Global Thermoelectric Model 7120) to the condenser end of the heat pipe, which is outside of the flue. A heat pipe is a sealed, evacuated tube containing a small amount of working fluid (for the temperatures of interest here, possible fluids include sodium and potassium) and a wick. The working fluid is evaporated by the waste heat applied to one end of the heat pipe (the end inserted in the exhaust gas flue), and condenses back to a liquid at the point where the heat pipe contacts the inner cylinder of the TEG. As the liquid condenses, it gives up its latent heat, which is used by the TEG to generate electricity. After condensing, the working fluid rapidly flows back down the heat pipe under gravity and the capillary forces produced by the wick, where it evaporates again, thereby restarting the heat transfer cycle. Heat pipes are known as "superconductors" of heat, as very little heat is lost in the vaporization/condensation cycle of the sodium liquid. Heat pipe technology has been under development for over 45 years, and currently has a number of commercial applications, including the efficient removal of heat from computer chips (with water as the working fluid). Heat pipes are attractive for use as heat exchangers in this application because of their excellent heat transfer efficiency, and excellent durability and reliability[28,29]. This design makes it possible to separate the problems of heat recovery and electricity generation; takes the TEG itself out of the flue environment, thereby greatly simplifying the requirements on its design and construction, making operation and maintenance of the TEG much more convenient, and allowing for both air and water cooling options; and efficiently transfers the captured heat to the TEG. Finally, the heat pipe module has a "heat concentrating" functionality; i.e., it collects heat from the flue along the entire surface area of heat pipe that is inside the flue, and (ideally) deposits heat only over the area where it contacts the TEG. For our geometry, this implies that the heat flux available inside the flue can be an order of magnitude lower than what is required to operate the TEG. For these reasons, the heat pipe module geometry was eventually chosen for the in-plant test as the most promising and most practical approach.

An additional geometry for heat collection proposed during this project was the "pin-fin" geometry. Pin-fin arrays are arrays of cylindrical posts placed such that turbulent flow is achieved inside the array for improved heat transfer, while maintaining fairly low pressure drops across the array and allowing air to enter the array from any direction. These arrays are used to cool chips in the computer industry. Arrays with posts consisting of biaxial cylinders, with cooling water flowing in the central cylinder, and TE modules placed between the inner and outer cylinder, were proposed. This arrangement provides for easy removal of individual posts for cleaning or other maintenance, as well as efficient use of cooling water. A downside to this concept is that thermal expansion

Cylindrical "Sleeve" TEG(s)

Heat pipe

Heat transfer fins
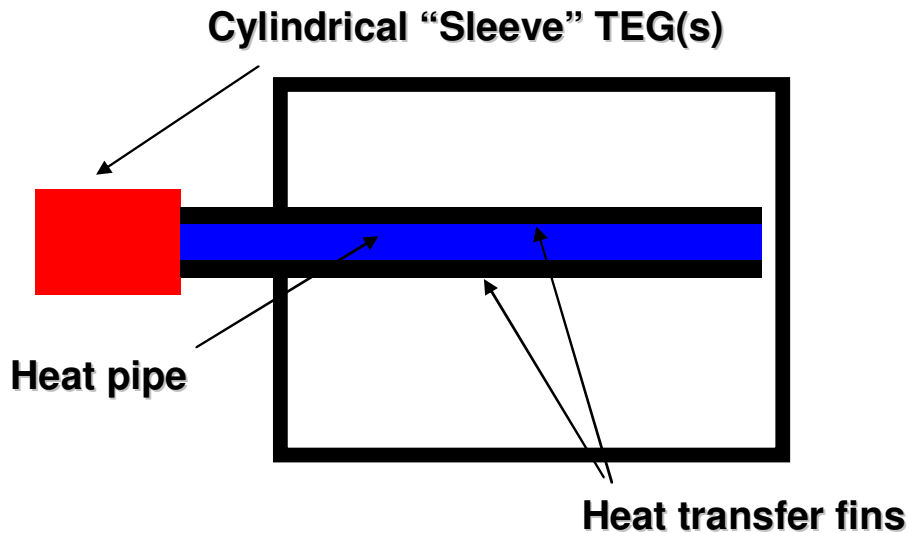
Figure 32 Heat pipe module geometry, looking down the length of the flue.

differences between the hot outer and cool inner cylinders could cause poor thermal contact to the TE modules upon inserting the device into the flue.

Working from the pin-fin concept, pin-fin arrays of heat pipes were also proposed, with TE modules attached to the pipes external to the flue. This arrangement also provides for easy removal of individual pipes, and the added advantage of having the modules external to the flue where they can be easily accessed and cooled via air, water, or a combination of both.

Initial Economic Analysis

Given these potential module geometries, PNNL performed an initial economic analysis of the diverter and boom geometries. The analysis involved the use of a spreadsheet that calculates net present values using either target costs or the best cost projections available at the time for the various components of the system. These were derived assuming reasonable performance and cost improvements anticipated to result from further development.

The analysis involved the following assumptions:

- Thermal power available - 58.3 MMBTU/hr (17×10^6 $W_{T)}$
- Total thermal energy intercepted – 50%
- Unit TEG cost $1000
- Electrical output corresponding to conversion efficiency and number of TEGs deployed.

Generic cost data were used as the basis for estimating balance of plant costs, for example, the supply and circulation system that supports the water cooled converter option. When no currently reliable cost information existed, balance of plant costs were estimated as a fixed percentage increment based on the target capital cost of the TEG.

Table 1 summarizes results showing years to payback vs. the market value of generated electricity for two of the principal TEG configuration alternatives. The option of mounting the TEG in an opening in the flue wall can, in principle, be cooled by ambient air flowing over fins external to the flue, whereas, the boom-mounted option that inserts the converter fully into the flue gases is cooled by direct water flow through the TEG mounting plate. The yellow highlighting in Table 1 indicates viable options that would satisfy a 2-year payback criterion.

The results tend to indicate the generally lower cost of air cooling especially when the coolant can be naturally aspirated by the flue. In contrast, water cooling extracts more heat from the flue gases than just the heat rejected by the cold shoe of the TEG. This heat must then be rejected to the atmosphere or delivered to some other process in the plant by an auxiliary circulation system. Neither option shows any economy of scale versus power output because of the manner in which costs are linearly based on the assumed unit cost of the TEG. However, the effect of converter efficiency is demonstrated and

Table 5 Sample case studies showing present value payback v generated power value.

Case Description	Years to Payback vs. Energy Value				
	2¢/kWh	4¢/kWh	6¢/kWh	8¢/kWh	10¢/kWh
Wall Mounted TEG; Natural Draft Cooling; 1 MW Output; 20% Eff.	6.33	2.39	1.47	1.07	<1
Wall Mounted TEG; Natural Draft Cooling; 1.7 MW Output: 20% Eff	6.33	2.39	1.48	1.07	<1
Wall Mounted TEG; Natural Draft Cooling; 1.3 MW Output: 15% Eff	11.12	3.46	2.07	1.48	1.15
Wall Mounted TEG; Natural Draft Cooling; 850 KW Output: 10% Eff	>20	6.33	3.46	2.39	1.82
Water Cooled TEG; Adds 50% Capital; 1.7 MW; 20% Eff.	18.98	4.45	2.58	1.82	1.4
Water Cooled TEG; Adds 100% Capital; 1.7 MW; 20% Eff.	>20	7.05	3.77	2.58	1.96

shows that, if the target converter cost assumption is reasonable, there are cost-effective system configurations even when TEG efficiency is considerably less than 20%. It is important to note that the converter cost assumption used here is roughly $0.60/W. Typical costs per watt for commercially available TEGs today are typically an order of magnitude higher than this.

PPG In-Plant Test of Waste Heat Recovery with TE Technology

Because waste heat recovery from an oxy-fuel exhaust gas stream had never been attempted (to our knowledge) with TE technology, the project team felt that it was worthwhile to test conventional (3-5% efficiency) TE technology at PPG while PNNL was developing the materials for the advanced TEG. With this approach, it was hoped that many of the expected challenges related to integrating TE technology into a glass furnace environment would be identified and resolved before receiving the advanced TEG, thereby accelerating project progress. In addition, some of the findings from such a test were expected to be valuable inputs for the design of the advanced TEG.

Recall from the Background section that combustion exhaust gases exit the oxy-fuel furnace through four ports. These gases then are pulled via natural draft down vertical sections of the flue known as "downcomers". From here, they flow into two horizontal "connecting flue" sections (one on either side of the furnace) before being ejected out the stacks. The flue is at a slight negative pressure relative to the ambient, so a small number of bricks are removed from the flue walls to allow ambient air to flow into the downcomers and connecting flues to cool the combustion exhaust gases before ejection. When the gases leave the furnace and enter the downcomers, the gas temperature is around 2700°F, with composition roughly 50% water, 35% carbon dioxide, and the remainder nitrogen and a small quantity of oxygen. At the bottom of the downcomers, entering the connecting flue, the gas temperature is around 800°F, with composition roughly 75% nitrogen, 20% oxygen, and the remainder equally split between carbon dioxide and water. Thus by the time the gas reaches the bottom of the downcomers, it has composition very close to that of normal ambient air, indicating that the combustion gas has been highly diluted by the aspirated ambient air. The gas velocity is quite low; in the connecting flue area just beyond the downcomer, gas velocities below 5 ft/sec are typical. The bottoms of the four downcomers are the hottest points in the exhaust flue that are easily accessible from the basement floor of the furnace building. In addition to being the closest points to the furnace that are also easily accessible, they are in line-of-sight of the very hot upper downcomer region, which is heated by radiation emitted by the furnace. For these reasons, it was proposed to perform the in-plant test at the bottom of the right downtank downcomer.

Before proceeding with the expense of the in-plant test, further characterization experiments on the proposed in-plant test site were performed. The purpose of these was to confirm that the temperatures required to power the TEG could be obtained at the site, and to better understand heat transfer mechanisms at the test site in order to design the most effective heat recovery module.

Spoon Run 0: Flue Temperature Characterization

"Spoon" is a generic term used by PPG to describe a probe, generally cooled by air or water, that can be inserted into a hot environment (such as the exhaust stream) to collect certain data on the hot environment. A spoon known as the "Materials Testing Spoon"

was custom-fabricated for this project. It was designed to measure directly both spoon surface temperature and heat flux through the spoon as condensates built up over time on the spoon surface. It also proved useful for simple characterization of temperature inside the flue.

In Run 0 of the Materials Testing Spoon, a heat flux transducer (HFT) obtained from Thermonetics[30] was cemented to the top surface of the spoon and placed in the exhaust stream at 1400°F gas temperature, 1150°F spoon top surface temperature, for three days. The HFT wires corroded and broke in the flue environment over this time, and the thermal connection between the HFT and the spoon weakened to the point that the HFT was easily removed from the spoon top surface. However, important information for the in-plant test was obtained in Run 0, which is therefore described in some detail below.

Run 0: A high-temperature heat flux transducer for use up to 1650°F was obtained from Thermonetics Corp. This HFT is ¾"x ¾" thermopile covered with a glass frit glazing. Chromel wire was spot-welded to the ends of the HFT wires to make them long enough to extend into the exhaust flue. Then the Thermonetics HFT was cemented to the top surface of the spoon using Sauereisen[31] Aluseal Adhesive Cement #2. After drying overnight, the cement was further dried at elevated temperature. The HFT calibration constant varied with temperature, 280 BTU/hr/ft^2/mV at 1200°F and 345 BTU/hr/ft^2/mV at 1600°F.

TOP VIEW
MATERIALS TESTING
SPOON

Air inlet/outlet
pipes shown
offset for clarity;
in actual, inlet
pipe should be
directly over
outlet pipe

Combined valve/meter to
throttle and measure air flow

Heat Flux Transducer
cemented to top surface
of spoon

Brick pattern shows placement of
insulation during ITI HFT Run
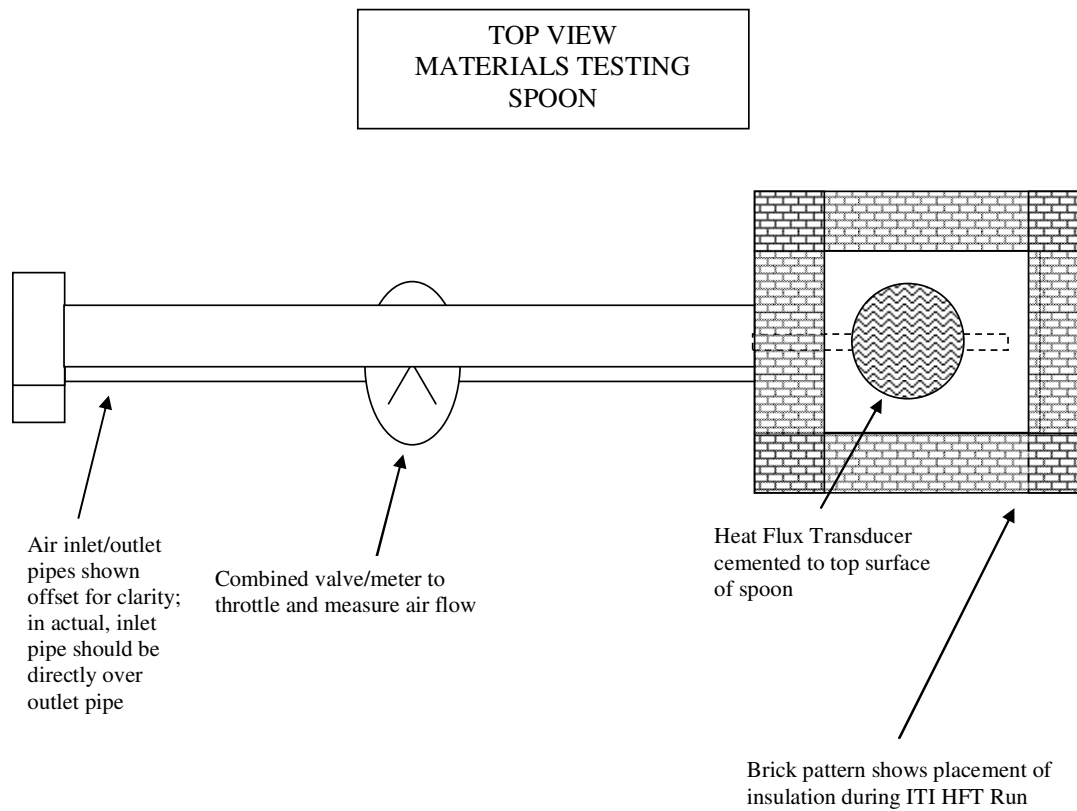
Figure 33 Top view of Materials Testing Spoon in configuration used for Run 1. In Run 0, insulation was also applied around the inlet and outlet pipes.

SIDE VIEW

Air Out

Air In

T_{int}

T_{GS}

Internal spoon temperature (Tint)
measured here

Gas stream temperature
measured here

***Dashed arrows show path of air
through spoon***
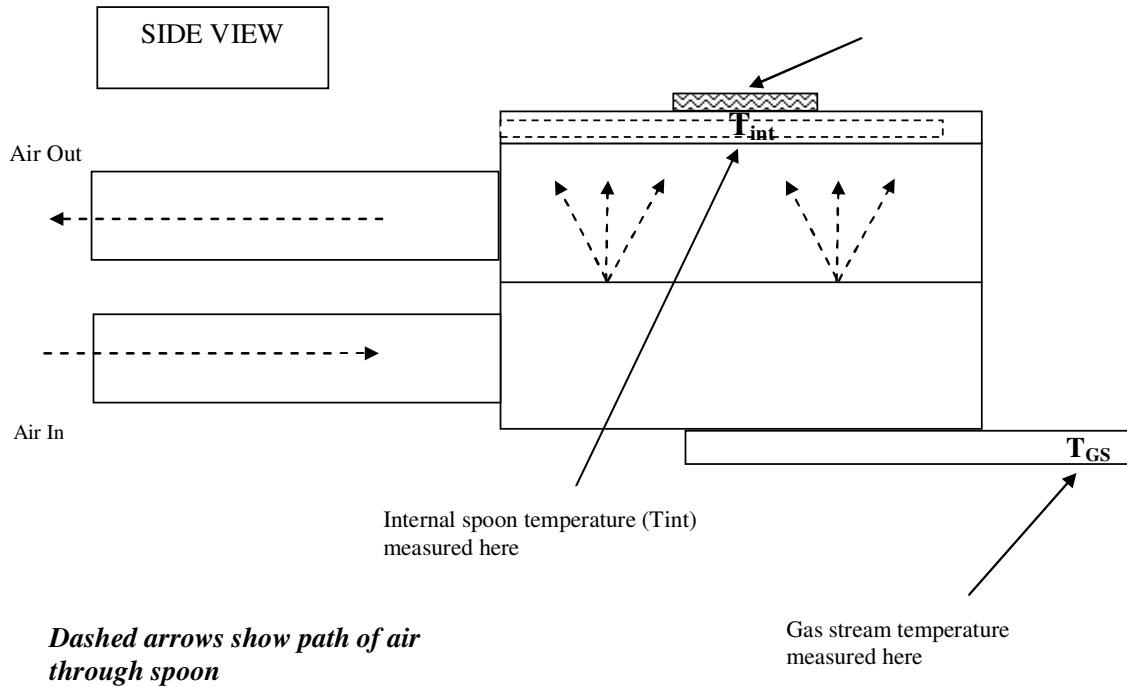
**Figure 34 Side view of Materials Testing Spoon in configuration used for Runs 0,1. Insulation is not
shown in this drawing for clarity.**

The configuration of the spoon as used in this experiment is shown in Figure 33 and
Figure 34. Kaowool[32] was used to insulate all surfaces of the spoon except for the top
surface, so that the heat flux measured by the spoon would be primarily through the top
surface and would be absorbed by the cooling air impinging on the top surface.
Insulation was also applied over the inlet and outlet air pipes in this experiment only in an
attempt to measure the temperature change of the cooling air as it picked up heat from the
spoon.

The objectives for this run were:

1. To assess whether the temperatures required for the in-plant
   demonstration (800°C gas temperature, 650°C heat pipe surface)
   could be achieved at the bottom of the downcomer.
2. Assuming the first objective could be met, measure the heat flux
   through the heat flux transducer under the surface and gas
   temperatures relevant for the in-plant demonstration. Compare the
   result to the heat flux required to power the 7120 TEG.

Given that a heat pipe module was proposed for the in-plant test, and given that the spoon geometry is not the same as the heat pipe geometry, there may be some question about how useful the second objective is. Indeed,

$$(1/A) \, \mathrm{d}Q/\mathrm{d}t = h \, (\Delta T)$$

Where $(1/A) \, \mathrm{d}Q/\mathrm{d}t$ is the heat flux, h is the heat transfer coefficient, and ΔT the temperature difference between the gas and the surface. If h for the heat pipe and for the spoon geometries are significantly different, measuring sufficient heat transfer for the spoon does not guarantee sufficient heat transfer for the heat pipe. However, we would argue that the spoon geometry is actually quite similar to what would be expected for a (short) cross section of the heat pipe. The heat pipe is a 3.42" diameter cylinder and, with insulation over all but the top surface of the spoon, the spoon presents a roughly 3" x 4" rectangular cross section to the gas stream. Given the similarities of these two geometries, we expect measurements with the spoon to give at least a rough idea of heat fluxes that could be obtained with a heat pipe.

For Objective 1, the spoon was placed in the flue opening at the bottom of the right downtank downcomer (easily accessed from floor level), and various holes in the middle of the downcomer were plugged to increase the temperature at the bottom. The plugging was done either with Kaowool or bricks. Recall that generally these holes are left open so that room air will be sucked into the flue (which is at around 0.25" negative pressure) to cool the exhaust gas. There are 14 holes, each 2.5" wide and 6.125" high, in the middle of both the down tank and uptank sides of the downcomer. The temperature was measured using a K-type thermocouple that was inserted into a 5.5 inch long steel bobbin and extended 4.25 inches from the end of the spoon (see Figure 34). The thermocouple was approximately 31 inches from the inner wall of the downcomer (the downcomer opening is 39 inches across from wall to wall). The table below shows the resulting temperatures that were achieved for various configurations of plugs.

Table 6 Gas stream temperatures achieved by plugging brick-sized holes on the down and uptank sides of the right downtank downcomer.

# holes plugged	Gas Stream Temp	Downtank Holes Plugged	Uptank Holes Plugged
7	1206 F	2,4,6,8,10,12,14	none
14	1289	all	none
21	1450	all	2,4,6,8,10,12,14
19	1490	2,3,4,5,6,7,8,9,10,11,12,13	2,4,6,8,10,12,14
17	1506	3,4,5,6,7,8,9,10,11,12	2,4,6,8,10,12,14
15	1430	4,5,6,7,8,9,10,11	2,4,6,8,10,12,14
13	1386	5,6,7,8,9,10	2,4,6,8,10,12,14

 The gas temperature desired for the in-plant demonstration is 800°C, or 1472°F. Clearly we are able to achieve this temperature (and more) by plugging holes in the downcomer. After demonstrating that the desired temperatures could be achieved, the air cooling system on the spoon was activated and the air flow tuned to achieve a spoon internal temperature reading (measured as T_{int}, see Figure 34) 300°F lower than the gas stream

temperature. This is consistent with the temperature difference estimated by the heat pipe manufacturer to drive sufficient heat into the unfinned heat pipe for the 7120 TEG. It was found that 1.5scfm was sufficient to achieve the temperature difference desired. The data taken with air flow at 1.5scfm are shown in Table 7.

Table 7 Summary of heat flux data taken on air-cooled spoon.

Run	Day/Time	Statistic	Internal °F	HFT mV	Inlet °F	Outlet °F	Gas Stream °F	HFT Heat Flux BTU/hr/ft2	Enthalpy to Air BTU/hr	GS-Int °F
plug 19	1/29 pm -	avg	1182	33	69	320	1490	9113	385	308
	1/30 am	max	1209	37	72	337	1523	10485	407	
		min	1144	28	67	307	1450	7722	367	
plug 15	1/30 late am	avg	1116	26	73	259	1430	7209	282	313
		max	1165	35	74	301	1441	9672	346	
		min	1030	20	72	192	1416	5501	175	
plug 13 0	1/30 early pm	avg	1159	15	74	309	1408	4257	358	249
		max	1168	19	75	314	1427	5219	366	
		min	1153	12	74	302	1392	3222	348	
plug 13 1	1/30 pm -	avg	1159	9	75	304	1386	2596	349	228
	2/2 am	max	1197	16	78	313	1429	4363	360	
		min	1127	3	72	289	1345	970	330	

In the table above, "Run" signifies the name of the data run. The names correspond with the number of downcomer holes that were plugged for that run. "Day/time" signify the time frame over which data were acquired for that run. For each quantity, average, maximum, and minimum values are reported to give a sense for variation in each quantity during the run. Since there were slight, non-statistical, variations in the flue conditions during the run, we report max and min values rather than a standard deviation. "Internal" is the internal spoon temperature (see Figure 34). "HFT" is the voltage read from the Thermonetics heat flux transducer, which can be multiplied by a temperature-dependent calibration constant to obtain the heat flux in BTU/hr/ft^2. "Inlet" and "Outlet" are the temperatures measured on the outside of the inlet and outlet pipes carrying the cooling air to and from the spoon. "Gas stream" is the gas stream temperature measured by the thermocouple enclosed in a steel bobbin and extended past the end of the spoon (see Figure 34). "HFT Heat Flux" is the increase in heat flux measured by the Thermonetics HFT upon turning on the 1.5scfm cooling air to the spoon (and waiting for equilibrium to be re-established). It is computed by subtracting a "background" heat flux measured when no cooling air was flowing to the spoon from the heat flux measured when cooling air was flowing. "Enthalpy to Air" is the calculated enthalpy transferred to the cooling air as it flows from the inlet to the outlet pipe, and includes enthalpy picked up while traveling through the pipes as well as in the spoon itself. The inlet and outlet pipes were covered with Kaowool insulation to minimize the amount of heat transferred to the cooling air while in the pipes, but we did not do experiments to separate out enthalpy transferred through the pipes versus through the spoon. "GS-Int" is the difference between the gas stream and internal temperatures.

As the table shows, the temperatures of the gas environment (as measured by T_{GS}) and of the spoon surface (as measured by T_{int}) were close to those desired for the in-plant test (1472°F environment, 1200°F surface) for all of the runs. The heat flux measured by the Thermonetics HFT started near 9113 BTU/hr/ft^2, then dropped consistently for subsequent runs to a minimum of 2596 BTU/hr/ft^2 in the last run. In these units, the heat flux that must be collected by the heat pipe to power the 7120 TEG is 1966 BTU/hr/ft^2 (0.62 W/cm^2). The measured heat fluxes are at least comparable to this, although clearly a dramatic decline in measured heat flux occurred over the course of these experiments. Another measure of heat flux to the spoon is the enthalpy transferred to the cooling air. While this shows some decrease in later runs compared to the first run, the decline is much less dramatic than what was seen by the HFT (10% versus a factor of 3). One explanation for the dramatic decline in HFT heat flux could be rapid collection of particulate. However, even after the extended "plug 13 1" run, there was not enough white powder on the HFT to collect for measurement. There were also some solid "grains" of material on the HFT, although these were sparse on the HFT. After removing the probe from the flue after "plug 13 1", a large buildup of solid material was noticed over the insulation covering the air pipes, and a red glow was seen just under this buildup, indicating that the area was very hot. Also, the voltage on the HFT rapidly climbed to saturation starting around 2100 hours on 1 February. After removing the buildup and insulation, it was noticed that an HFT electrical lead had broken in that region, most likely due to the excessive heating observed at that point. Also, the cement bond between the HFT and the spoon surface had degraded to the point where the HFT could be easily removed from the spoon surface by hand. Hence, we believe that the decline in heat flux over the course of these experiments was most likely due to degrading thermal contact between the HFT and the spoon surface, and the sharp rise in voltage after 2100 hours was due to the HFT wires breaking.
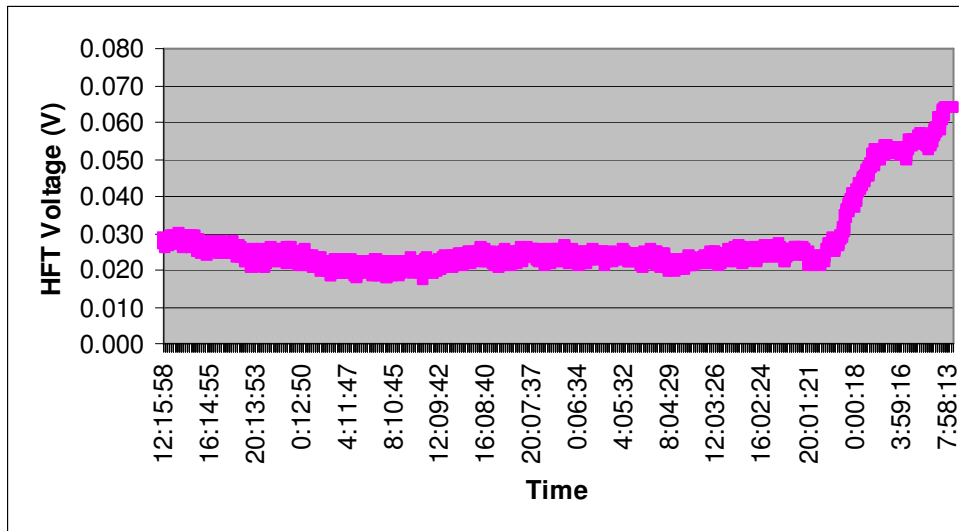
Figure 35 Heat flux transducer voltage towards the end of run "plug 13 1".

The overall conditions of the downcomer did change due to the plugged holes and resulting increase in temperature in that region. The inside walls of the downcomer are generally covered with an "ice" composed of solid sodium sulfate and other

condensibles. Further downstream at lower temperatures, only a "snow" of sodium sulfate remains, and this powder collects at the bottom of the downcomer and further downstream in the connecting flue (as well as on cooled surfaces such as the spoon). After plugging holes in the downcomer, the walls of the downcomer became hotter and some of the "ice" on the walls loosened and fell to the bottom of the downcomer (some of these "ice" particles also fell on the HFT). Also, pools of liquid sodium sulfate seemed to form at the bottom of the downcomer and eventually solidified to form ice.

A last piece of learning from this experiment was to observe the impact on various readings from applying the cooling air to the spoon. Figure 36, Figure 37, and Figure 38 below show the impact on various sensors from suddenly applying 4 scfm of air to the spoon (at 16:09), then progressively throttling the flow back to various levels, ending around 1.5scfm at 17:55.
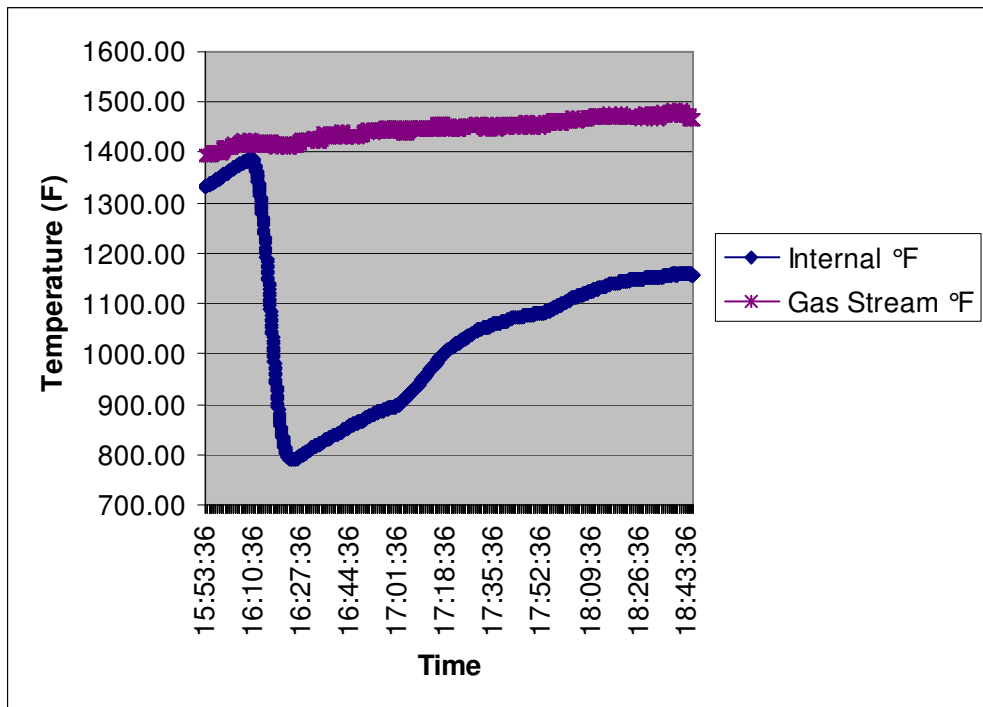
Figure 36 Internal temperature and gas stream temperature. Air flow to the spoon was started at 16:09. Cooling of the spoon due to air flow is apparent.
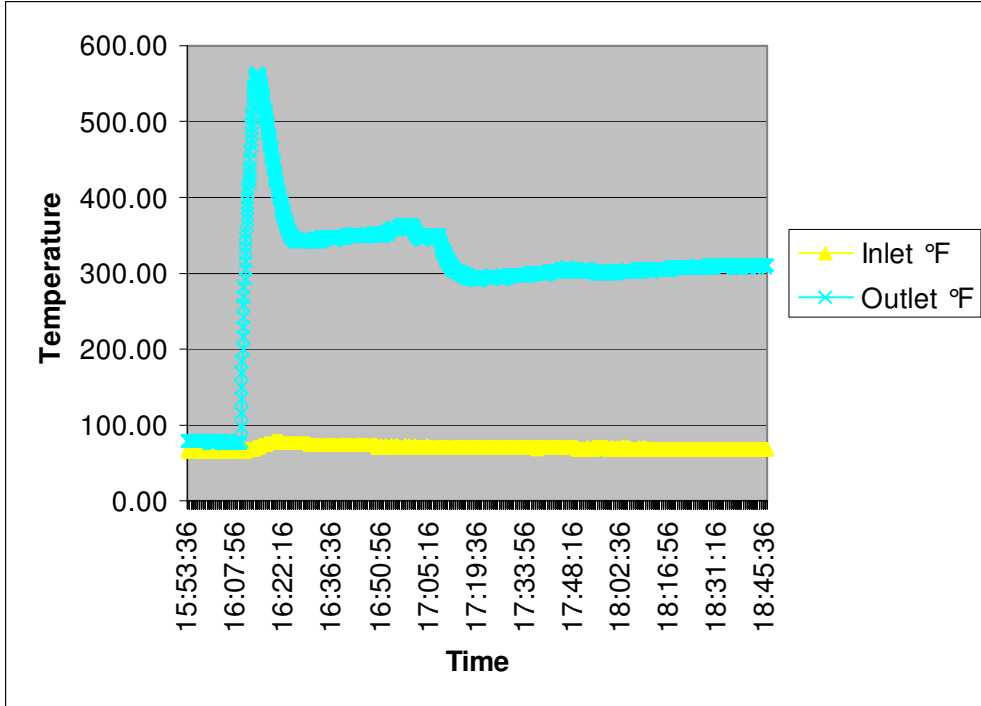
Figure 37 Response of inlet and outlet air temperatures to introducton of air flow to the spoon at 16:09.

Figure 38 Response of Thermonetics HFT to introduction of air flow to the spoon at 16:09. The HFT was saturated from 16:09 through 17:28.

The Materials Testing Spoon was used again later in the project to characterize the impact of particulate buildup on heat transfer to the air-cooled surface. This experiment is described later in this report.

Gardon Gage Radiometry

In order to increase our understanding of the convective and radiative heat sources and sinks at the site for the in-plant test, we measured radiant heat flux using a water cooled Gardon gage radiometer (Vatell Corp. Thermogage Circular Foil Heat Flux Gage Model No. 1000-34). The radiometer is constructed such that it generates a signal from a sensor that is proportional to radiant heat flux received. It measures this heat flux over a cone with a 62° total included angle. The emissivity on the sensor surface is 0.94 and is shielded from convection by a thin sapphire window. The temperature of the sensor is effectively the water temperature. Assuming gray body behavior, the effective temperature of the source of the radiation can be estimated via the Stefan-Boltzman equation. As a result of the procedure for calibrating the radiometer, the view factor would be 1.0.

Using a relatively high emissivity, typical of ceramic or corroded surfaces, of 0.7 and a view factor of 1.0 the effective temperature of the surroundings in the direction noted was calculated, see Table 8. This data was taken at the in-plant test location, viz. the bottom of the right, down tank, downcomer. In addition to the effective temperature the effect of position in the flue was explored. This was limited by the length of the heat flux probe. Additionally, the Gardon gage was checked by measuring a heated metal plate both before and after the in plant measurements to assure the sensor was operating properly.

It must be noted that the data in Table 8, and for that matter all the data in this report, has been collected at certain operating conditions. These are subject to change without compromising the operation of the process. The effective radiant source temperatures given in Table 8 have to be looked at in concert with spoon and suction pyrometer measurements.

Table 8 Gardon gage radiometer data.

Radiometer facing up

dist. Protruding (in.)	effective temp (F)
24	1300
24	1313
24	1318
36	1352
36	1373

Radiometer facing down

24	1094
24	1107

| 36 | 1169 |
| 36 | 1159 |

Radiometer facing outer wall

dist. Protruding (in.)	effective temp (F)
24	1075
24	1079
36	1106
36	1088

Radiometer facing inner wall

24	1117
24	1105
36	1134
36	1181

As we have mentioned elsewhere, a significant amount of air leaks into the flues on both sides of the furnace both intentionally and by accident thus dropping the exhaust gas temperature from probably in excess of 3000 °F (in the furnace) to nominally 700 °F in the connecting flue between the two downcomers. Based on the spoon and Gardon gage experiments, we hypothesized that a surface placed at the in-plant test site was heated primarily by radiant heat from the furnace at the top of the downcomer, and the surface was convectively *cooled* by the relatively cold room air that made up the majority of the exhaust stream at the bottom of the downcomer. A combined suction pyrometer / spoon experiment was performed to confirm this hypothesis, as described below.

August 2007 Suction Pyrometry/Spoon Experiment

Because of the radiation sources within view it was determined a simple thermocouple suspended in the flow may not give an accurate gas temperature. A thermocouple, simply suspended in a gas, will come into thermal equilibrium with its surroundings. This usually involves radiation and convection. For example, with relatively low flow of cool gas and intense radiation sources within view, an exposed thermocouple can read much higher than the gas temperature. To obtain the gas temperature a thermocouple must be shielded from radiation in a small tube with insulation on the tube's exterior, and the gas drawn at high velocity through the tube and over the thermocouple. To do this, the tube is placed in the gas, the temperature of which is to be determined, and placed under a partial vacuum with an air ejector attached to the other end of the tube outside of the hot environment. The thermocouple is read as a function of gas velocity across the thermocouple junction. When increasing gas velocity (i.e. vacuum) produces no discernable change in temperature, the correct gas temperature has been found. This procedure simply increases the convective heat transfer to a point where it overwhelms the radiation and/or conductive heat transfer.

This was done at the proposed location for the in-plant test using a suction pyrometer normally used for measuring combustion gas temperature in the tank. The results are shown in Figure 39.
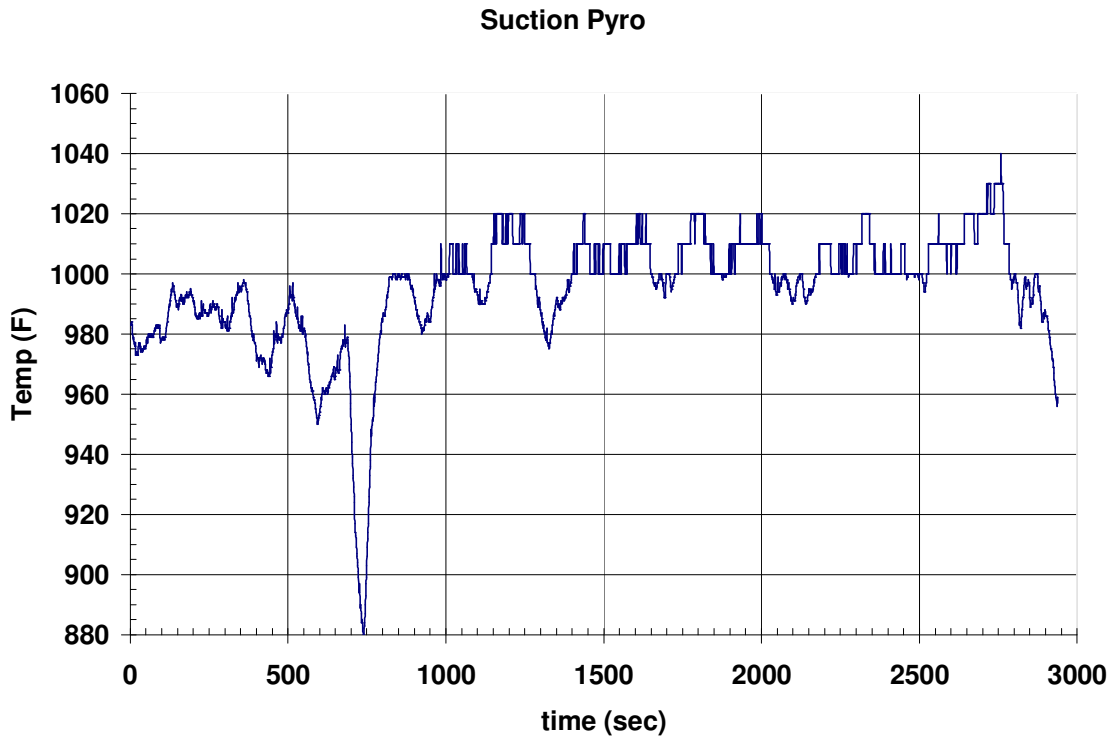
Suction Pyro

Figure 39 Suction pyrometer data at in-plant test site versus time.

The Results of the suction pyrometer measurements indicate the true temperature of the gas stream to be nominally 1000 °F. The effects of mixing of cooler air with the combustion gases at this location are quite evident from the temperature fluctuations in the graph. Just above this location (≈ 6 feet) two opposing rows of brick have periodic openings to atmosphere thus diluting and cooling the combustion gases. In Figure 40, the comparison of the suction pyrometer to a thermocouple simply suspended in the stream (gas stream plot) is shown. Radiation from the upper reaches of the downcomer heats the unshielded suspended thermocouple while this heat is convected away to the cooler air. The equilibrium temperature of the thermocouple is approximately 150 °F higher than the ambient gas temperature.

Manufacturer's data for the TEG indicates it consumes ≈ 4.5 Kw of heat (15,358 btu/hr) at the optimum operating temperature of 1200 °F. The heat pipe module will have to supply this heat at this temperature from the cavity environment. Gardon gage radiometer

measurements (Table 8) indicate the walls and floor of the downcomer are colder than 1200 °F and thus would tend to prevent the heat pipe from reaching 1200 °F under present operating conditions. If the heat pipe were perfectly insulated from these radiation sinks (floor and walls), the view factor to the upper source were close to 1.0, the combined emissivity were 1.0, and the convective losses were eliminated, there would be enough heat due to radiation to supply the TEG through the heat pipe.

Spoon heat flux data on Figure 41 shows that at about 3500 sec into the experiment, the spoon temperature was in excess of 1100 °F but the heat flux to the spoon was less than 1500 btu/(hr ft^2). However, this is without any thermal load applied to the spoon. When cooling air is applied to the spoon (simulating the thermal load of the TEG), it appears that the required heat flux of 3430 btu/hr/ft^2 can be drawn from the flue while incurring a temperature drop of around 300 °F.

For the in-plant test, the overall temperature inside the flue will need to be raised by plugging holes in the downcomer. According to thermal modeling for the heat pipe, if the heat pipe surface is held at 1200 °F, the TEG hot surface will be at roughly 1100°F, the required hot surface temperature for optimal operation. Assuming the spoon and heat pipe have similar heat transfer coefficients, the heat pipe will need to be at a temperature of 1500°F without any thermal load on it. As described above, we can reach 1500°F at the in-plant test site by plugging holes in the downcomer.

Based on these experiments, fins were added to the heat pipe used for the in-plant test, and were designed so that the maximum surface area faces the top of the downcomer, which is the primary radiation source. By plugging holes in the downcomer, we expected to be able to reduce convective cooling, increase the flue wall temperatures, and increase the effectiveness of the radiation source and therefore the temperature of the heat pipe. We expected that it would be possible to operate the TEG at optimal power output provided the heat pipe surface is clean. We also expected that over the course of two weeks, the output would be reduced dramatically by the collection of particulate on the heat pipe surface. We planned to apply an air lance through an existing hole that would have good visibility to the heat pipe to try to clean the heat pipe surface during the test.

Spoon Temperatures
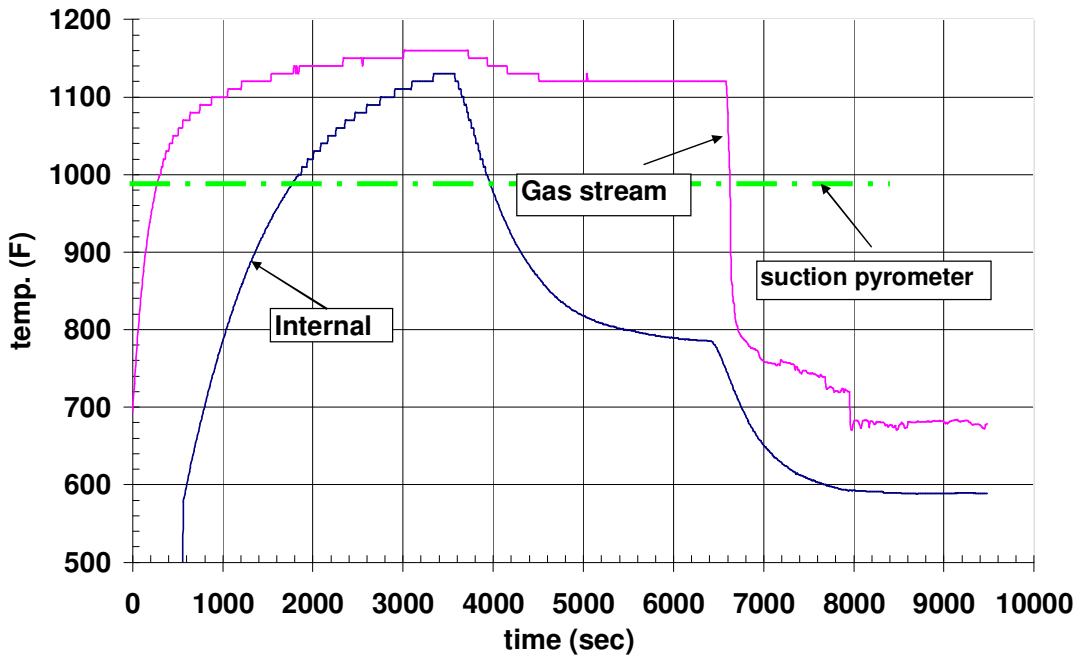
Figure 40 Various temperatures measured on the suction pyrometer and Materials Testing Spoon.

Spoon Heat Flux
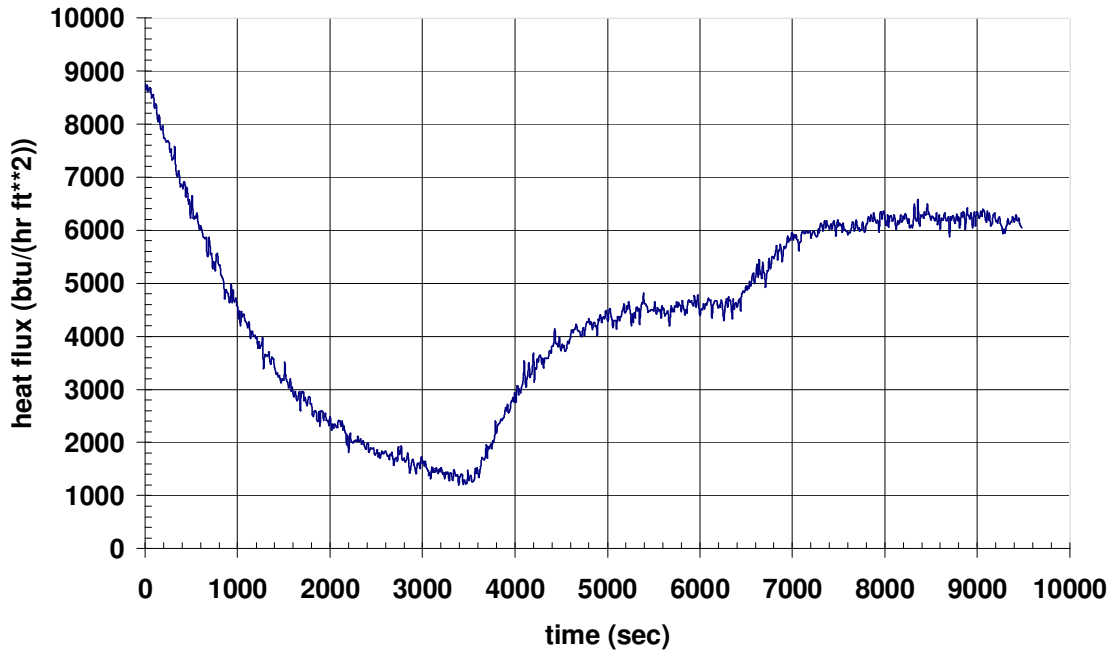
Figure 41 HFT data from the combined suction pyrometer / Materials Testing Spoon experiment.

As stated above, it was most convenient to locate the in-plant test at the bottom of one of the downcomers, given that this area had the best combination of high temperature and ease of access from floor level. Also, given our desire to perform a demonstration at reasonably high temperature (1000°F) and generate a significant amount of electricity (in the hundreds of watts range), we were limited to using the cylindrical TEG geometry provided by (for example) the Global Thermoelectric Model 7120 TEG. Global Thermoelectric has a Model 5120 power unit that incorporates a flat plate TEG, but it was not possible to obtain this TEG in the form needed for the boom or diverter modules. Also, we considered connecting several small flat plate submodules (as made by, for example, Marlow or Hi-Z) together to generate a larger flat plate module, but did not have the resources to design and build such a module, nor was it clear that the heat flux available at the downcomer bottom was sufficient to power such a module without some heat flux concentration. Given that we were constrained to use a commercially available TEG designed only to withstand high temperatures at the inner cylindrical surface, it seemed preferable to operate the TEG outside the flue environment and bring the waste heat to the inner cylindrical surface. Operating the TEG outside the flue environment also made TEG cooling much more efficient and provided convenient access to the TEG should it require maintenance.

Given these design constraints, we chose to attach the TEG to one end of a large sodium heat pipe that would be inserted in the flue to capture heat and transfer it to the inner cylindrical surface of the TEG. As mentioned earlier, a heat pipe is a sealed, evacuated tube containing a small amount of working fluid, in this case sodium metal, and a wick. As applied in our in-plant test, liquid sodium is evaporated by the waste heat applied to one end of the heat pipe (the end inserted in the exhaust gas flue), and condenses back to a liquid at the point where the heat pipe contacts the inner cylinder of the TEG, giving up its latent heat to the TEG where it is used to generate electricity. After condensing, the liquid sodium rapidly flows back down the heat pipe under gravity and the capillary forces produced by the wick, where it evaporates again, thereby restarting the heat transfer cycle.

A schematic of the in-plant test, looking down from the top of the downcomer, is shown in Figure 42. The heat pipe is seen to extend across the entire dimension of the downcomer cross-section, and has "heat transfer fins" attached to it to increase the surface area available to collect radiant heat from above. The fins are made of nickel to maximize thermal conductance to the heat pipe surface. The heat pipe itself is made of Inconel 601, to ensure that the heat pipe would be as durable as possible during the in-plant test. There was concern that using a less expensive material such as stainless steel could lead to the heat pipe sagging over time in the high-temperature flue environment. The surfaces of the heat pipe and fins facing the radiant source were painted with a high-emissivity paint[33] to enhance radiant heat transfer. The cylindrical TEG (Global Thermoelectric Model 7120) is fitted over the end of the heat pipe outside of the exhaust

flue. The fit is accomplished by tapering the inner cylindrical surface of the TEG with a complementary tapering of the outer surface of the heat pipe.

Cylindrical "Sleeve" TEG(s)

Heat pipe

Heat transfer fins
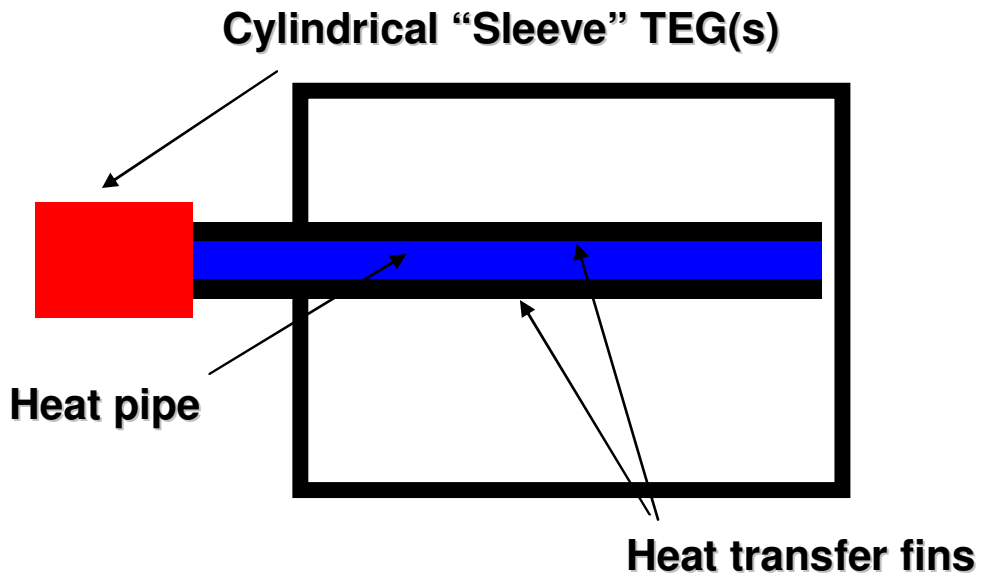
Figure 42 Basic schematic of the in-plant test design, looking down from above.

In addition to the waste heat recovery module itself (consisting of the heat pipe and the TEG), a support frame and trolley were required for the installation and removal of the module from the flue. Also, an electrical panel was required for measuring the electrical power produced by the TEG.

PPG worked with a number of companies to execute the in-plant test. The heat pipe was designed and built by Thermacore (Lancaster, PA). Thermacore, PPG, and Global Thermoelectric worked together on the design and execution of the tapered fit between TEG and heat pipe. After verifying the electrical performance of a Model 7120 TEG, Global machined the taper on the inner cylindrical surface and sent the TEG to Thermacore so that Thermacore could match the taper on the heat pipe to the taper on the TEG. In addition to tapering and TEG electrical testing, Global provided an engineer who was present during start-up of the in-plant test to ensure that the TEG was brought up to operating conditions safely. River Consulting (Pittsburgh, PA) was contracted to design the support frame and trolley, and Carlson Manufacturing (Carnegie, PA) built the support frame and trolley. The electrical panel was designed by PPG, and built by Premier Automation (Monroeville, PA). Local contractors near the Meadville plant were engaged to install the support frame and trolley, the cooling water plumbing for the water jacket used to cool the outside surface of the TEG, and the installation of the electrical panel and connection to the TEG.
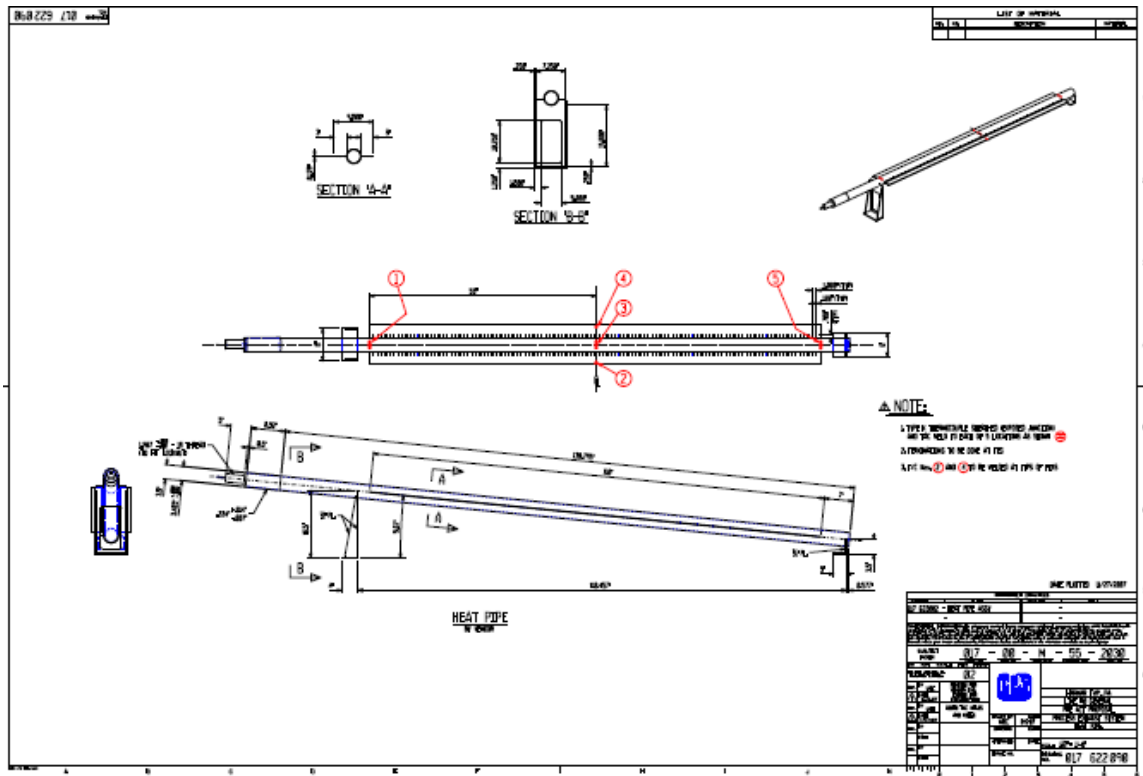
Figure 43 Engineering drawing of heat pipe used for the in-plant test.

An engineering drawing of the heat pipe is shown in Figure 43. The heat pipe was supported on both ends by brackets, and extended across the entire length (roughly 10

feet) of the flue. Thermocouples were attached at 6 locations on the heat pipe surface for diagnostic purposes.
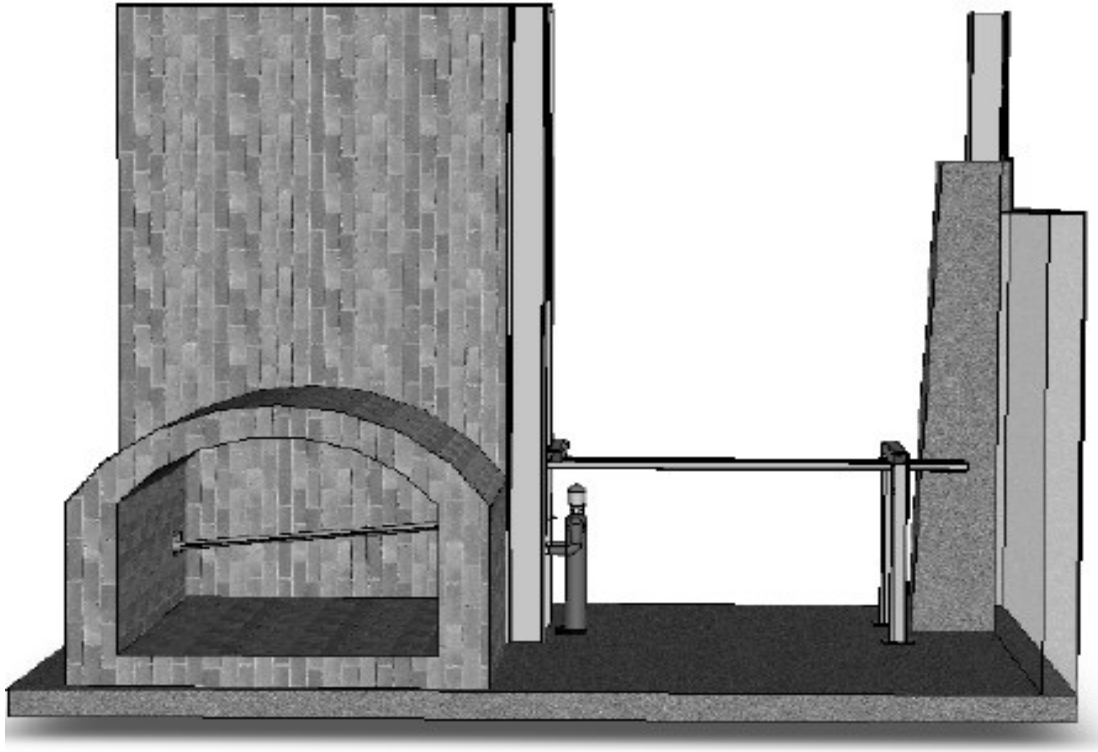
Figure 44 Drawing of in-plant test site. This view is looking downtank (i.e. in the direction of glass motion). The downcomer is shown to the left, with the heat pipe extending at an angle across the downcomer. The external support structure used to support the heat pipe and move it in and out of the flue is shown above and behind the man.

The in-plant test site is shown schematically in Figure 44. Not shown in the Figure is the support that was placed in the middle of the heat pipe during installation in the flue. This support was added due to concerns about thermal stresses on the heat pipe during installation. After heat pipe installation, the support was moved back along the overhead support bar and folded for storage. In Figure 45, a photograph of the support structure is shown after installation of the heat pipe, including the folded support.

Figure 45 Photograph of in-plant test site, showing overhead support bar (blue) and the support used to minimize stress to the heat pipe during installation (folded back, orange) by supporting the heat pipe from below.

Before discussing the results of the in-plant trial in detail, it is worth noting that an important (and unforeseen) delay that we encountered while preparing for the trial was finding a Department of Transportation – approved method to ship the heat pipe from Thermacore to PPG Meadville. It was necessary to build special wooden crates and subject them to DOT approved testing before shipping the heat pipe. The main reason for this was the large size of the heat pipe and the fact that it contained sodium metal. Typical sodium heat pipes sold by Thermacore are smaller in size and can be shipped in 55-gallon drums.

After successfully completing the shipping container testing and certification in mid-January 2008, the heat pipe manufacturer shipped the heat pipe to Works – 8 Meadville, PA. In late January 2008 the heat pipe was delivered to the plant. At that time plans were implemented to install the heat pipe and TEG.

On February 4, 2008 we (PPG team and plant personnel, engineer from Global Thermoelectric, and workers from the piping, electrical, and mechanical contractors) completed the final installation of the support frame, heat pipe mounting, electrical and cooling water connections. At that time we slowly (to avoid thermal shock and to let the TEG output settle out) inserted the heat pipe into the bottom of the downstream right furnace flue.

Upon installation, we began to see TEG open circuit voltage climb steadily. We blocked holes in the flue in order to raise the temperature around the heat pipe to see if we could achieve maximum TEG output. We achieved 301W of output (23.9 Amps at 12.6V) with

open circuit voltage above 28V. This constitutes the maximum output achievable for this TEG model.

After achieving maximum output, we opened holes in the flue to return the power output level to a more sustainable level (the TEG lifetime would be shortened if operated constantly at 300W). We reduced the power to 264W and set up the data acquisition system to monitor TEG output. TEG output, as well as temperature data from the thermocouples attached to the heat pipe and cooling water temperature data, were recorded until the waste heat recovery module was removed from the exhaust flue on 8 May, 2008 (see Figure 46).
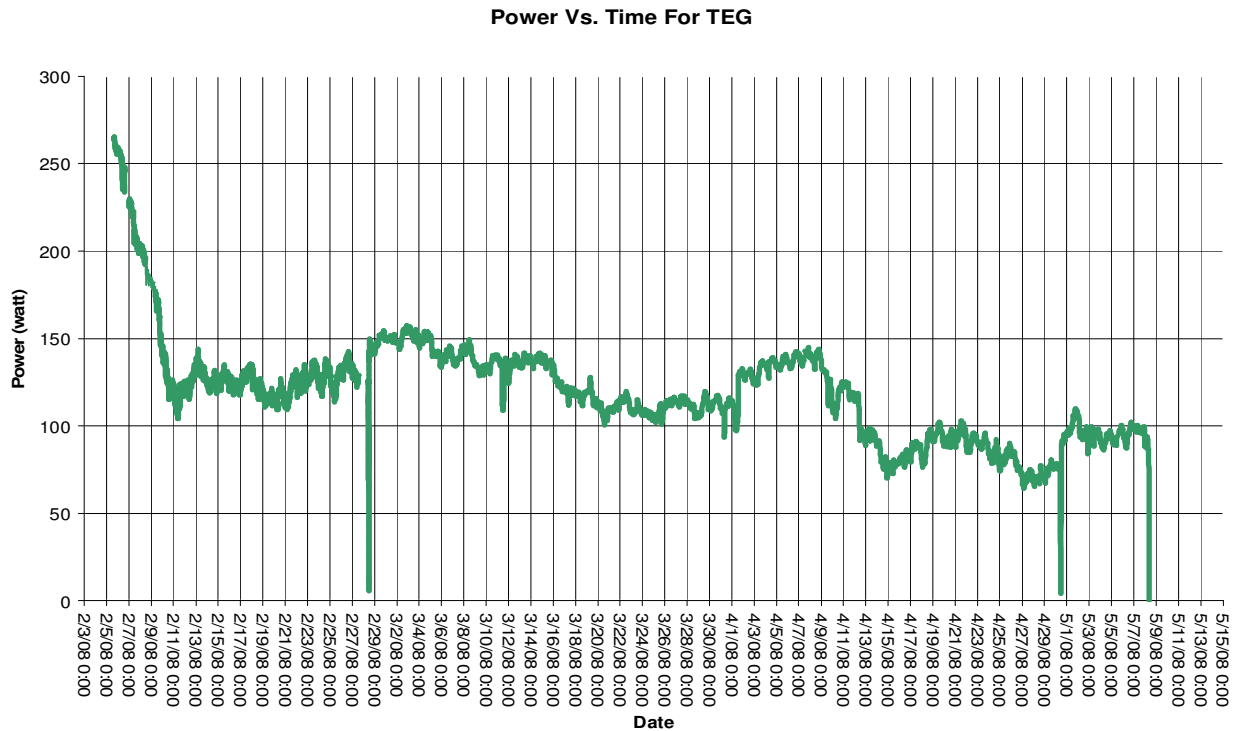
Figure 46 Electrical power output of TEG versus time during the in-plant trial.
A rapid and large drop in power was observed over the first week of the plant trial. We believe this was due to change in the thermal contact between the heat pipe and the TEG, or due to an internal degradation in heat pipe performance. This is evidenced by Figure 47, which shows the TEG power output decline correlating with a decline in cooling water temperature change, which in turn correlates with the amount of heat flowing through the TEG to the cooling water. However, the heat pipe temperatures, while apparently declining slightly during the steep drop in power output, recover to their initial values soon after, while the TEG power does not recover. Also, the temperature of the heat pipe surface near the TEG was 1233°F on 5 February (when the power output was still high), whereas on 28 February that temperature was 1291°F. Thus it appears that while the surface temperatures of the heat pipe did not change substantially, the amount of heat transferred to the TEG dropped by a large amount. This points to either a thermal contact problem between heat pipe and TEG or to a problem internal to the TEG.

The TEG was connected to the heat pipe with a shallow tapered fit (0.04" diametrical change in the 3.5" nominal diameter over 5.5"). To allow for ease of assembly and later disassembly the taper was coated, both surfaces, with boron nitride lubricant. Upon examining the cylindrical cavity which forms the hot face of the TEG after disassembly it was noticed only half the length of the taper had intimate thermal contact but there was no sign of degradation of the lubricant or corrosion of the metal. From this it appears the tapers were not perfectly matched; however, there is no obvious signs of degradation that would explain the power loss in the first week of operation. Another explanation is that somehow the thermal resistance of the TEG changed, possibly a thermal induced separation of materials inside. To further check on this possibility, the TEG was shipped back to the manufacturer (Global Thermoelectric) for evaluation. However, Global's testing indicated that the TEG was performing within factory specifications.
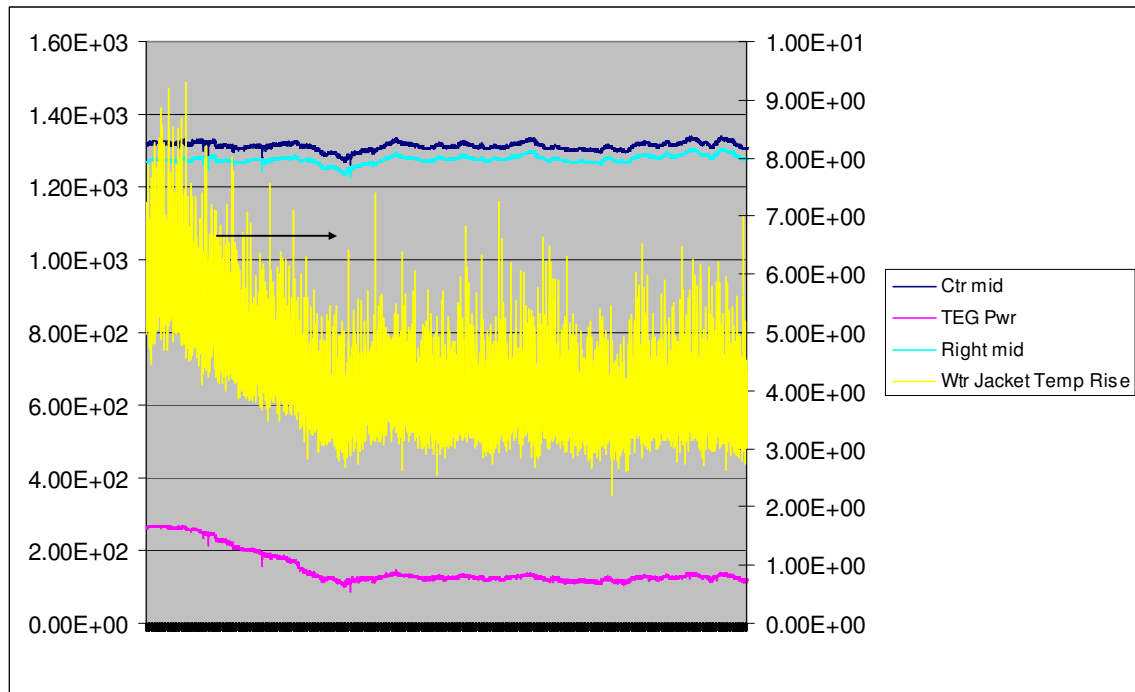
Figure 47 Behavior of a number of different parameters during the initial fast drop in power during the in-plant trial.

Also, particulate was cleaned off the heat pipe using a high-pressure air lance on two occasions, 28 February and 1 April. After these cleaning events, the electrical power output increased from roughly 110-120W back to 140-150W. The time required for the power output to degrade after the 28 February clean was roughly 3 weeks, which is somewhat longer than, but comparable to, the time of 2 weeks required for heat transfer degradation to stop in the spoon experiments (see discussion below under "Characterization of Emission and Impact on Heat Transfer"). After the 4/30 clean it did

not recover to the same level as after the 2/28 clean and the 4/1 clean. It is possible that additional buildup occurred during the interval between 4/1 and 4/30 that was not removable with air lance cleaning.

On Thursday, May the 8th, the heat pipe, along with the thermoelectric generator (TEG), was removed from the flue on line 1 Meadville. Before removal a final set of operating data was retrieved. Plant personnel opened up the right side wall exposing a thick layer of molten sodium sulfate fusing the heat pipe to the wall. Two jack hammers were used to cut the molten sodium sulfate from the heat pipe. Because the sodium sulfate had built up so deep under the heat pipe it could not be removed once it was freed from the wall. The build up also prevented the insertion of the mid-span bottom support of the transport frame. Because of the Inconel construction of the heat pipe and the drop in temperature from opening up the flue it was decided that the heat pipe could be safely elevated by lengthening the two turnbuckles in the transport frame. This effectively made the heat pipe into a cantilever which once risen was easily pulled back out of the flue, clearing the deposits. During this time the water cooling was maintained to the TEG and was left on until the heat pipe was cool enough to touch. All the water and electrical connections were then disconnected. The TEG/heat pipe assembly was then unfastened from the transport frame and manually moved to rest on the shipping container.

It was then decided to remove the TEG from the heat pipe in order to preserve the original approved shipping configuration of the heat pipe. The TEG was coupled to the heat pipe along a tapered fit. The taper was sprayed on both surfaces with boron nitride to prevent galling. Because of the construction of the TEG it could easily be damaged if pounding with a hammer was used to remove it thus it was decided to use a gear/bearing puller for removal. This was successful and the heat pipe was placed in the shipping container and shipped to GTC.

Economic Analysis After In-Plant Trial

Based on the amount of space required by the heat pipe used in the in-plant trial, and the area of the flue we were able to block before impacting the glass production process (see "Flue Damper Experiment" described earlier under "Glass Furnace Exhaust Flue Characterization Experiments"), we believe that a practical system would use 24 heat pipes per furnace (6 per downcomer). Assuming that each heat pipe could transfer up to 15kW of heat (based on input from Thermacore), each heat pipe could in principle support 3 TEG's (requiring 5kW each to produce 250W each). This system design was assumed for the economic analysis described below.

For a 24 heat pipe system, with 3 TEG's per heat pipe producing 250W each, a total of 18kW could be produced. This leads to a yearly energy production of 156,000 kWhr per year. Assuming 5 cents per kWhr as a typical industrial electricity charge, the yearly savings for the system would be $7800.

The estimated cost for a 72 TEG system on 24 heat pipes (including installation) is $970,000. Hence the payback time for this system would be 124 years, much longer than industry can support.

The cost breakdown of the $970,000 is as follows:

35% Heat Pipe
22% TEG with water Jacket
17% Support Frame, Electrical & Piping materials
11% Installation
6% Engineering
9% Contingency

This cost breakdown assumes that stainless steel heat pipes can be used. In our in-plant trial, we used an Inconel heat pipe due to concerns about stainless steel sagging when continuously exposed to the 1200°F flue conditions.

Clearly, the major cost elements of the system are heat pipes and TEGs. Even if TEG efficiency could be increased from 5% to 100%, the payback time would still be over 6 years, which is still quite long from an industry point of view. The first point of attack for improving the economics of the module would be to find a means to capture the heat that is significantly less expensive than a heat pipe.

Obviously, the economics calculated here do not show the promise of the original economics. This is due to a number of factors, including the high cost of TEGs and the high cost to capture the heat (represented by the heat pipes). Also, a much lower fraction of heat (2% versus 50% assumed earlier) is captured by the system, which limits its utility.

Characterization of Emission and Impact on Heat Transfer

A number of experiments were performed in the oxyfuel furnace combustion gas exhaust flue to understand the impact of condensates in the gas stream on heat transfer to surfaces placed in the stream. These experiments included three different spoon experiments in which water- or air-cooled spoons were placed in the flue for a period of time to characterize temperature, heat flux, and/or condensate collection rate. Each experiment is discussed in some detail below.

Water Cooled Block Spoon

In the first spoon experiment, a water-cooled carbon steel block was placed in the flue at the in-plant test site. None of the holes in the downcomer walls were blocked, and a

thermocouple placed in the gas stream measured 800°F during the testing. The block surface temperature was 200°F. The block was held in the flue for 3 1-day exposures. After each 1-day exposure, the white powder that collected on the surface was carefully brushed into a bag and weighed to determine a mass deposition rate. Finally, a 3-day exposure was performed. A deposition rate of 25 mg/day/in2 was measured. The powder composition was characterized via x-ray fluorescence (XRF) and found to be primarily sodium sulfate.

Gradient Spoon

The second spoon experiment was a "gradient spoon" experiment. The gradient spoon geometry is shown in Figure 48.
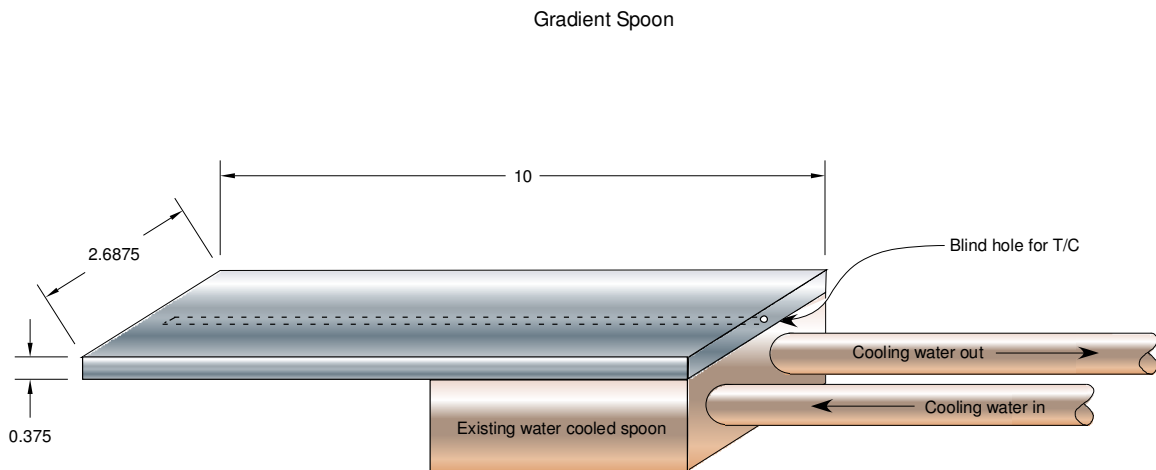
Gradient Spoon

Figure 48 Gradient spoon.

As shown in the drawing, the spoon consists of a water-cooled block with a 10" long steel plate welded to it. The plate has a blind hole drilled into it. A long rod with a thermocouple at the end of it fits snugly into the hole, and can be moved so that the temperature at various points on the plate can be measured. When the gradient spoon is inserted into the flue, a range of temperatures is realized on the steel plate. A sample temperature profile is shown in Figure 49.
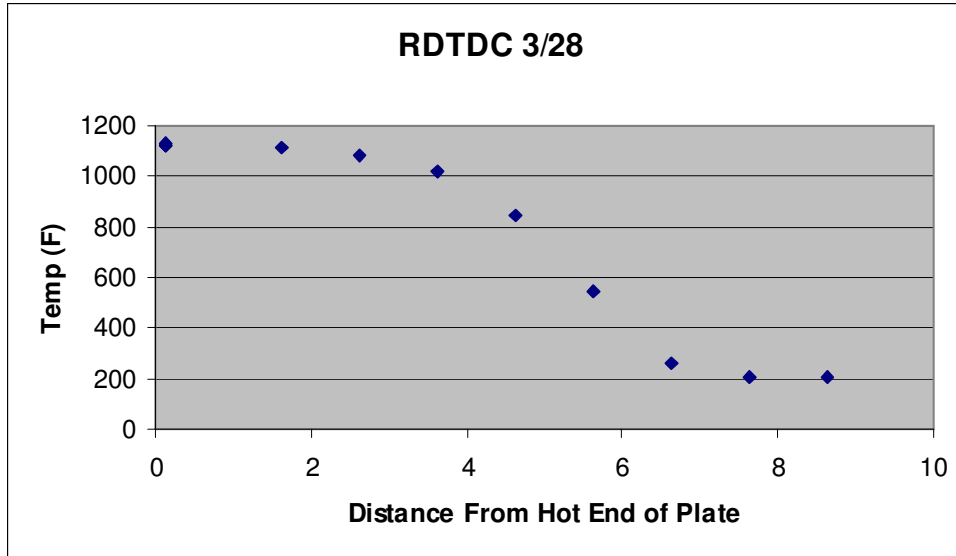
Figure 49 Temperature variation of gradient spoon across plate.

The block edge is 6 inches from the hot end of the plate. Thus for distances significantly greater than 6 inches, we expect the temperature to be roughly constant and low due to the effect of the cooled block. Close to the hot end of the plate, the cooling effect of the block is minimal, leading to a roughly constant and high temperature at that end. In the intermediate region between the hot and cold ends, heat is flowing via conduction at a rate governed by

$$\mathrm{d}Q/\mathrm{d}t = k\,A\,\mathrm{d}T/\mathrm{d}x$$

where $\mathrm{d}Q/\mathrm{d}t$ is the rate of heat flow in Watts, k is the thermal conductivity in Watts/cm/K, A is the cross sectional area of the plate in cm^2, and $\mathrm{d}T/\mathrm{d}x$ is the temperature gradient in K/cm. Given the temperature profile data and the known cross-sectional area of the plate, and observing that k for steel is fairly constant over the 250°F – 1000°F range, it is possible to estimate the heat flow across the plate. For the profile shown above, we calculated heat transfer across the plate of 650-1300W and heat flux of 100-200W/cm2, for thermal conductivity in the range 2-4 W/cm/K. This heat transfer across the plate is related to the heat transfer from the flue environment to the plate. In addition, the gradient spoon defines a range of temperatures that is available at a given position in the flue. Finally, the gradient spoon provides the ability to study how much condensate would accumulate on a surface at a range of different temperatures at a specific location in the flue.

The gradient spoon was used to characterize the Meadville flue at 3 different locations, all on the right side of the flue: the bottom of the uptank downcomer, the bottom of the downtank downcomer, and 10 feet above the bottom of the downtank downcomer. In the furnace diagram shown in Figure 50, the right uptank downcomer is labeled "RUTDC", and the right downtank downcomer is labeled "RDTDC".
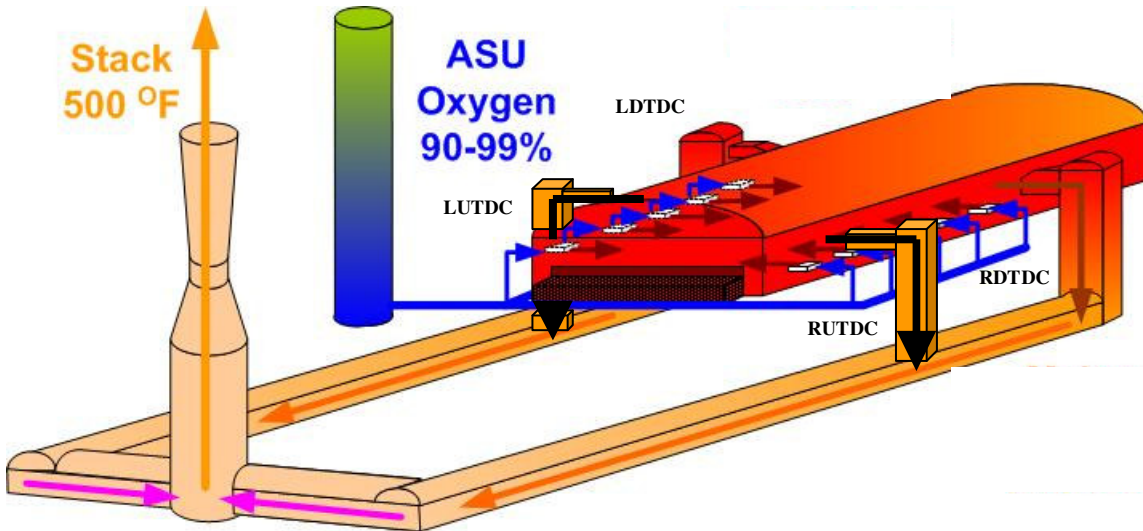
Figure 50 Oxyfuel melter diagram showing right uptank downcomer (RUTDC) and right downtank downcomer (RDTDC).

Table 9 summarizes the results of these experiments.

Table 9 Data collected in first gradient spoon experiments.

Flue Location	Plate Orientation	Plate Hot End Temp	Plate Cold End Temp	Plate Heat Conduction	Total Heat Transfer	Particulate
RUTDC Bottom	Horizontal	1030°F	190°F	600-1200W	900W	Collect below 600°F (4.8" from hot end)
RDTDC Bottom	Horizontal	1100	200	700-1400	1000	Collect below 700°F (4.8-5" from hot end)
RDTDC Bottom	Vertical	1070	200	700-1400		
RDTDC 10 ft up	Vertical	1620	730	350-700	4000	

In the table, Plate Orientation refers to whether the plane of the plate is horizontal or vertical. The Plate Hot (Cold) End Temp is the temperature of the plate at the hot (cold) end. These data show good agreement between temperatures at the bottoms of the two downcomers, and as expected much higher temperatures are seen 10 feet up the RDTDC. Plate Heat Conduction is the calculated amount of heat conducted through the plate using the calculation method described above and considering thermal conductivity values

between 2 and 4 W/cm/K. Again, the data are comparable at the bottom of the two downcomers. The Plate Heat Conduction 10 feet up the RDTDC is surprisingly lower than that at the bottom of the two downcomers. This could be due to a combination of factors. First, some insulation of the cooling water pipes was lost while inserting the spoon into the (narrow) slot in the downcomer, so the cooling water may have warmed significantly before entering the spoon. Second, the heat flux at that point in the downcomer is quite high, and may overwhelm the cooling power of the spoon. Upon removing the spoon from this section of the downcomer, the hottest 5 inches of the spoon were glowing red-hot, indicative of the high temperatures and heat transfer occurring in that section. Total Heat Transfer was computed by measuring the surface temperature of the cooling water in and out pipes, and using the measured water flow rate and properties of water to compute the amount of heat added to the water stream by the flue. Specifically, the formula

$$\frac{dQ}{dt} = C\rho \frac{dV}{dt} \Delta T$$

was used, where dQ/dt is the heat transferred to the water; C is the heat capacity of water; ρ the density of water; dV/dt the volume flow rate of water; and ΔT the temperature difference measured between the two pipes. This calculation overestimates the amount of heat actually transferred to the spoon, since it includes heat transferred to the cooling water pipes as they conduct the cooling water to and from the spoon. The total heat transfer numbers are fairly consistent between RUTDC and RDTDC, and a much higher heat transfer is seen 10 feet up in the RDTDC, consistent with the higher temperatures at that location. Finally, it was noted that particulate did not collect on the hottest 5 inches of the gradient spoon when placed at the bottom of the 2 downcomers, even after 16 hours of exposure. The hottest 5 inches of the spoon had temperatures above 600F or 700F for the RUTDC and RDTDC, respectively.

Additional gradient spoon experiments were performed at Meadville. An estimate of the impact of insulating the water cooling pipes to the spoon was made. Temperature profiles and particulate collection were studied for short (1/2-1 hour) exposures at three different flue locations to verify the initial results discussed above.

To estimate the impact of insulating the water cooling pipes to the spoon, the spoon was inserted into the bottom of the right down tank downcomer without any insulation over the cooling pipes. The temperatures of the inlet and outlet cooling pipes were measured. Using the formula

$$\frac{dQ}{dt} = C\rho \frac{dV}{dt} \Delta T$$

we found that the non-insulated cooling pipes plus spoon absorbed roughly 2500W from the exhaust stream. After applying a new layer of insulation to the pipes, the device absorbed 600W from the exhaust stream. Given that the spoon length is roughly 1/5 of the total length inserted into the flue, and the other 4/5 is the cooling pipes, and assuming

that the insulation eliminated heat transfer to the cooling pipes, this ratio can be roughly explained based on the ratio of areas exposed to the exhaust stream. Also, given that the cooled water block on the spoon had a temperature of 200°F, and the temperature of the pipe outside the flue was 100°F, we estimate that the average temperature in the cooling water pipes is around 150°F. Given the dimensions of the tubes, and knowing the gas temperature in this region to be around 1000°F, we can estimate a heat transfer coefficient in this region without insulation, and find h ~ 60 W/m^2/K. However, it is clear that it is important to minimize the length of exposed cooling water pipe to minimize the amount of stray heat transferred to the cooling water, and that insulation can dramatically improve this situation. These observations would be most relevant for a boom-type design.

The following results were obtained in the second round of gradient spoon experiments.

Table 10 Results of second round of gradient spoon experiments.

Flue Location	Plate Orientation	Plate Hot End Temp	Plate Cold End Temp	Total Heat Transfer	Particulate
RDTDC Bottom	Horizontal	1130	200	600W	Collect below 700°F (4.8-5" from hot end)
RDTDC 10 ft up	Vertical	1680	300	3000	Collect below 650°F (5.5-6" from hot end)
Right Connecting Flue	Horizontal	770	150	300	Collect below 400°F (5" from hot end); collect differently above 400F?

The hot end temperatures obtained are quite similar for the two data sets. However, the cold end temperature is significantly lower for RDTDC 10ft up, and the total heat transfer is reduced for both RDTDC bottom and RDTDC 10 ft up. We believe this is due to much better insulation on the cooling water pipes during this quarter's experiments. Also, while the emissions collected between 5" from the hot end and 10" from the hot

end were the same, easily removed white powder for each location, the surface between the hot end and 5" from the hot end was different at the three locations. For RDTDC 10 ft up, the surface was roughened and slightly charred, and indeed was glowing red hot upon removal from the flue. For RDTDC bottom, the surface was clean and undamaged. For right connecting flue, the surface seemed to have a thin, difficult-to-remove white film on it. Fortunately, the right connecting flue area is not under consideration for the current in-plant test, but if different TEGs involving lower temperature materials are used, the character of deposition there will become more important. Some pictures of the spoon are shown below.

Figure 51 Gradient spoon after removal from right connecting flue before cleaning with brush and scraping region between hot end and 6" from hot end.
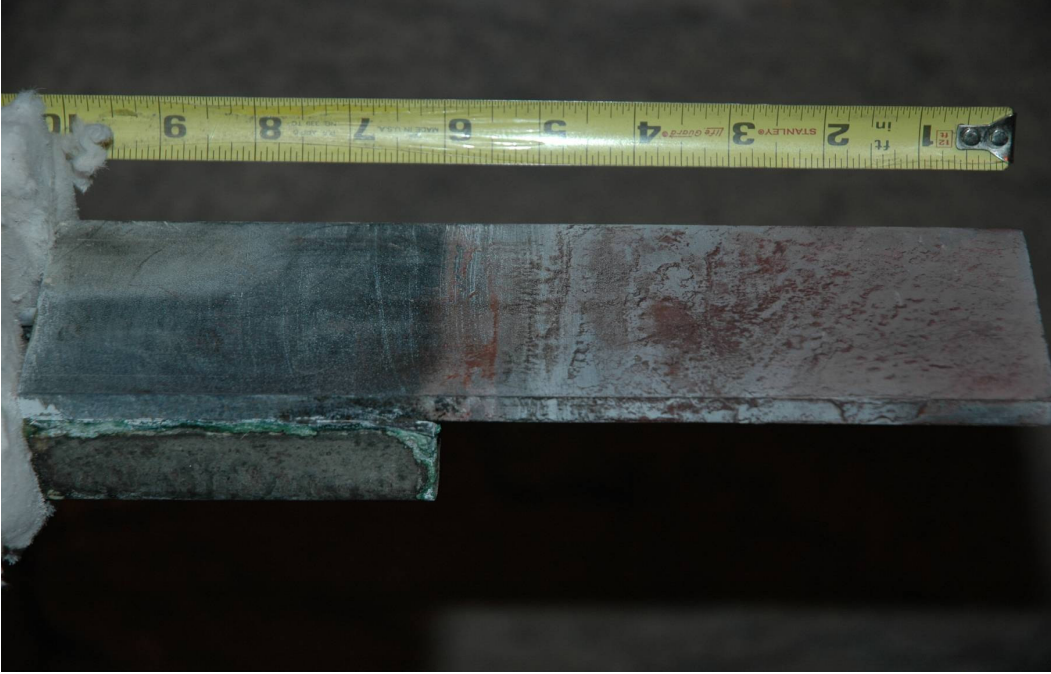
Figure 52 Gradient spoon after removal from right connecting flue and after cleaning with brush and scraping region between hot end and 6" from hot end.

Figure 53 Gradient spoon just after removal from RDTDC 10 feet up.
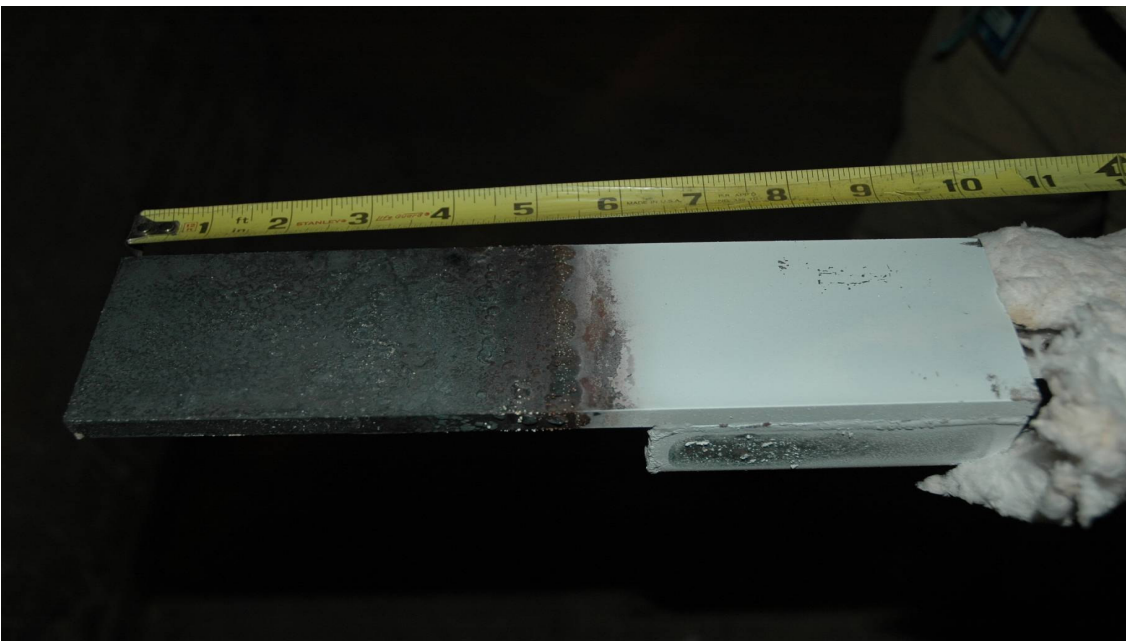
Figure 54 Gradient spoon removed from RDTDC 10 feet up, after cooling.

For all locations measured, an easily removable white powder collects over the area of the spoon covered by the water cooling block (6" and greater from hot end). In the downcomer (bottom and 10 ft up), locations above 650-700°F again seem to have no

particulate collected. In the connecting flue, locations above 400°F seem to have a more tenacious film deposited on them that is difficult to remove.

Materials Testing Spoon

In Run 1 of the Materials Testing Spoon (Run 0 was described above as part of the In-Plant Test report), a HFT obtained from ITI[34] was cemented to the top surface of the spoon and placed in the exhaust stream at around 1100°F gas temperature, 850°F spoon top surface temperature, for twelve days. The HFT survived this exposure, and a reduction in thermal conductance from the gas to the spoon surface was observed over this time. At the end of the twelve day test, white powder particulate was cleaned off the top surface and collected, and the thermal conductance measured to return to its original value after removal of the white powder. The experiment is explained in detail below.

Run 1: The major change from Run 0 to Run 1 was to switch from the Thermonetics HFT to the ITI Model HT-50 HFT. The ITI HFT is encased in stainless steel, and was therefore hoped to be more robust than the Thermonetics. Also, the ITI HFT has a K-type thermocouple integrated into it, which gives a direct measure of temperature at the surface of the spoon, in addition to the measurement of the spoon internal temperature (Tint). In addition, we dropped the measurement of heat transferred to the cooling air, and removed the insulation from the cooling air pipes.

The ITI Model HT-50 HFT is a ¾" diameter and 1/8" high Gardon gauge-type transducer inside a stainless steel case, welded to a 1" diameter stainless steel flange. The wiring as received from ITI was long enough to extend out of the flue and to the data acquisition board. The ITI HFT was cemented to the top surface of the spoon using Sauereisen Aluseal Adhesive Cement #2. After drying overnight, the cement was further dried at 140°F for 6.5 hours. The HFT calibration constant did not depend on temperature, and was 18.59 BTU/hr/ft^2/µV, significantly (70 times) less sensitive than the Thermonetics HFT.

The configuration of the spoon as used in this experiment was shown in Figure 33 and Figure 34 above. Kaowool was again used to insulate all surfaces of the spoon except for the top surface, so that the heat flux measured by the spoon would be primarily through the top surface and would be absorbed by the cooling air impinging on the top surface. Again, insulation was not applied over the inlet and outlet air pipes in this experiment.

The objectives of this run were:
1. Compare performance of ITI HFT versus Thermonetics. However, temperature would not be elevated by plugging downcomer holes in this experiment, in order to increase the chances of the HFT surviving the entire experiment.
2. Measure heat flux and compare to heat flux required for heat pipe module.
3. Demonstrate impact of condensate on heat transfer, and quantify.

The ITI HFT remained firmly fixed to the spoon throughout Run 1. Also, the integrity of all wires was good throughout the run. Part of this was due to the more robust design of the ITI HFT, but part was also due to maintaining normal flue conditions and not plugging holes. While this does not exactly simulate the conditions desired for the in-plant demonstration, it was shown to be possible to introduce a 300°F temperature gradient between the gas stream and internal thermocouples (using 3.3scfm of air), and the heat transfer properties are not expected to change greatly between the gas stream temperature used in this experiment (around 1130°F) and that expected for the in-plant demonstration (1472°F).

As described in more detail below, heat fluxes measured with the clean (i.e. without particulate on the surface) ITI HFT were on average 3700 BTU/hr/ft^2, with gas stream temperature around 1110°F, internal spoon temperature 850°F, and HFT thermocouple temperature 870°F. The temperature difference here between gas stream and spoon is 260°F. For similar temperature difference with the Thermonetics HFT, heat flux of 4257 BTU/hr/ft^2 was measured ("plug 13 0" experiment). However, given uncertainties in the Thermonetics HFT contact to the spoon at that point, it is suspect at best to compare numbers between the two HFTs. If we assume the Thermonetics was still in good contact during the "plug 19" experiment, and reduce that heat flux proportionately for a 260°F temperature difference rather than the measured 308°F, we find 7700 BTU/hr/ft^2 from the Thermonetics HFT. Assuming the 7700 BTU/hr/ft^2 number is closer to the real value for the Thermonetics, there is a large discrepancy between the ITI and Thermonetics measurements. This discrepancy could be attributed to differences in furnace conditions, but we do not know of any significant differences in furnace conditions between Run 0 and Run 1. It could be attributed to differences in spoon geometry for the two experiments. However, the only major difference is the use of insulation on the air pipes for Run 0 versus no insulation on the air pipes for Run 1, and this seems unlikely to have a major impact on the heat flux to the HFT. Another possibility is a difference in radiant heat transfer to the two HFTs, given that the ITI HFT is made of stainless steel and so is expected to have a lower emissivity than the Thermonetics HFT, which has a glass frit coating. This difference in HFT emissivity seems like the most reasonable explanation, especially given the high intensity of red (and certainly infrared) light from the furnace that will be seen by a HFT at the bottom of the downcomer.

Since the HFT was the only calibrated sensor available for measuring absolute heat flux, we used data taken from the HFT to quantify heat flux available for the in-plant test (objective 2). Three separate measurements were done with the spoon in a clean or nearly-clean state (i.e. no particulate collected). The result from these measurements was 3.7 +/- 0.3 kBTU/hr/ft^2, well in excess of the 1966 BTU/hr/ft^2 computed requirement for the in-plant test. These measurements were taken while measuring thermal conductance to the spoon, as described below.

The spoon was left in the downcomer for twelve days to collect particulate and to monitor changes in heat flux over an extended exposure. The readings from the heat flux transducer showed a surprising amount of variation, and discontinuous jumps when data

collection was stopped and restarted in one day increments. An example of this behavior is shown in Figure 55. The jumps are almost certainly related to the interaction of the data acquisition electronics and the HFT, and the large drifts may be as well. The data used to calculate the heat flux above (3.7 kBTU/hr/ft^2) were taken during thermal conductance measurement experiments. These required only short data collection times (few hours) during which the HFT behavior was continuously monitored, and during which air flow to the spoon was varied and the same air flow value repeated at the beginning and end of the run to ensure that there were no significant drifts in the HFT reading.
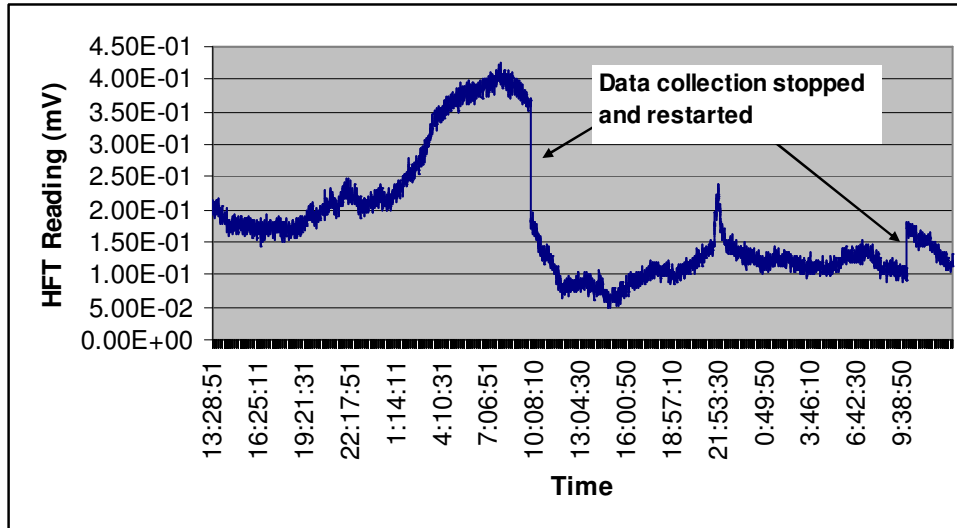
Figure 55 Jumps in HFT reading upon stopping and restarting data collection. Also shown are large, slower changes in HFT reading that did not correlate with other sensor readings.

However, because of our incomplete understanding of HFT data, we used two other methods to characterize changes in heat flux during exposure. One was to monitor the difference between the HFT thermocouple temperature and the internal spoon temperature. Because these two thermocouples are located in the path heat would take from the spoon surface to the air cooling stream, the difference in temperature between them should be proportional to the heat flux through the surface. The second method was to measure thermal conductance from the furnace environment to the spoon. This was done by varying the air flow to the spoon from 0scfm to 3.3scfm, and recording HFT voltage, HFT and internal thermocouple readings, and gas stream temperature after equilibrium was achieved at each air flow. Then by plotting HFT heat flux (making use of the known calibration constant) as a function of the difference between HFT temperature at zero flow and HFT temperature at given flow, the slope of the resulting line gave the thermal conductance. This method is based on the relationship

$$\frac{dQ}{dt} = hA(\Delta T)$$

and taking the thermal conductance to be *hA*.

THE

Alternatively, one could plot the difference between HFT temperature and internal temperature as a function of the difference between HFT temperatures at zero and given flow, since the difference between HFT temperature and Internal temperature should be proportional to heat flux through the spoon. It was assumed in these measurements that with zero air flow, the heat flux through the spoon was zero. This assumption was borne out by the very low HFT voltages measured at zero air flow, and the less than 1F temperature difference between HFT temperature and Internal temperature at zero flow. Table 11, Figure 56, and Figure 57 below show an example of the conductance measurement.

Table 11 Data collected for conductance measurements.

Flow (scfm)	Internal T (F)	HFT (mV)	HFT TC (F)	Gas Strm (F)	HFTC-Int (F)	HFT Temp-HFT Temp(0 flow) (F)	Corrected HFT (mV)	Heat flux (Btu/hr/ft2)
3.3	848	0.2016	871	1135	23	-292	0.1786	3573
0	1163	0.0230	1163	1138	1	0	0.0000	0
1.5	1000	0.1397	1013	1137	13	-151	0.1167	2334
3.3	851	0.2265	874	1128	22	-289	0.2035	4070
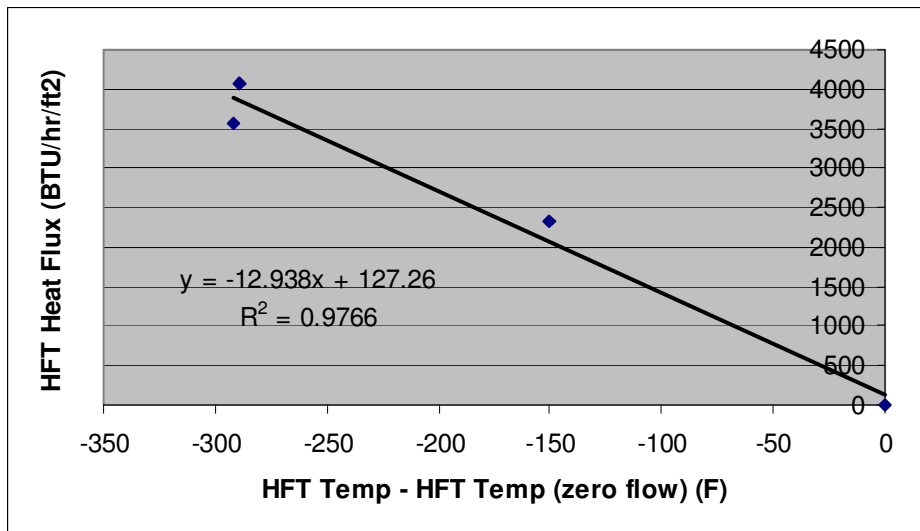
Figure 56 Fit of data for conductance measurement with HFT heat flux.

The chart shows a linear fit with equation $y = -0.0754x + 0.9546$ and $R^2 = 0.9993$.
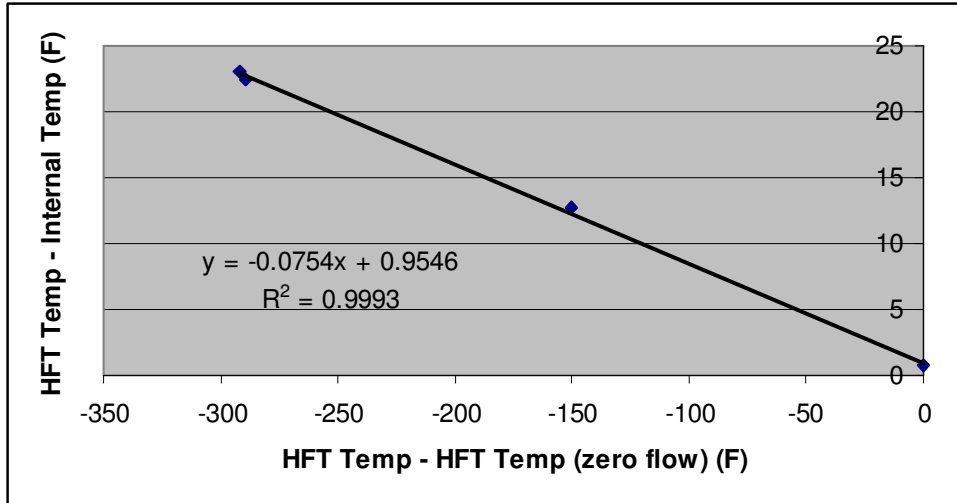
Figure 57 Fit of data for "conductance" measurement using difference between HFT temperature and internal temperature, which is proportional to heat flux.

Given these tools for monitoring the impact of condensate on heat transfer (viz. HFT voltage, thermal conductance, and temperature difference between HFT and Internal), two experiments were done to look at the impact of condensate. In the first experiment, a quantity of white powder that had collected on the floor of the downcomer was scooped up and dumped on a clean spoon. This experiment was done to show quickly whether there was an impact of particulate on heat transfer, and to quantify how much particulate generated that impact. In the second experiment, as already mentioned above, the spoon was left in the exhaust stream for 12 days and the heat flux monitored. At the beginning and end of the 12 day exposure, the thermal conductance was also measured. The spoon was pulled out after the 12 day exposure, and accumulated particulate was removed from the spoon and measured to quantify particulate deposition rate. Finally, the spoon was reinserted after cleaning, and thermal conductance and heat flux measured to verify that any changes in heat transfer were due to the accumulated particulate.

The data obtained from dumping powder on the spoon are shown in Table 12. After dumping powder, the sensor readings were monitored and data recorded only after equilibrium was re-established.

Table 12 Readings on various sensors before and after deliberately dumping a large quantity of powder on the spoon. Changes are also computed.

Condition	Internal T (F)	HFT (mV)	HFT TC (F)	Gas Stream T (F)	HFT TC - Internal T (F)
Before Dump	849	0.187	869	1109	21
After Dump	804	0.131	816	1113	13
Change	-45	-0.056	-53	4	-8

The two measures of heat flux, the HFT reading and the difference between the HFT and Internal spoon temperatures, both declined due to the powder. Also, the HFT and Internal temperatures themselves declined, indicating the powder insulated the spoon

from the heat of the exhaust stream. The powder directly over the HFT was observed to cover about 90% of the HFT area, and formed a layer 1/8" thick, plus or minus 50%. This layer was easily brushed off with a soft paint brush, and collected for measurement. 62mg of powder were collected. This first experiment showed a clear effect of powder on heat transfer. Also, it suggests that 62mg of powder reduces heat transfer by around 30%.

As noted already above, it was difficult to use the long-term HFT readings to monitor changes in heat transfer over the entire 12 day experiment. However, the difference between HFT and Internal spoon temperatures showed a clear decrease over the experiment, indicating reduced heat transfer (see Figure 58). The size of the decrease was roughly 1/3. After removing the spoon at the end of the 12 day experiment and collecting the accumulated particulate, then reinserting the cleaned spoon, the temperature difference recovered to 24°F. This verifies that the decline in heat transfer can be attributed to the accumulation of particulate on the spoon.
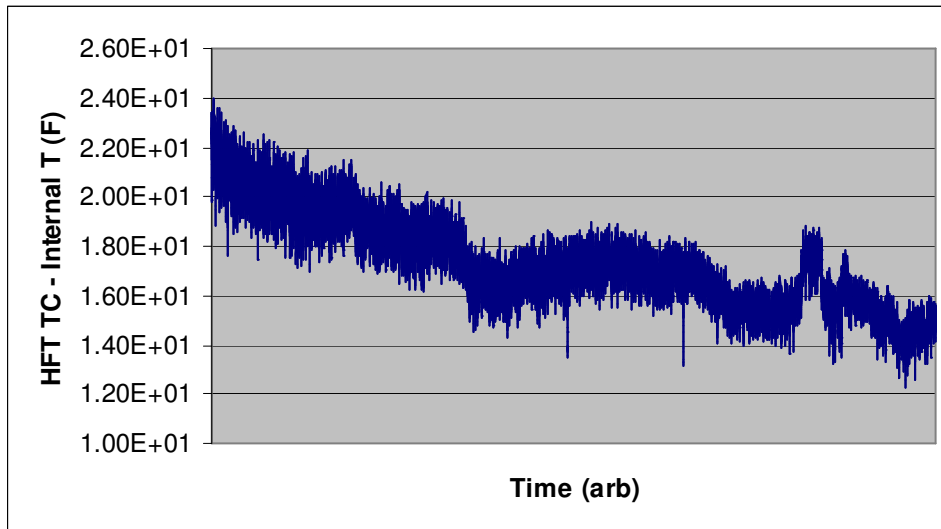
Figure 58 Decline in heat flux through the spoon over the extended exposure, as measured by the difference between HFT and Internal thermocouple temperatures.

The conductance measured using the HFT method, as well as the quantity proportional to conductance measured using the temperature difference of the HFT and Internal thermocouples, are tabulated for various exposure times in Table 13. According to both measurements, the conductance from the environment to the spoon is reduced by half over the 12 day exposure, and recovered to its original value after the particulate was brushed off of the spoon. 130mg of powder was collected from the HFT surface. Given the total exposure time of 306 hours, and the area of the spoon from which particulate was collected (the HFT itself and surrounding area), gives a collection rate of 5 mg/day/in^2. This is a factor of four lower than what was measured earlier (in the very first spoon experiment, see above) on a water-cooled surface (200°F, as opposed to the 850°F of the air-cooled spoon used here), showing lower particulate collection rate on a surface closer to the temperature of the surrounding gas.

Table 13 Conductance from flue environment to spoon, and quantity proportional to that conductance, as a function of exposure time. The "2 hr (after 12 day)" data were taken after cleaning particulate from the spoon after 12 day exposure and reinserting the spoon at the same location.

Exposure Time	HFT Conductance (BTU/hr/ft2/F)	HFT TC - Internal T "Conductance"
2 hr	12.2	0.065
18 hr	12.9	0.075
12 days	5.7	0.037
2 hr (after 12 day)	14.1	0.084

Summary: The major results of Run 1 are summarized below.

- The heat flux available at the bottom of the downcomer should be sufficient to power the 7120 TEG. Measurements taken with both the Thermonetics and ITI HFT's indicated at least a factor of 2 margin over the heat flux requirement for Thermacore's heat pipe.
- Radiant heat transfer may be very important at the bottom of the downcomer.
- Particulate collection rates are reduced as the temperature difference between surface and gas environment is reduced. 5 mg/in^2/day were observed for a 300°F difference, while earlier data showed 20 mg/in^2/day for a (roughly) 900°F difference.
- Particulate buildup can have a major impact on heat transfer. At this particular point in the exhaust stream, heat transfer fell by about 4% per day due to particulate buildup.
- Particulate collected on the spoon surface could be easily removed by light brushing with a soft brush.

A third run (Run 2) of the Materials Testing Spoon was also conducted. The purpose of this run was to repeat Run 1 with improved configuration of the data acquisition software in hopes of eliminating the large drifts in the HFT readings that were seen in Run 1 over time. Data collected over a 15 day run showed that the large drifts were indeed eliminated with this new configuration. After about 7 days in the flue environment, very little additional degradation in heat transfer was observed by HFT measurements.

Run 2: The hardware used for Run 2 was identical to that used for Run 1, with the exception that a new (and presumably identical) data acquisition board was used.[35] We enabled the "continuous calibration" feature in the data acquisition board software in hopes of eliminating the large drifts seen in the HFT data in Run 1. This feature is used specifically to eliminate drift in the analog circuitry of the board due to changes in the electrical environment or temperature of the board over time.

The objectives of this run were:
1. Confirm data taken in Run 1 for heat flux and degradation of heat flux over time at the proposed site for the in-plant demo.

2. Test whether the large drifts and jumps in HFT data could be reduced or eliminated.

The Materials Testing Spoon was insulated as shown in Figure 33 and inserted into the flue at the bottom of the right downtank downcomer, the proposed site of the in-plant test. Thermal conductance was measured as described above, and found to be 13.1 BTU/hr/ft^2/°F. This is in good agreement with values of 12.2, 12.9, and 14.1 BTU/hr/ft^2/°F measured in Run 1. The spoon was then left in the flue at that location for 14 days, and the usual data collected (internal spoon temperature, HFT temperature, HFT heat flux, and gas stream temperature).

Figure 59 below shows the HFT readings in mV as a function of time over the course of the 14 day run. Clearly, these data do not show these drifts and jumps that were seen in Run 1 (see Figure 55). We attribute this to the continuous calibration feature on the data acquisition software, although we did not turn off this feature during the run to verify that it was the cause.
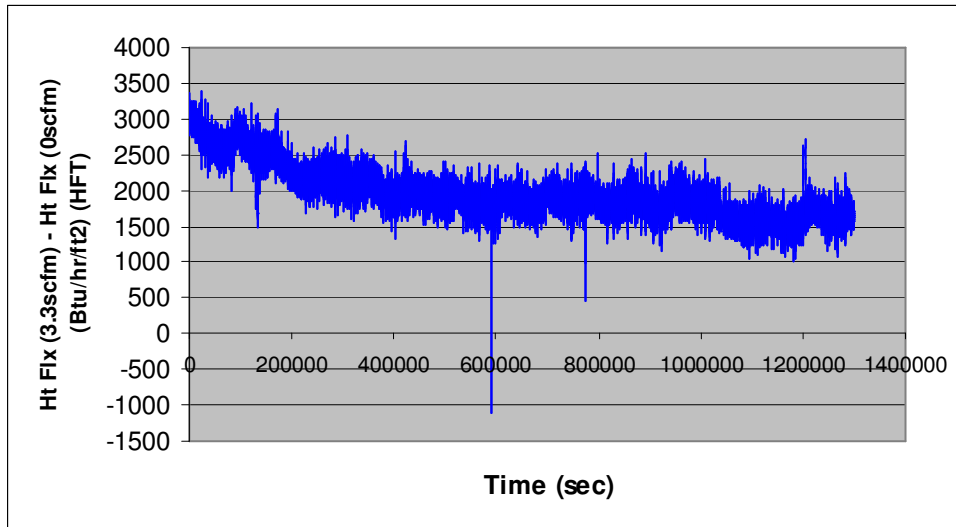
Figure 59 Heat flux (less zero flow heat flux) as a function of time over 15 days of continuous exposure to the flue environment at the proposed in-plant test site. No drifts or steps are observed.

The average heat flux over the first hour that the spoon was in the flue was 3026 BTU/hr/ft^2. This is somewhat lower than the Run 1 result of 3.7 +/- 0.3 kBTU/hr/ft^2. The average heat flux for data taken after day 7 of the experiment was 1739 BTU/hr/ft^2. This represents a decrease in heat flux of nearly 40%. The maximum reduction in heat flux is about ½, judging by the upper and lower bounds of the data set. In Run 1, a reduction in heat flux of ½ was found for a 12 day exposure, based on conductance measurements. We conclude that the "clean" spoon heat flux value for Run 2 is somewhat lower than Run 1, while the reduction in heat transfer due to particulate collection in Run 2 is similar to slightly less than was measured in Run 1 using different methods. Note that all heat fluxes here did not include the heat flux with zero air flow to the spoon.

Run 2 of the Materials Testing Spoon continued to 28 days exposure to the flue environment at 3.3scfm air flow to the spoon. Heat flux and temperature data were collected with the heat flux transducer. The data are shown in Figure 60 below. Apparently, the heat flux stops decreasing after about 15 days flue exposure. The large drop in heat flux at the end of the run was due to a wire breaking on the HFT as it was removed from the flue.
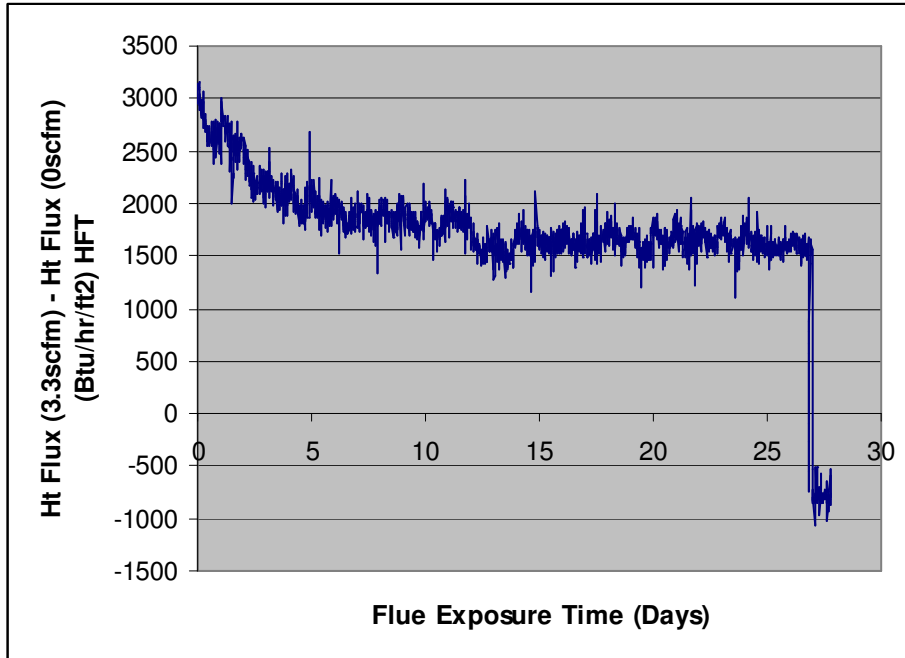
Figure 60 Heat flux as a function of time as measured during Run 2.

Strategies to Minimize Emissions Impact

Dr. John H Johnson and his student Kiran Premchand set out to study the literature on formation and control of particulate in the glass furnace exhaust, including ways of controlling particulate formation or periodic cleaning of the surface to minimize the impact of the particulate formation on the performance of the heat pipe.

Dr. John H Johnson has more than 40 years of experience working with particulate matter formation and its control as related to the mining and the automotive industry. It was proposed that a thorough study of the problem involving a literature review on the topic will reveal possible solutions.

The major tasks involved in this study are summarized as follows:

1. Gather existing literature and information already known to PPG from PPG personnel.

2. Perform a literature review about the chemical and physical characteristics of the particulate of interest, i.e., Na_2SO_4,

3. Based on the preliminary study of the particulate characteristics, perform a literature review about means to prevent and/or control Na_2SO_4 particulate formation on the heat pipe,

4. With the help of available literature, come up with possible means of controlling particulate formation or provide means of periodic cleaning of the heat pipe surface,

5. Write, review and submit a brief report (in electronic format - MSWord) about the study to PPG industries.

6. Propose and make cost estimates for two or more 1-2 day experiments that PPG could perform in conjunction with its heat pipe / TEG test to test recommendations of the report for cleaning or controlling Na_2SO_4 particulate formation, and assist PPG with these experiments. Also include in the cost estimates assistance to PPG for these experiments.

The literature review concentrated in four general areas:

   i.   Properties of Na_2SO_4 and how it forms as a particulate including size distribution data,
   ii. Na_2SO_4 particles and the methods of control, and
   iii. EPA New Source Standards that apply to glass manufacturing.
   iv. Possible materials that could be applied to the heat pipe surface that would reduce the tendency of Na_2SO_4 to adhere to the heat pipe.

The literature review focused on the following journals and electronic databases:

- Journal of the American Chemical Society,
- Environmental Science and Technology (online journal),
- Journal of the Air and Waste Management Association,
- Journal of Chemical and Engineering Data,
- Chemical Engineering Journal,
- Environmental Sciences and Pollution Management (online database), and
- Environmental Protection Agency – Standards – Information Services.

Other journals and/or databases were searched for material as and when found to be necessary. Also, relevant books were acquired and/or loaned to complete the literature review.

The other area of study was to come up with approaches/ideas for cleaning/preventing the formation of particles on the heat pipe. These were recorded in the brief report delivered at the end of the project.

The main conclusions of the study were:

- Rate of deposition of Na_2SO_4 is critical to degradation of heat pipe performance

- Majority of degradation of heat pipe performance is expected due to change in absorptivity of heat pipe surface (from 0.94 to 0.06-0.39) due to covering of surface with Na_2SO_4, a loose white powdery deposit and change in outer surface temperature of heat pipe due to Na_2SO_4 particulate formation

- Online mechanical cleaning methods seem to be the most promising in restoring heat pipe performance

- Experiments can be conducted to study the effect of particulate formation on heat pipe performance and to determine which cleaning method is most suitable and effective for restoring heat pipe performance

The full text of the report is found in Appendix I.

Accomplishments

Although the primary objective of demonstrating waste heat recovery with 20% efficiency in an industrial process was not achieved, the project did accomplish many of the objectives that were integral to achieving the primary objective, including:

- Defined a strategy (modular waste heat recovery) for implementing TE technology in an industrial process, and suggested several possible module designs
- Calculated the economics of one module, namely the heat pipe module, based on real heat pipe, TEG, and installation costs from vendors, and demonstrated the importance of heat collection technology and TEG efficiency in those economics
- Identified a new class of thin-film TE materials and showed how they could be implemented in commercially available TEG designs
- Performed (to our knowledge) the first demonstration of high temperature waste heat recovery with TE technology in an industrial environment, using heat collection and TE technology capable of generating a significant amount of power (100W) given today's technology
- Characterized temperatures and heat transfer in an oxyfuel glass melter exhaust system
- Quantified the long-term impact of condensate buildup on heat transfer in the exhaust system using a custom-designed spoon device
- Reviewed existing knowledge of condensates in a glass furnace and existing technology that may be useful for mitigating the impact of those condensates on heat transfer

In addition to these accomplishments, the following invention disclosures and/or patent applications were made:

- "PbTe-based N-Type Thermoelectric Materials", disclosure submitted by PNNL.
- "Waste Heat Recovery with Photovoltaics", disclosure submitted by PPG. PPG chose not to pursue.
- "Heat Pipes and Use of Heat Pipes in Furnace Exhaust", patent application submitted by PPG.
- "A Device for Use in a Furnace Exhaust Stream for Thermoelectric Generation", patent application submitted by PPG.

Also, the following presentation was made:

"Advanced Thermoelectric Materials for Efficient Waste Heat Recovery in Process Industries", Presented at the DOE Industrial Materials for the Future Annual Review, June 1, 2005, Chicago, IL.

Conclusions

The primary conclusion to be drawn from this project is that TE technology is still far from ready to be used for waste heat recovery on an industrial scale. The Si/SiGe and B_4C/B_9C materials systems that motivated this project were found to be impractical for use in real devices. Thick film GAST material appears to show promise as a material that can achieve ZT ~ 1.5 at 300°C temperature. While this is a remarkable accomplishment in a field that has struggled to achieve ZT of 1 after 100 years of research, additional improvement in high temperature ZT is required to make an economical device. Also, while recent research has suggested that thin films and other new materials structures may lead to higher ZT materials, incorporating these new structures into a TEG may require new TEG device designs. We have demonstrated a novel technique for depositing thin films on Kapton substrates and then winding them to obtain thermoelements that could be integrated into TEG designs that currently use bulk thermoelements. However, this technique is limited to the useful temperature range of Kapton, which is 400°C or below.

We successfully demonstrated that waste heat could be collected, transferred to a TEG, and converted to electricity in a real industrial process, and that this could be done for a period of at least several months with only minimal maintenance by plant personnel. This was achieved using heat pipe technology to efficiently transfer collected heat to the TEG hot surface, and relied on a relatively large heat pipe to collect a sufficient amount of heat through primarily radiative heat transfer from the hot glass furnace. The presence of condensates in the exhaust gas stream led to heat transfer reductions of about 50% after 2 weeks, but leveled off after that. The impact of particulate collection on waste heat recovery efficiency was observed, and it was found that some of the efficiency loss could be reversed by manually cleaning the heat pipe surface on a monthly basis. Commercially available, automated cleaning technologies were identified that could reduce this maintenance cycle even further. However, given current TEG costs and efficiencies, as well as current heat pipe costs, this approach to waste heat recovery is far from ready for adoption by industry.

Recommendations

As a result of the findings of this project, we would recommend the following:

- Additional basic science work on high-temperature thermoelectric materials such as GAST, with the recognition that such work is high-risk and may require years of additional device work after benchtop demonstration of the material properties before a practical TEG with high efficiency would be realized
- Applied R&D and engineering work focused on developing inexpensive heat collection and heat transfer methods that could be applied across multiple industries
- Applied R&D work on inexpensive materials (either bulk or coatings) that would improve survivability of heat exchangers at high temperatures (>500°C)
- Exploration of alternative heat-to-electricity conversion methods with higher efficiencies than thermoelectrics

References

[1] Mahan, G., Sales, B., and Sharp, J. *Physics Today*, March 1997, page 42.

[2] Pellegrino, J. *Glass Industry of the Future: Energy and Environmental Profile of the U.S. Glass Industry, April 2002*. Published by Office of Industrial Technologies, U.S. DOE.

[3] Margolis, N. and Brindle, R. *Energy Profile of the Steel Industry, August 2000*. Published by Office of Industrial Technologies, U.S. DOE.

[4] Choate, W. and Green, J.A.S. *U.S. Energy Requirements for Aluminum Production, February 2003*. Published by Office of Industrial Technologies, U.S. DOE.

[5] Margolis, N. *Energy Profile of the U.S. Aluminum Industry, July 1997*. Published by Office of Industrial Technologies, U.S. DOE.

[6] Pellegrino, J. *Energy Profile for the Chemical Industry, May 2000*. Published by Office of Industrial Technologies, U.S. DOE.

[7] Trier, W. *Glass Furnaces: Design, Construction, and Operation*. Sheffield, UK: Society of Glass Technology, 1987.

[8] Rowe, D.M. *CRC Handbook of Thermoelectrics*. Introduction. Boca Raton: CRC, 1995.

[9] Hicks, L.D. and Dresselhaus, M.S. *Physical Review B* **47**, 12727 (1993).

[10] Venkatasubramanian, R., Silvola, E., Colpitts, T., and O'Quinn, B. *Nature* **413**, 597 (2001).

[11] Hsu, K.F. et al. *Science* **303**, 818 (2004).

[12] Goldsmid, H.J. *CRC Handbook of Thermoelectrics*, Chapter 3. Boca Raton: CRC, 1995.

[13] Sales, B.C., Mandrus, D., Willaims, R.K. *Science* **272**, 1325 (1996).

[14] Nolas, G.S., et al. *J. Appl. Phys.* **79**, 4002 (1996).

[15] Chen, N. et al. *Appl Phys. Lett*. **87**, 171903 (2005).

[16] Skrabek, E.A. and Trimmer, D.S. *CRC Handbook of Thermoelectrics*, Chapter 22. Boca Raton: CRC, 1995.

[17] Khinkis, M. Ya., et al. *Steklo i Keramika* **1**, 15 (1968).

[18] Shapiro, M.D. Tyurin, A.I., and Lashenkov, Yu. V. *Steklo i Keramika* **11**, 24 (1980).

[19] Nycz, J.A. and Sturgill, D.T. *The Glass Industry*, June 1980, p. 12.

[20] Rozendaal, N.A. *Glass International* December 2007 / January 2008, p. 32.

[21] Kobayashi, et al. *Ceramic Engineering and Science Proceedings* **26**, 1 (2005).

[22] Kobayashi, et al. Glass Problems Conference Energy Workshop. October 2005, Champaign IL.

[23] Glass Manufacturing Industry Council. *Glass Melting Technology: A Technical and Economic Assessment*. October 2004.

[24] http://www.hi-z.com/hz20.php

[25] Enerac Inc., Westbury, NY.

[26] Dwyer Instruments Inc., Michigan City, IN.

[27] Setra Systems Inc., Boxborough, MA.

[28] Kumar, V., Gangacharyulu, D., and Tathgir, R.G. *Heat Transfer Engineering* **28** 954 (2007), and references therein.

[29] Rosenfeld, J.H. and Ernst, D.M. *Heat Pipe Science and Technology: Proc. 11th Int. Heat Pipe Conf., Tokyo-Japan 1999*, p 407.

[30] Thermonetics Corp., La Jolla, CA

[31] Sauereisen Cements Company, Pittsburgh, PA.

[32] Thermal Ceramics, Augusta, GA.

[33] HiE Coat 840-M, Aremco Products, Inc.

[34] International Thermal Instrument Co., Del Mar, CA.

[35] Personal DAQ/56. IOTech, Cincinnati, OH.

Study of the Characteristics and Control of Sodium Sulfate Particulate Cake Formation on a Heat Pipe Used for Energy Recovery from the Exhaust Gas of a Glass Manufacturing Furnace

Prepared and submitted by:

Dr. John H Johnson

1500 Ravine Side Drive

Houghton, MI – 49931

Tel: (906) 482-6413

Fax: (906) 482-7155

&

Kiran C Premchand

June 30, 2008

Contents

1. Introduction

This report describes a study conducted on available research literature about Na_2SO_4 particulate properties and formation which leads to fouling of the outer surfaces of a heat pipe intended for use in the exhaust flue duct of a flat-glass manufacturing furnace as part of a heat recovery system.

1.1. Background

Flat-glass is one of the intermediate products that PPG manufactures at the plant in Meadville, PA. PPG has two furnaces – a regenerative type furnace and an oxy-fuel furnace. In a regenerative type furnace, air is used as the oxidant for combustion whereas in the oxy-fuel furnace, oxygen is used instead of air as the oxidant. The furnace that is of interest to this project is the oxy-fuel furnace.

Exhaust gas from the oxy-fuel furnace exits through vertical ducts called 'downcomers', numbering two on each side of the line, one each from the 'uptank' and the 'downtank'. Downcomer lengths for this furnace are approximately 17 ft, and these merge into a connecting flue 6.5 ft by 9.3 ft and roughly 60 ft long, connecting the downcomers to the stack. The junction of the downcomer to the connecting flue is the area where the heat pipe is planned to be placed. From initial measurements obtained from PPG, this area has a temperature range of 500-700 ºC, whereas the gas temperatures at the top of the downcomers have been measured to be approximately 1500 ºC. The pressure in the connecting flue is slightly less than atmospheric pressure. Also, there are small openings in the connecting flue which let atmospheric air enter the flue through the openings via natural draft, thereby assisting in cooling the flue gas.

The heat pipe is a slender cylindrical metal (Inconel) pipe with a liquid metal (sodium) filled inside the pipe. It also has two lateral fins attached length-wise to two diametrically opposite sides on the cylindrical pipe. While in operation, these fins will be placed horizontally, as the primary heat transfer mechanism will be radiation from the furnace above the heat pipe. The TEG and the furnace flue ducts are described in more detail in Appendix A. Appendix A also describes the letter to potential suppliers of heat exchanger fouling control equipment and the enclosure with the letter describing the furnace flue and the TEG.

An important issue that needs to be addressed when attempting to recover heat energy from the flue gases is the fouling of the heat transfer surfaces of the heat pipe. From an initial inspection of the flue, the formation of a white powdery deposit was observed to take place. This powdery particulate matter was determined to be sodium sulfate (Na_2SO_4), from analyses conducted by PPG. Sodium sulfate, especially in its powder form is a poor conductor of heat and will cause deterioration of the heat pipe performance over time.

The Environmental Protection Agency (EPA) has regulated the total particulate emission rates from new glass manufacturing plants. The standards are given in Reference [1], and Table 1 gives a comparison of

particulate emission rates (measured in grams of particulate per kilograms of glass produced) for various segments of the glass manufacturing industry.

Table 1: EPA Standards - Particulate emission rates *(g of particulate/kg of glass produced)* for glass manufacturing plants [1]

Glass manufacturing plant industry Segment	Furnace fired with gaseous fuel	Furnace fired with liquid fuel
Container glass	0.1	0.13
Pressed and blown glass		
(a) Borosilicate recipes	0.5	0.65
(b) Soda-Lime and Lead recipes	0.1	0.13
(c) Other than Borosilicate, Soda-Lime and Lead recipes (including opal, fluoride and other recipes)	0.25	0.325
Wool fiberglass	0.25	0.325
Flat glass	0.225	0.225

This report provides an understanding of particulate formation on heat exchanger surfaces and ways and means to prevent and/or control it. The report suggests methods to clean the heat pipe surfaces and provides references/contacts in the industry that can be of assistance in providing equipment for the prevention/cleaning processes.

1.2. Project Work Plan and Outline of the Report

The following are the specific tasks that were carried out in accordance with the PPG/John H Johnson contract.

1. Gather existing literature and information already known to PPG from PPG personnel,
2. Perform a literature review about the chemical and physical characteristics of the particulate of interest, i.e., Na_2SO_4,
3. Based on the preliminary study of the particulate characteristics, perform a literature review about means to prevent and/or control Na_2SO_4 particulate formation on the heat pipe,
4. With the help of available literature, come up with possible means of controlling particulate formation or provide means of periodic cleaning of the heat pipe surface,
5. Write, review and submit a brief report (this document - in electronic format - MSWord) about the study to PPG industries, and
6. Propose and make cost estimates for two or more 1-2 day experiments that PPG could perform in conjunction with its heat pipe/TEG test, to test recommendations of the report for cleaning or controlling Na_2SO_4 particulate formation, and assist PPG with these experiments. Also include in the cost estimates assistance to PPG for these experiments.

Appendix B contains the details of the literature review for items 1-4 above. A rating system from 1-10 (1 – lowest and 10 – highest) was used to rate the significance of various papers/books. Papers/books that were rated as 5 or above were used to write this report and they are listed in the 'References' section at the end of this report. Section 2 in this report contains the physical, thermal and chemical properties of Na_2SO_4 from the literature, followed by section 3 which contains a discussion on particulate cake formation and its effects on the heat transfer rates. The approaches for prevention and control of Na_2SO_4 particulate matter are contained in section 4. Also, Appendix C contains additional tables that are referenced from within sections of the main body of this document. Section 5 contains a description of experiments that can be conducted by PPG to determine the optimal cleaning method for the heat pipe used for heat recovery of flue gases from the glass furnace. Finally, section 6 summarizes our findings from this study.

2. Characteristics of Sodium Sulfate

Sodium sulfate is, next to sodium chloride, by far the most common of the naturally occurring saline salts [2]. Some of its common minerals are Thenardite (Na_2SO_4), Mirabilite – also called Glauber's salt ($Na_2SO_4.10H_2O$), Glauberite ($Na_2SO4.CaSO_4$), Astrakanite – also called Bloedite ($Na_2SO_4.MgSO_4.4H_2O$) and Burkeite ($2Na_2SO_4.Na_2CO_3$). A fairly steady amount of sodium sulfate has been used in glass manufacturing for many years, averaging 0.5% of the charge (by weight) for flat glass. A small amount of sodium sulfate is helpful in reacting with silica scum on the melter surface, and thus limiting the formation of silica scum. Also, it helps in increasing the melting speed of the original charge, reduces the amount of unmelted solids in the melt and improves the workability of high-silica glass and for being formed into complex shapes. On the other hand, the SO_2 and SO_3 that are formed during the decomposition of sodium sulfate are corrosive, regulated gases and must at least be partially removed from the flue gas. Also, even if the sodium sulfate is not decomposed, about 50% of the unused sodium sulfate is volatilized [2].

The next three sub-sections list a set of physical, thermal and chemical characteristics of sodium sulfate and its various forms.

2.1. Physical Characteristics

Sodium sulfate is a white crystalline solid of the formula Na_2SO_4, formed as a result of the cooling of the flue gases. Reference [3] states that the dust particles formed in the flue gases from glass furnace have diameters between 0.02 and 0.6 μm (also in Reference [4]). Also, the particles formed in soda-lime glass furnaces are mainly sodium sulfate [3]. It is assumed that majority of the sodium sulfate that is formed is in the anhydrous state, since the gaseous composition of the PPG flue gases shows low (4-5% vol.) moisture content.

Reference [1] lists a set of physical properties of sodium sulfate. Table 2 below (reproduced from Reference [1]) shows solubility and density of various sodium sulfate in water at different temperatures. Table C1 in Appendix C shows various properties of different sodium sulfate minerals.

Table 2: Solubility and Density of Sodium Sulfate in Water (wt %) [1, 5]

Table 7.1

Solubility and Density of Sodium Sulfate in Water (wt%) (Seidell, 1965)[a]

Temp. (°C)	Solubility (wt %)	Density (g/cc)	Temp. (°C)	Solubility (wt %)
−1.25[1]	4.15	—	110	29.58
0[2]	4.31	1.041	120	29.48
5[2]	5.84	1.0575	130	29.53
10[2]	8.26	1.0795	140	29.58
15[2]	11.66	1.1085	150	29.68
20[2]	15.97	1.149	160	29.82
25[2]	21.88	1.2085	170	30.07
27.5[2]	25.15	1.241	180	30.26
30[2]	29.18	1.2795	190	30.46
32.38[3]	33.20	1.334	200	30.60
			210	30.65
−3.55[4,5]	12.8	—	220	30.94
−1.25[4]	4.15	—	230	31.32
0[6]	15.11	—	233[5,10]	31.7
5[6]	18.90	—	241[10]	31.88
10[6]	23.02	—	250	30.56
15[6]	27.11	—	260	29.48
20[6]	31.13	—	270	27.95
23.7[7]	34.38	—	280	26.04
24.25[5,7]	34.3	—	290	23.55
			300	19.87
35[8]	32.93	1.329	300[5]	20.3
40[8]	32.48	1.3205	310	15.61
45[8]	32.07	1.3123	320	11.58
50[8]	31.69	1.3052	324.5[5]	10.0
60[8]	31.13	1.292	330	6.80
70[8]	30.65	1.280	340	4.03
80[8]	30.17	1.267	350	2.34
90[8]	29.87	1.2552	354[5]	1.62
100[8]	29.68	1.246	360	0.89
101.9[9]	29.68	1.2450	382	0.38

[a]The solid phases in equilibrium with these solutions are: 1, ice + $Na_2SO_4 \cdot 10H_2O$; 2, $Na_2SO_4 \cdot 10H_2O$; 3, $Na_2SO_4 \cdot 10H_2O$ + Na_2SO_4 (ortho); 4, ice + $Na_2SO_4 \cdot 10H_2O$ + $Na_2SO_4 \cdot 7H_2O$ (metastable); 5, data from Strakhov (1970); 6, $Na_2SO_4 \cdot 7H_2O$ (metastable); 7, Na_2SO_4 + $Na_2SO_4 \cdot 7H_2O$ (metastable); 23.47°C, Dyson (1962); 8, Na_2SO_4 (ortho) at temperatures from 32.38 to 233, 235 or 241°C; 9, boiling point; 10, Na_2SO_4 (ortho) + Na_2SO_4 (mono); mono alone at higher temps; 234.5 or 235°C; Dyson (1961).

The heat capacities of two forms of sodium sulfate (anhydrous – Na_2SO_4 and decahydrate – $Na_2SO_4.10H_2O$) are given in Table 3. It can be observed that the heat capacity of $Na_2SO_4.10H_2O$

(decahydrate) is 8-9 times higher than that for Na_2SO_4 (anhydrous) at the same temperature. The decahydrate loses water at 100°C to form the anhydrous form and the anhydrous form melts at 844°C.

Table 3: Heat Capacity of Na_2SO_4 and $Na_2SO_4.10H_2O$ [1]

T (K)	Cp (cal/mole.K)		T (K)	Cp (cal/mole.K)	
	Na_2SO_4	$Na_2SO_4.10H_2O$		Na_2SO_4	$Na_2SO_4.10H_2O$
15	0.222	1.940	90	14.440	50.970
20	0.581	4.200	100	15.930	56.190
25	1.213	7.300	120	18.450	65.930
30	1.990	10.530	140	20.500	75.100
35	2.980	13.960	160	22.250	83.680
40	4.077	17.510	180	23.820	91.540
45	5.222	21.180	200	25.230	99.180
50	6.423	24.950	220	26.510	106.800
60	8.743	32.380	240	27.670	114.700
70	10.850	39.250	260	28.730	122.900
80	12.760	45.430	280	29.670	131.400
			300	30.510	140.500

Another set of relevant data for sodium sulfate is the set of thermodynamic properties shown in Table 4.

Table 4: Thermodynamic values of Na_2SO_4 [1]

Enthalpy *(kcal/g mol, 25°C)* of			Free Energy	Entropy
Formation	Fusion	Solution	*(kcal/g mol)*	*(cal/° g mol)*
-330.9	+5.83	+0.28	-303.4	35.7

2.2. Thermal Characteristics

Thermal conductivity of sodium sulfate is another important property that is required for calculations later in this report. Although the references that were reviewed as part of this study do not cite values

for the thermal conductivity of Na_2SO_4, Reference [6] gives a range of values for the thermal conductivity of non-metallic solids as **0.3 – 60** *W/m.K*. Reference [7] cites the thermal conductivity of sodium thiosulfate ($Na_2S_2O_3 \cdot 5H_2O$) as **1.36** *W/m.K* at *295 K* (*22°C*), and the thermal conductivity of sodium hydrogen sulfate ($NaHSO_4$) as ranging from **0. 626** *W/m.K* at *443 K (170°C)* to **0.515** *W/m.K* at *518 K (245°C)* as shown in Table 5.

Table 5: Thermal conductivity of sodium hydrogen sulfate ($NaHSO_4$) at various temperatures [7]

Temperature *(K)*	Thermal conductivity *(W/m.K)*
443.0	0.626
450.0	0.604
460.3	0.480
470.2	0.502
502.2	0.509
518.3	0.515

The thermal conductivity of Inconel 600 is given in Reference [6] as **14.9 W/m.K**.

Absorptivity values of sodium sulfate are also important for the calculations in Appendix D of this report. While the absorptivity values of Na_2SO_4 are not directly available from the literature that was reviewed, absorptivity of white non-metallic coatings is known to be less than that for a metal alloy like Inconel. Emissivity values of Inconel sheet are reproduced from Reference [7] in Table 6. Absorptivity values of Inconel are also assumed to be equal to their emissivity values (gray surface approximation).

Table 6: Emissivity of Inconel at various temperatures [7]

Material	Temperature (°C)	Emissivity ε (.)
Inconel sheet	538	0.28
Inconel sheet	649	0.42
Inconel sheet	760	0.58
Inconel X, polished	24	0.19
Inconel B, polished	24	0.21

The absorptivity values of the heat pipe surface may be different from those of Inconel, because of the presence of a special coating on the heat pipe surface. Table 7 reproduced from Reference [9], gives the values for normal-total absorptivity (for receiving material at 300 K or 27°C) of common paint coatings for incident solar radiation. The black paint coatings listed in Table 7 have absorptivity values in the range of *0.88 – 1*, while white coatings have absorptivity values associated with them in the range of *0.06 – 0.39*. According to private communication with PPG [23], the emissivity of the ceramic coating on the heat pipe is **0.94**.

Table 7: Normal-total absorptivity of common coatings for incident solar radiation (receiving material at 300 K or 27°C) [9]

Coating	Normal-total absorptivity *(.)*
Black coatings:	
Anodize black	0.88
Carbon black paint NS-7	0.96
Ebanol C black	0.97
Martin black velvet paint	0.91
3M black velvet paint	0.97
Tedlar black plastic	0.94
Velestat black plastic	0.96
White coatings:	
Barium sulfate with polyvinyl alcohol	0.06
Catalac white paint	0.23
Dow Corning white paint DC-007	0.19
Magnesium oxide white paint	0.09
Potassium flourotitanate white paint	0.15
Tedlar white plastic	0.39
Titanium oxide white paint with methyl silicone	0.20
Zinc oxide with sodium silicate	0.15

2.3. Chemical Characteristics

The chemical structure of sodium sulfate is given in Figure 1.
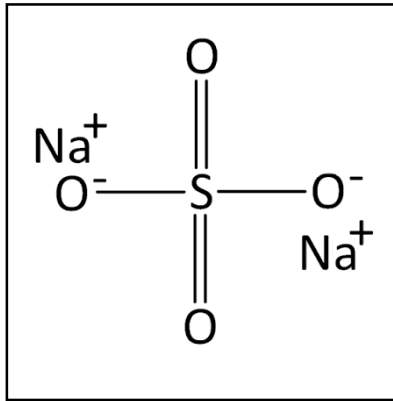
Figure 1: Chemical structure of Na_2SO_4 [10]

Sodium sulfate is odorless and chemically very stable, being unreactive toward most oxidizing or reducing agents at normal temperatures. At high temperatures, it can be reduced to sodium sulfide. It is a neutral salt, which forms aqueous solutions with pH of 7. The neutrality of such solutions reflects the fact that Na_2SO_4 is derived, formally speaking, from the strong acid sulfuric acid and a strong base sodium hydroxide.

Sodium sulfate is an alkali sulfate formed in exhaust flue gases of glass furnaces due to several (at least four) intermediate reactions [5] resulting in the following overall chemical reaction:

$$2NAOH (g) + SO_2 + 0.5O_2 \quad Na_2SO_4 (g) + H_2O$$

Reference [5] gives a thermodynamic characterization of condensation products from glass furnaces, which says "solid or liquid alkali sulfates are the main compounds formed during the cooling of alkali-rich and sulfur-rich flue gases". The condensation is also thought to be occurring due to two mechanisms – firstly, the increased supersaturation of salt vapors at decreased temperatures leads to condensation in the bulk flue gas, and secondly, condensation will occur due to presence of relatively cold surfaces in the exhaust gas flow, leading to the deposition of liquid or solid salts on these surfaces. Reference [5] also states that "deposition of alkali sulfates is observed in regenerators at brick temperatures below 1350 K", which is consistent with the observations from the PPG plant. The mechanism of formation on the heat pipe surfaces could be both the condensation due to supersaturation of salt vapors in bulk flue gas, and condensation due to the lower temperature of the heat pipe surface.

Solubility and phase data for different aqueous solutions containing sodium sulfate are given in Chapter 7 of Reference [1]. A solubility plot of Na_2SO_4 in water at various temperatures from 0°C to 200°C is given in Figure 2 (References [11] and [5]). Its solubility rises more than tenfold between 0 °C to 32.4 °C, where it reaches a maximum of 49.7 g Na_2SO_4 per 100 g water. At this point the solubility curve changes slope and the solubility becomes almost independent of temperature.
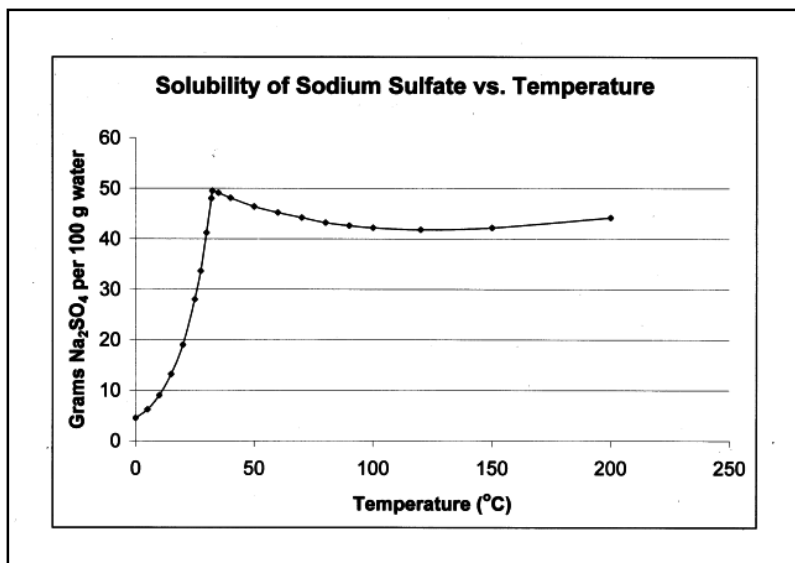
Figure 2: Solubility of Na$_2$SO$_4$ vs. Temperature [11, 5]

3. Particulate Cake Formation and its Effect on Heat Transfer Rates

During the cooling of flue gases such as those in glass furnaces, some of the constituents of the flue gases condense and form solid particulate matter. Research literature [5] is available on the chemical changes occurring during the cooling of exhaust gases in a glass furnace, which also gives a calculation of the equilibrium composition of the waste gas mixture for temperatures from 1000 to 1800 K. A typical waste gas composition from a gas-fired glass furnace is given in Table C2 in Appendix C. This section gives a brief description of formation of particulate matter, especially on external surfaces and its effect on heat transfer rate.

3.1. Particulate Formation Mechanisms

Beerkens et al. [3] mention that "fouling of heat exchanging surfaces, which are relatively cold compared to the flue gases, is caused by either:

(a) Mass transfer of gaseous components from flue gases to channel surfaces and condensation of these compounds at the surfaces, or

(b) Mass transport of dust particles from the flue gases towards the heat exchanging surfaces."

Also, the available literature on the topic [3, 12] points out that in secondary heat exchangers, the mechanism responsible for fouling is b). At temperatures below 1000 K, the product of condensation from flue gases consists mainly of sub-micrometer particles. These particles are deposited on external surfaces and occur mainly due to one or more of the mechanisms mentioned below occurring separately or simultaneously:

1. Gravitational settling,

2. Deposition by inertia of the dust particles,

3. Interceptional deposition (only important for very rough surfaces),

4. Deposition by Brownian diffusion,

5. Deposition by thermophoretic forces (important for small particles).

There are three basic stages of deposition on surfaces from a moving fluid [13]:

1. Diffusional transport of the particulate matter that forms the deposit (or its precursors) across the boundary layers adjacent to the solid surface within the flowing fluid,

2. Adhesion of the deposit to the surface and to itself, and

3. Transport of the deposit material away from the solid surface.

In mathematical terms, the rate of deposition can be given as [13]:

$$\frac{dm}{dt} = A_{dep}(\emptyset_D - \emptyset_R)$$ -- (1)

where:

m -- Mass of deposit (kg),

A_{dep} -- Area of deposition (m^2),

$\emptyset_D$ --- Deposit mass flow rate per unit area of surface $(kg/m^2.s)$ and,

$\emptyset_R$ ---Removal mass flow rate per unit surface area $(kg/m^2.s)$

Equation (1) can be used to calculate deposit thickness evolution with time, provided the density at which the deposit gets accumulated is known. Mathematically,

$$\frac{dm}{dt} = \frac{d}{dt}\left(w_{dep}A_{dep}\rho_{dep}\right) = \rho_{dep}A_{dep}\frac{d\left(w_{dep}\right)}{dt}$$ --- (2)

where:

w_{dep} --Deposit thickness (m), and

ρ_{dep} ---Density of particulate matter accumulation (kg/m^3)

From Equation (2), the important variables determining the particulate deposition rate are the particulate accumulation density $\left(\rho_{dep}\right)$ and particulate layer thickness growth (or depletion) rate $\left(w_{dep}\right)$, for a given surface area of deposition $\left(A_{dep}\right)$.

Figure 3 shows a graph of the deposit growth rate on a typical heat exchanger surface (reproduced from Reference [13]). In region A, adhesion of particulate matter is initiated. Region B represents the steady growth of deposit on the surface. In this region, the adhesion and removal rates are competing with each other. Finally, the rate of removal becomes equal to the rate of deposition in region C, so that a "steady" state is reached when the deposit thickness remains constant with respect to time. So, in such a scenario, the fouling resistance of the heat transfer system reaches a steady value after a certain period of time.
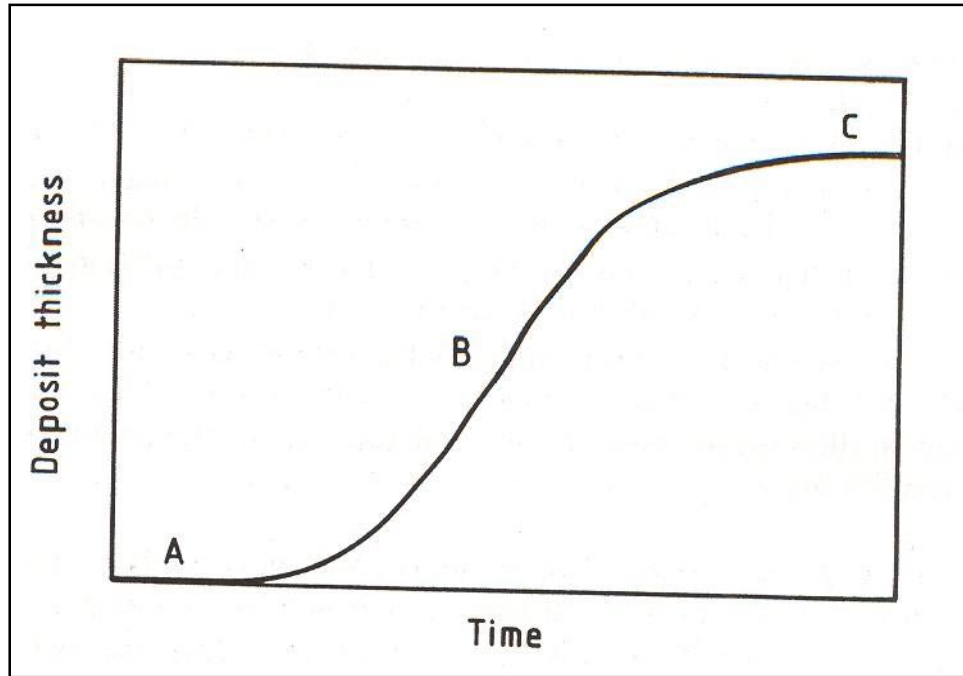
Figure 3: Idealized representation of change in deposit thickness with time [13]

If the particulate removal mass flow rate (for a specific case) can be considered negligible, Equation (1) becomes:

$$\frac{dm}{dt} = \emptyset_D \qquad \text{--} \qquad (3)$$

In case this assumption is valid, the rate of change of deposit thickness will always be non-negative, and hence the fouling resistance - R_f - (which depends on the deposit thickness) of the entire heat transfer system keeps increasing or remains steady with time.

3.2. Fouling and its Effects on Heat Transfer Rates

As the particulate deposition rate changes with time differently in various heat exchangers, the fouling resistance R_f also increases in different ways. Reference [14] shows examples of linear, falling, asymptotic and saw-tooth rates of change in fouling resistance in different heat exchangers, and is qualitatively depicted in Figure 4.

Figure 8: Possible fouling resistance versus time curves
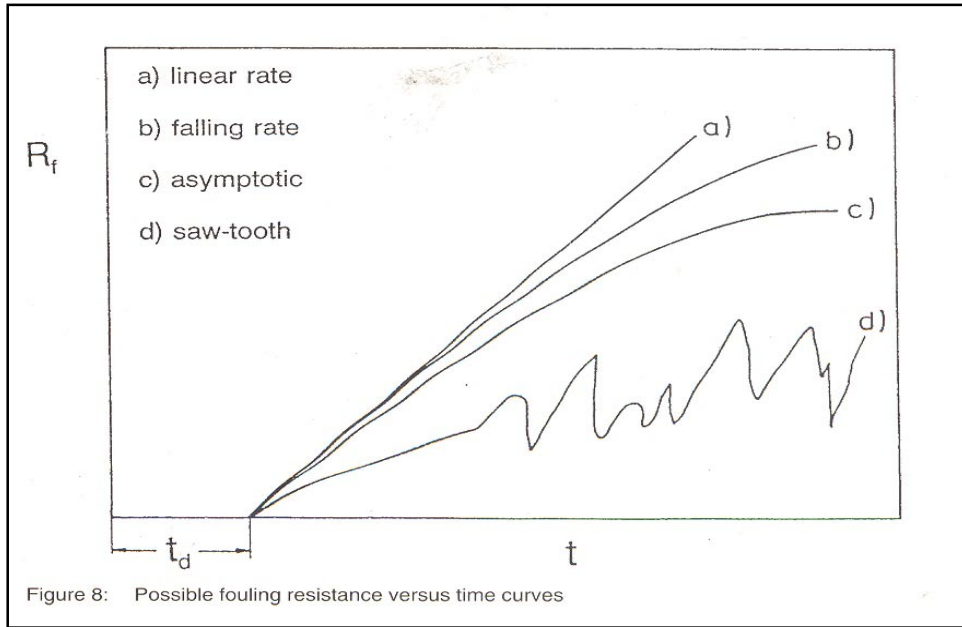
Figure 4: Possible fouling resistance versus time curves [14]

Particulate control has been used in industries using heat exchangers for decades, for revival of heat exchanger effectiveness. Periodic cleaning of heat exchangers is necessary, even for a well-designed heat exchanger, since the deposition of particulate matter is a characteristic of the system, and depends on the medium of cooling and the chemical composition of the particles.

Now, since we are interested in finding out the effect of particulate deposition on heat transfer performance of the heat pipe, we need to take a closer look at the energy balance of the heat pipe at steady state. Figure 5 shows a schematic of the same.

Note - control volume boundary shown in this figure in dotted lines coincides with the external surface of the heat pipe. It is, however, drawn slightly off for graphic purposes only.
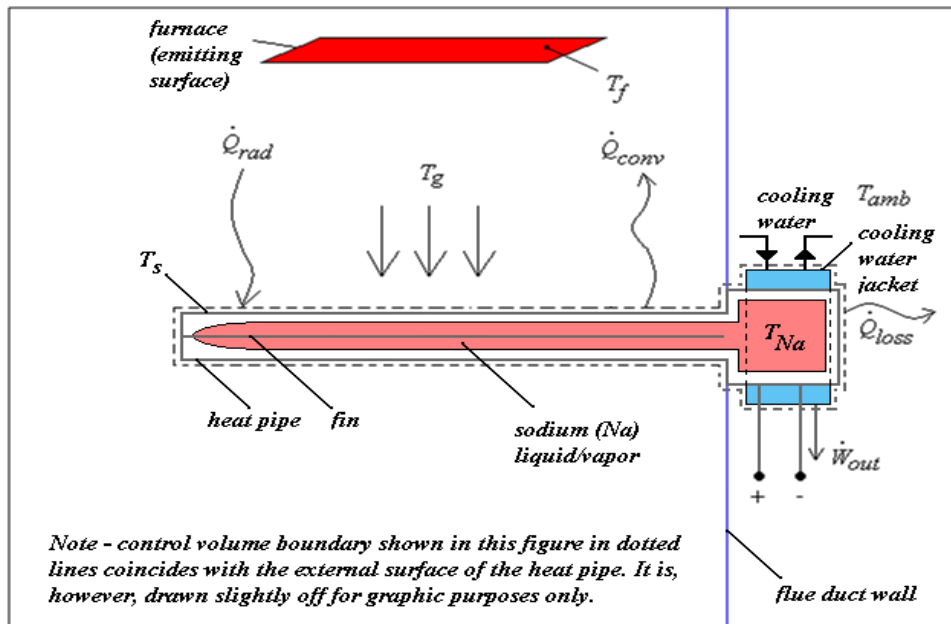
Figure 5: Energy balance schematic of the heat pipe at 'steady' state

Since the control volume is chosen such that the mass flows in and/or out of the system are the mass flow of cooling water into and out of the cooling water jacket on the outer surface of the TEG, this becomes an open system problem. The energy balance of this open system expressed mathematically is:

$$\dot{E}_{st} = \dot{Q} - \dot{W} + \dot{m}_{H_2O}\left(\hat{h}_{in} - \hat{h}_{out}\right) \qquad \text{--} \qquad (4a)$$

where:

$\dot{E}_{st}$ -- Rate of change of energy stored in the system *(W)*,

$\dot{Q}$ -- Net rate of heat transfer into or out of the system *(W)*,

$\dot{W}$ -- Net rate of work into or out of the system *(W)*,

$\dot{m}_{H_2O}$ -- Mass flow rate of water (kg/s), and

$\hat{h}_{in} - \hat{h}_{out}$ - Difference in specific enthalpy of water entering ('in') and leaving ('out') the system *(J/kg)*

Here, it should be noted that according to the convention used for energy balance of open systems at steady state from References [15, 6], heat transfer into the system is considered '+' and heat transfer out of the system is considered '-'. Also, work output by the system is considered '+', whereas work input to the system is considered as '-'.

For a constant specific heat of water, the enthalpy difference term in Equation (4a) can be written as:

$$\dot{m}_{H_2O}\left(\hat{h}_{in} - \hat{h}_{out}\right) = -\dot{m}_{H_2O}c_{p,H_2O}\left(T_{out,H_2O} - T_{in,H_2O}\right) \qquad \text{--} \qquad (4b)$$

For the system that is considered in Figure 5, at steady state, we know that the internal energy of the system is constant, since when the fluid (liquid sodium) completes one cycle through the heat pipe, it returns to the same state for a given location of the heat pipe (and hence, $\dot{E}_{st} = 0$).

Now, Equation (4) can be modified, knowing that:

1. Heat transfer into the system occurs via radiation,

2. Heat transfer by convection takes place out of the heat pipe and into the flue gas since the heat pipe outer surface is at a temperature greater than the gas temperature,

3. Heat loss from the TEG to ambient (through natural convection on the outer surfaces of the TEG and heat pipe end) are taking place, along with heat transfer internal to the system in Figure 5 which causes specific enthalpy of water exiting the system $\left(\hat{h}_{out}\right)$ to be higher than that of water entering the system $\left(\hat{h}_{in}\right)$,

4. Work output from the system is the electrical power that is obtained from the TEG module, and

5. At steady state, the rate of energy storage (or accumulation) of the system is zero. In other words, the total energy of the system is constant at a state of equilibrium.

So, from Equation (4),

$$\dot{E}_{st} = \dot{Q}_{rad} - \dot{Q}_{conv} - \dot{Q}_{loss} - \dot{W}_{out} - \dot{m}_{H_2O}c_{p,H_2O}(T_{out,H_2O} - T_{in,H_2O}) = 0 \qquad \text{------------ (5a)}$$

From Equation (5a), the power output from the system may be calculated as:

$$\dot{W}_{out} = \dot{Q}_{rad} - \dot{Q}_{conv} - \dot{Q}_{loss} - \dot{m}_{H_2O}c_{p,H_2O}(T_{out,H_2O} - T_{in,H_2O}) \qquad \text{------------------------------ (5b)}$$

In order to calculate $\dot{W}_{out}$ for the system (the entire heat pipe and TEG including the water jacket), the following need to be calculated:

1. $\dot{Q}_{rad}$,

2. $\dot{Q}_{conv}$, and

3. $\dot{Q}_{loss}$.

Also, $\dot{m}_{H_2O}$, T_{out,H_2O} and T_{in,H_2O} need to be known for calculating the RHS of Equation (5b).

First, we look at how to estimate $\dot{Q}_{rad}$. For deriving the radiation heat transfer rate, the geometry of the system of two bodies – emitting and absorbing - is assumed to be simplified as shown in Figure 6.

Here, the upper surface of the heat pipe is approximated to be a flat surface of area equal to the sum of the upper curved surface area of the pipe having an outer diameter of 3.5 inches and 9.3 feet long, and flat surface area of two fins 3 inches wide and 9.3 feet long. The assumed values of the dimensions depicted in Figure 6 used for the calculations in Appendix D are:

$w_i = 3.3 \, ft., \, w_j = 9.5 \, in., \, L = 16.7 \, ft.,$ and $b_i = b_j = 9.3 \, ft.$

The rate at which total radiation of the emitting surface (in this case, the furnace) is absorbed by the heat absorbing surface (upper half of heat pipe) assuming the furnace as a blackbody can be calculated as:

$$\dot{Q}_{rad} = A_s F_{fs} \sigma \alpha_s (T_f^4 - T_s^4) \qquad \text{-- (6)}$$

where:

A_s --Area of heat pipe surface absorbing radiation (m^2),

F_{fs} ---View factor of heat pipe surface from furnace $(.)$,

σ --Stefan-Boltzmann constant $(= 5.67 \times 10^{-8}\ W/m^2\text{-}K^4)$,

α_s --Absorptivity of heat pipe surface $(.)$,

T_f --Absolute temperature of heat emitting surface (furnace) (K),

T_s --Absolute temperature of heat absorbing surface (heat pipe) (K)

For finding out the view factor F_{fs}, an empirical relation given in Reference [6] applicable for a system of two bodies as shown in Figure 6 can be used, which is as follows:

$$F_{ij} = \frac{\left[\left(\frac{w_i}{L} + \frac{w_j}{L}\right) + 4\right]^{1/2} - \left[\left(\frac{w_i}{L} - \frac{w_j}{L}\right) + 4\right]^{1/2}}{2\left(\frac{w_i}{L}\right)} \qquad \text{---} \qquad (7)$$

where:

w_i -- Width of emitting surface (m),

w_j -- Width of absorbing surface (m), and

L --Normal distance between the two surfaces (m)

$\dot{Q}_{rad}$ can also be expressed in terms of a radiation heat transfer coefficient (h_{rad}) [6] as:

$$\dot{Q}_{rad} = h_{rad} A_s \left(T_f - T_s\right) \qquad \text{---} \qquad (8)$$

where:

h_{rad} ---Radiation heat transfer coefficient $(W/m^2.K)$

By a comparison of Equations (6) and (8),

$$h_{rad} = F_{fs}\sigma\alpha_s\left(T_f^2 + T_s^2\right)\left(T_f + T_s\right) \qquad \text{--} \qquad (9)$$

By the definition of thermal resistance, radiation thermal resistance R_{rad} is defined as the reciprocal of h_{rad} from Equation (9) as:

$$R_{rad} = \frac{1}{h_{rad}} = \frac{1}{F_{fs}\sigma\alpha_s\left(T_f^2 + T_s^2\right)\left(T_f + T_s\right)} \qquad \text{---} \qquad (10)$$
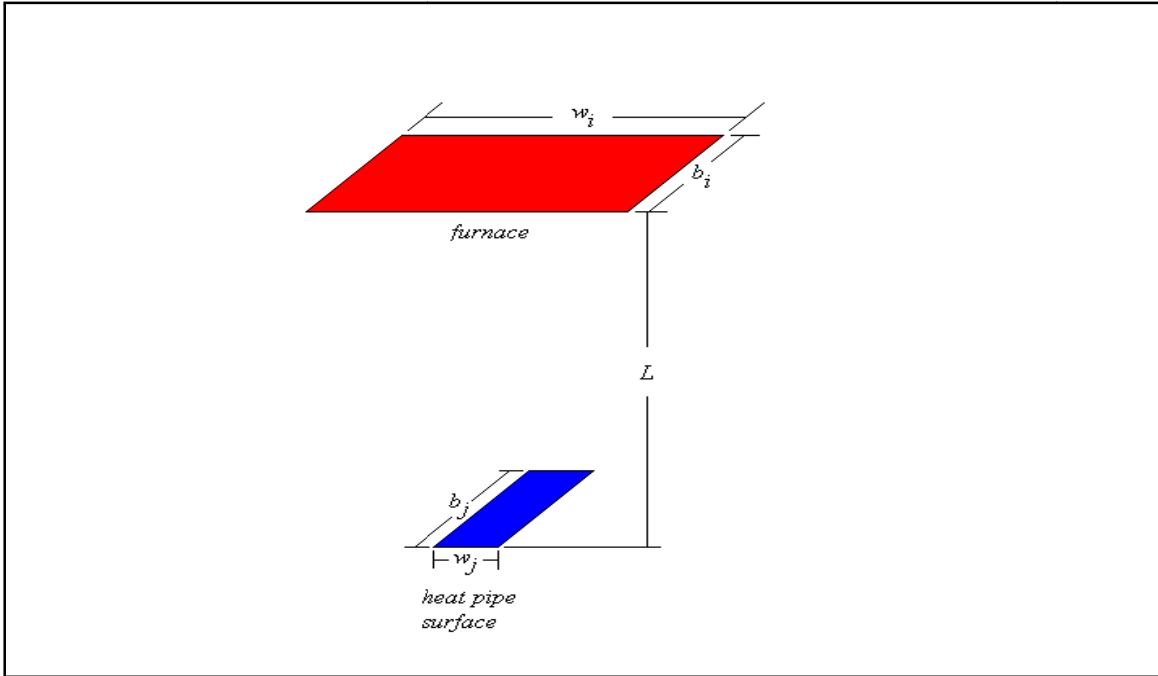
Figure 6: A schematic representation of the furnace and heat pipe surfaces for radiation heat transfer calculations

Forced convection heat transfer rate to a fluid (exhaust flue) from a cylindrical external surface in cross-flow is given as [6]:

$$\dot{Q}_{conv} = \bar{h}A_s(T_s - T_g)$$ -- (11)

where:

$\bar{h}$ --Average convective heat transfer coefficient *(W/m².K)*,

A_s --Total surface area of heat transfer *(m²)*,

T_s --Absolute temperature of heat transfer surface *(K)*, and

T_g --Absolute bulk temperature of exhaust gas *(K)*.

Note that in Equation (6), depending on the sign of the term on the right-hand side, $\dot{Q}_{conv}$ can be positive or negative, corresponding to heat being supplied to the part of the system in the flue duct (if $(T_g > T_s)$) or heat being removed from the system (if $(T_g < T_s)$) respectively.

In order to calculate the average convective heat transfer coefficient, certain correlations are commonly used according to Reference [6], one of which is the Zhukauskas correlation (used for a cylindrical surface in cross-flow). The Nusselt number based on the diameter is as follows:

$$\overline{Nu}_D = \frac{\bar{h}D}{k} = CRe_D^m Pr^n \left(\frac{Pr}{Pr_s}\right)^{1/4}$$ --- (12)

for

$$0.7 < Pr < 500$$

and

$$1 < Re_D < 10^6$$

where:

Re_D ---Reynold's number based on diameter of cylindrical surface (.),

Pr ---Prandtl number of the exhaust gas (.),

Pr_s ----------------------------Prandtl number of the exhaust gas calculated at the surface temperature (.),

D --Diameter of cylindrical surface *(m)*, and

k --Thermal conductivity of exhaust gas *(W/m-K)*

In Equation (7), the pre-determined constants C and m are given in Reference [6] as functions of Re_D and the constant n is given as a function of Pr, as given in Table 8 below.

Table 8: Constants C, m and n in Equation (7) for cylinder in cross-flow [6]

Re_D	C	m
1-40	0.75	0.4
40-1000	0.51	0.5
1000-2 x 10^5	0.26	0.6
2 x 10^5 – 1 x 10^6	0.076	0.7

Pr	n
≤ 10	0.37
> 10	0.36

From Equation (12), it follows that:

$$\bar{h} = \overline{Nu}_D \frac{k}{D} \quad\quad\quad (13)$$

Hence, $\bar{h}$ can be calculated for the given conditions of the exhaust gas flow and applied back to Equation (6), from which the convective heat transfer rate can be calculated, knowing the total surface area of heat transfer and the gaseous and surface temperatures. A sample calculation demonstrating calculation of $\bar{h}$ for a mean gas temperature $T_g = 600°C$ for various surface temperatures T_s is shown in Appendix D.

The next quantity that is of interest to calculate for solving Equation (5b) is $\dot{Q}_{loss}$. This is the additional heat loss from the TEG to the ambient, and is assumed to be occurring entirely due to free convection on the external surfaces of the TEG (although radiation heat transfer may also be occurring from the TEG external surfaces to the ambient). Equation (14) gives the quantitative expression for the same. If the external surfaces of the TEG can be approximated to be consisting of a sphere of the same diameter as the average dimension of the TEG setup, Equation (15) gives the average Nusselt number based on the diameter of an isothermal spherical surface exposed to natural convection [6], from which the average convection heat transfer coefficient $(\bar{h}^*)$ can be calculated.

$$\dot{Q}_{loss} = \bar{h}^* A_{int}(T_{m,o} - T_{amb}) \quad\quad\quad (14)$$

where:

$$\overline{Nu}_D = \frac{\overline{h}^* D_{int}}{k_{Na}} = \left\{ 0.60 + \frac{0.387 Ra_D^{(1/6)}}{\left(1 + \left(\frac{0.559}{Pr}\right)^{\frac{9}{16}}\right)^{\frac{8}{27}}} \right\}^2 \tag{15}$$

for $Ra_D \leq 10^{12}$

where:

D_{int} -- Internal diameter of the heat pipe *(m)*,

k_{Na} -- Thermal conductivity of liquid sodium *(W/m.K)*,

A_{int} -- Internal curved surface area of the heat pipe *(m²)*,

$T_{m,o}$ -- Heat pipe outer metal surface temperature *(K)*, and

T_{amb} -- Ambient temperature *(K)*.

As can be observed from Equation (14), the Rayleigh number based on the diameter of the spherical surface (Ra_D) needs to be calculated [6] as:

$$Ra_D = \frac{g\beta(T_{m,o} - T_{amb})D_{int}^3}{\vartheta\alpha} \quad \text{---} \tag{15a}$$

where:

g -- Acceleration due to gravity *(m/s²)*,

β -- Thermal compressibility *(m²/N)*,

ϑ -- Kinematic viscosity of liquid sodium *(m²/s)*,

$\alpha = \left[\frac{k}{\rho c_p}\right]_{Na}$ -- Thermal diffusivity of liquid sodium *(m²/s)*.

Another approach to consider in determining the effect of deposit formation on the heat pipe surface on convection heat transfer rate is to study the individual thermal resistances due to the deposit layer and the metal. Reference [13] gives such a representation of the heat transfer surface when particulate deposits are present on the 'hot-side' and 'cold-side' of a heat exchanger surface, where convection from the hot side is the only mode of heat transport into the system.
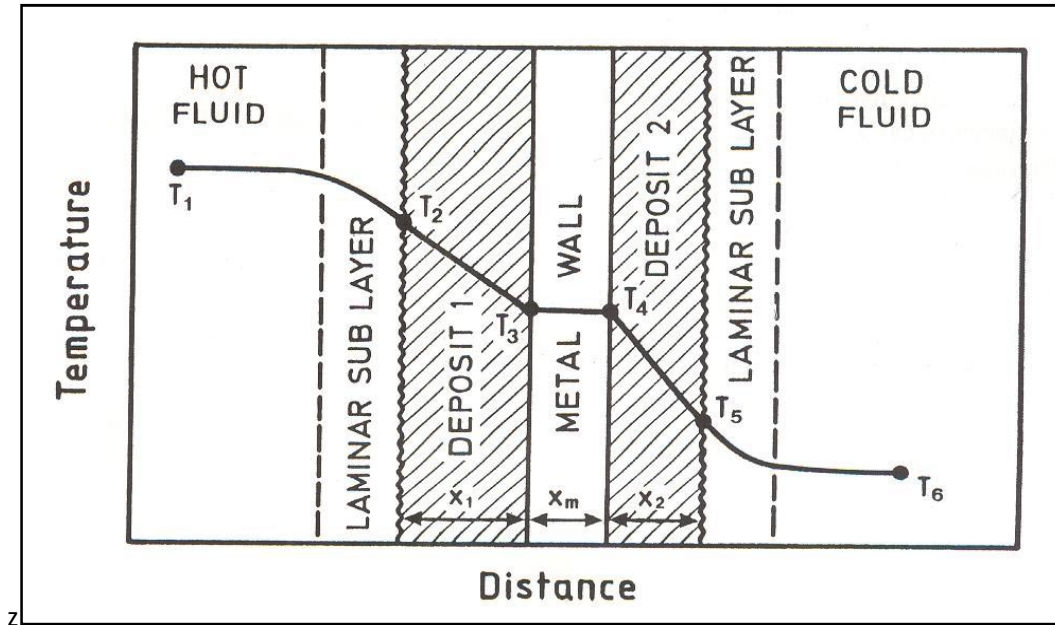
Figure 7: Temperature distribution across fouled heat exchanger surfaces for convection alone [13]

Figure 7 shows a typical temperature distribution across heat exchanger surface thickness (reproduced from Reference [13]) considering only a convection heat transfer, which is typical for two-fluid heat exchangers. The heat transfer rate from the hot fluid to the cold fluid for a composite wall is given as [6]:

$$\dot{Q}_{conv} = UA_s(T_1 - T_6)$$ -- (16)

and

$$U = \frac{1}{R_{tot}} = \frac{1}{\left[\left(\frac{1}{h_{hot}}\right) + \left(\frac{w_1}{k_1}\right) + \left(\frac{w_m}{k_m}\right) + \left(\frac{w_2}{k_2}\right) + \left(\frac{1}{h_{cold}}\right)\right]}$$ --- (17)

where:

U --- Overall heat transfer coefficient *(W/m².K)*,

A_s -- Surface area of heat transfer *(m²)*,

T_1 -- Absolute temperature of hot fluid *(K)*,

T_6 --- Absolute temperature of cold fluid *(K)*,

25

R_{tot} -- Total thermal resistance of the system *(m².K/W)*,

h_{hot} -- Hot-side convection heat transfer coefficient *(W/m².K)*,

h_{cold} --- Cold-side convection heat transfer coefficient *(W/m².K)*,

w_1 -- Thickness of deposit 1 [hot-side] *(m)*,

w_m --- Thickness of metal *(m)*,

w_2 --- Thickness of deposit 2 [cold-side] *(m)*,

k_1 -- Thermal conductivity of deposit 1 *(W/m.K)*,

k_m --- Thermal conductivity of metal *(W/m.K)*, and

k_2 --- Thermal conductivity of deposit 2 *(W/m.K)*,

From Equations (16) and (17), it can be observed that the heat transfer rate by convection will decrease with increasing particulate layer thickness, due to the increase in total thermal resistance of the system by an increasing magnitude of the deposit thermal resistance - $\frac{w_1}{k_1}$ term - in Equation (17).

If a radiation heat transfer is added into this scenario, a new temperature profile is expected at equilibrium, as schematically shown in Figure 8.
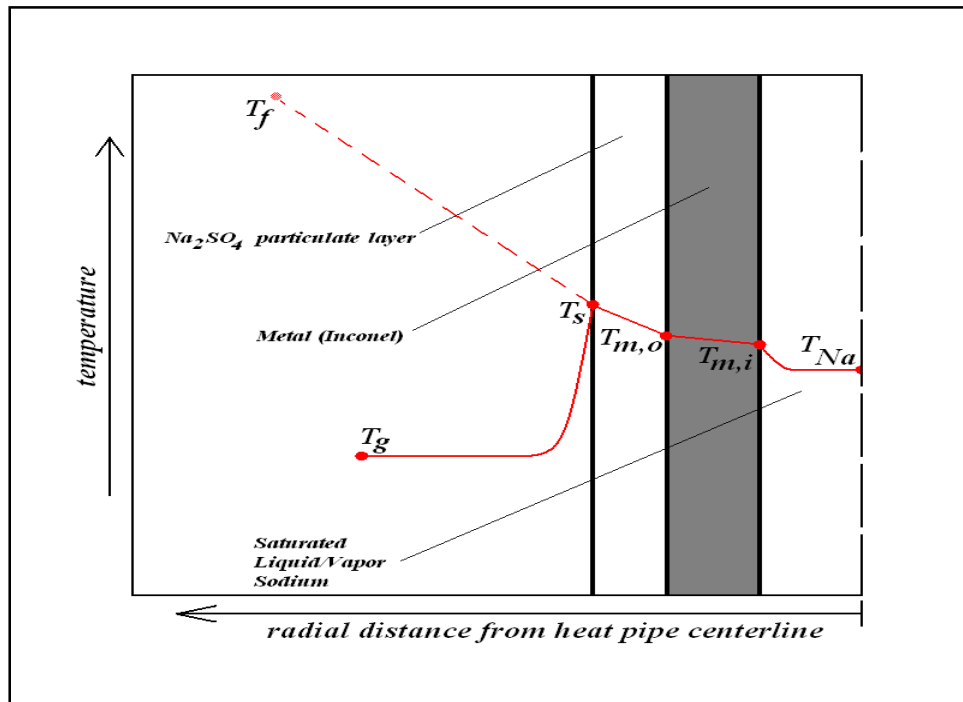
Figure 8: Schematic of temperature profile along radial direction from heat pipe axis

The equivalent thermal circuit of the system is shown in Figure 9.
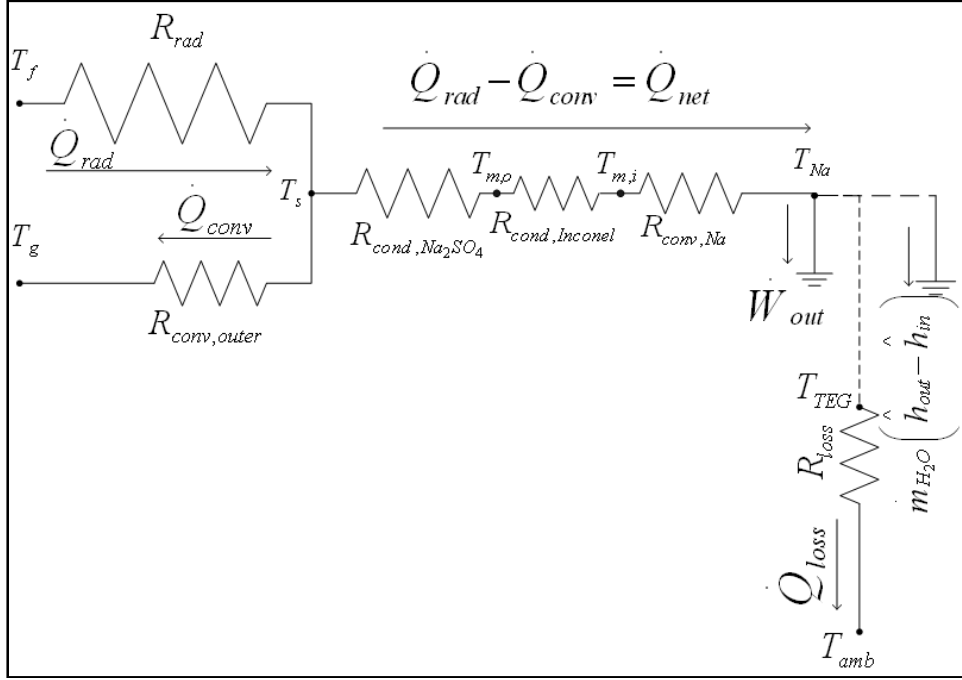
Figure 9: Equivalent thermal circuit of the heat pipe

For the conduction – convection mode heat transfer that takes place through the heat pipe, from Figure 9, the following equations can be developed:

$$\dot{Q}_{rad} = \frac{1}{R_{rad}} A_{up}\left(T_f - T_s\right) \quad \text{---} \quad (18)$$

where R_{rad} is given by Equation (10).

$$\dot{Q}_{conv} = \frac{1}{R_{conv,outer}} A_{up+dn}\left(T_s - T_g\right) \quad \text{---} \quad (19)$$

where $R_{conv} = \frac{1}{h_{conv}} = \frac{1}{\bar{h}}$ and $\bar{h}$ is given by Equations (13) and (12).

$$\dot{Q}_{net} = \dot{Q}_{rad} - \dot{Q}_{conv}$$
$$= \left[\frac{1}{R_{cond,Na_2SO_4} + R_{cond,inconel} + R_{conv,Na}}\right] A_{up+dn}(T_s - T_{Na}) \quad \text{-----------------} \quad (20)$$

where:

$$R_{cond,Na_2SO_4} = \frac{w_{dep}}{k_{dep}} \quad \text{--} \quad (21)$$

$$R_{cond,inconel} = \frac{w_m}{k_m} \quad \text{---} \quad (22)$$

27

$$R_{conv,Na} = \frac{1}{\overline{h}^*} \quad \text{--} \quad (23)$$

Combining Equations (18), (19) and (20), a single equation having T_s as the unknown can be arrived at as:

$$\frac{1}{R_{rad}} A_{up}(T_f - T_s) - \frac{1}{R_{conv,outer}} A_{up+dn}(T_s - T_g)$$

$$- \frac{1}{(R_{cond,Na_2SO_4} + R_{cond,inconel} + R_{conv,Na})} A_{up+dn}(T_s - T_{Na}) = 0 \quad \text{------------} \quad (24)$$

Equation (24) is of the 4th degree in T_s and can be solved for T_s for known values of T_f, T_g and T_{Na} and individual thermal resistances R_i's. Here, note that R_{rad} is also a function of T_s (from Equation (10)).

Looking at Figure 8 and Equation (23), it can be noted that:

1. When there is no Na_2SO_4 deposit present on the outer surface of the heat pipe, $R_{cond,Na_2SO_4} = 0$ and $T_s = T_{m,o}$.

2. As R_{cond,Na_2SO_4} increases, the value of T_s increases from that of $T_{m,o}$. From Equations (6) and (11), this causes a decrease in $\dot{Q}_{rad}$ and increase in $\dot{Q}_{conv}$ from their respective 'clean' values.

3. Also, from Equation (6), $\dot{Q}_{rad}$ decreases from its 'clean' value because of decrease in α_s, the absorptivity of the surface of the heat pipe.

4. Looking at Equation (5b), if all other variables on the RHS remain the same as before ('clean'), $\dot{W}_{out}$ at a time during operation of the heat pipe when there is a certain finite value of deposit thickness on the heat pipe will be less than its 'clean' value. This is precisely the degradation of heat pipe performance.

As a result of fouling of the heat pipe surface, the changes occurring in overall heat transfer rate are due to:

1. Decrease in radiation heat transfer rate into the heat pipe due to:

   a. Decrease in absorptivity (α_s) of the heat pipe surface, and

   b. Increase in temperature of outer surface (as the surface gets coated with Na_2SO_4 deposit) of heat pipe (T_s),

2. Increase in convection heat transfer rate out of the heat pipe due to:

   a. Increase in surface temperature (T_s)

In other words, $\dot{Q}_{net}$ as given by Equation (20) decreases with increasing fouling of the heat pipe.

Parametric equations of the heat transfer rates via convection and radiation and convection and radiation thermal resistances when the heat pipe surface is 'clean' and when a sodium sulfate particulate layer of an arbitrary thickness is present on the heat pipe surface is given in Appendix D.

The next section (section 4) gives a description of models developed to predict the condensation products from exhaust flue gases of glass furnaces and conclusions that were drawn by the authors of these models. Section 4 also lists commonly used cleaning methods for fouled heat exchanger surfaces and specific methods that seem to be potential solutions to the formation of Na₂SO₄ particulate on the heat pipe external surfaces.

4. Sodium Sulfate Particulate Prevention and Control

From physical inspection of the particulate formed on the surfaces of the exhaust flue at the PPG plant in Meadville, PA, the particulate formed is a white powdery substance, and an X-Ray Fluorescence (XRF) method analysis conducted by PPG showed that ~95% (by weight) of the particulate was Na_2SO_4. Hence the formation and cleaning methods that were looked into for this report were focused on Na_2SO_4 particulate formation and cleaning, although a list of commonly used cleaning methods is also given in this section.

4.1. Factors Affecting the Formation of Na₂SO₄ Particulate on Heat Exchanger Surfaces – Modeling Studies and Results

There are specific factors affecting the formation and rates of formation of condensation deposits on furnace surfaces. Kirkbride et al. [5] and Beerkens [3] describe the chemical changes taking place in flue gases from glass furnaces during cooling. In glass furnaces, the sodium sulfate dust particles have an average diameter of **0.10 to 0.15 μm** [3, 4]. Because these particle sizes can be considered as being in the 'small particles' range, the contributions of mechanisms 1 (gravitational settling) and 2 (inertial deposition) (mentioned in section 3.1 of this report) to overall deposit formation rate can be considered to be negligible. The deposition surface in question here is smooth (the heat pipe is made of Inconel alloy, and sanded and coated with a paint for high-temperature use), and hence mechanism 3 (interceptional deposition) also can be considered to be negligible. This means that only deposition by Brownian diffusion and by thermophoretic forces are important in the case under study. Also, the two major deposition products formed are sodium sulfate (Na_2SO_4) and sodium bisulfate $(NaHSO_4)$, depending on the temperature range of the surface of deposition: Na_2SO_4 if the surface temperature is greater than **570 K** and $NaHSO_4$ if the surface temperature is below **540 K** [3].

4.1.1. Kirkbride Model

Reference [16] outlines the changes occurring due to cooling of flue gases from a glass furnace. Reference [16] also defines flat glass as a soda-lime-silica glass of approximate composition 72% SiO_2, 12% Na_2O, 14% $(CaO + MgO)$, with small amounts of Al_2O_3 and K_2O. The raw materials for the production of flat glass are: sand (SiO_2), limestone $(CaCO_3)$, dolomite $(CaCO_3.MgCO_3)$, soda ash (Na_2CO_3) and saltcake (Na_2SO_4). These raw materials are heated together in large regenerative furnaces by burning either oil or natural gas, and the furnace temperatures can reach 1550-1600°C. This melting point leads to entrainment of some of the raw materials in the combustion gases and to volatilization of some of the constituents from both the raw materials and the 'melt' or the molten mixture. Exhaust gases leave the furnace and enter the exhaust flue at about 1500°C, and are cooled as they pass through the flue. According to Reference [16], "at some stage during the cooling process, the volatile material in the gas stream condenses and deposits material on the walls of the gas passages". Reference [16] presents:

1. The chemical thermodynamic calculation of the equilibrium molecular composition of the exhaust gas from a typical flat glass furnace as it leaves the furnace, and

2. The chemical changes which might be expected to occur as the exhaust gas cools down, leading to the condensation of one or more species.

Sodium sulfate gets entrained in the exhaust gas from the saltcake that is one of the raw materials used in the manufacture of flat glass. Sodium sulfate vaporizes congruently, that is, the vapor phase and the condensed (solid or liquid) phase have the same stoichiometric composition. This can be represented as [16]:

$$Na_2SO_4(s\ or\ l) \rightarrow Na_2SO_4(g)$$ --- (R1)
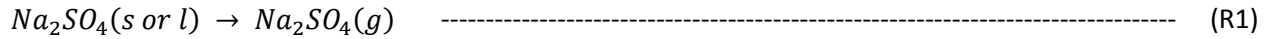
Also, a vapor pressure $p(Na_2SO_4)$ of sodium sulfate can be defined above the condensed phase, which gives a quantitative measure of sodium sulfate present in the vapor phase. In the vapor phase, $Na_2SO_4(g)$ can dissociate into other chemical species, according to the following likely chemical reactions (Reactions (R2), (R3) and (R4) and if the atmosphere is damp, Reaction (R5)) [16]:

$$Na_2SO_4(g) \rightarrow 2Na(g) + SO_2(g) + O_2(g)$$ -- (R2)

$$Na_2SO_4(g) \rightarrow Na_2O(g) + SO_2(g) + \frac{1}{2}O_2(g)$$ -- (R3)

$$Na_2SO_4(g) \rightarrow 2NaO(g) + SO_2(g)$$ --- (R4)

$$Na_2SO_4(g) + H_2O(g) \rightarrow 2NaOH(g) + SO_2 + \frac{1}{2}O_2(g)$$ --- (R5)
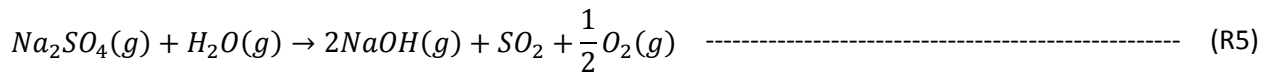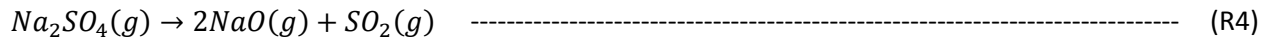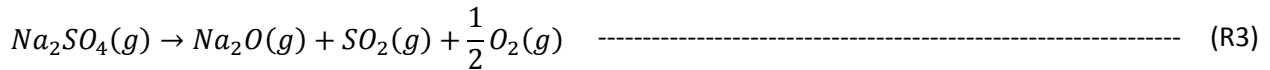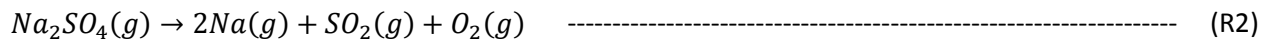
In order to calculate the equilibrium composition of the exhaust gas, the following steps are executed:

1. It is assumed that the significant constituents of the exhaust gas consist of the elements sodium, sulfur and chlorine. The chemical species containing these elements are:

    a. containing sodium – $NaO, Na_2O, NaOH, NaCl, Na_2CO_3, Na_2SO_4, Na$

    b. containing sulfur - SO_2, SO_3, Na_2SO_4

    c. containing chlorine – $HCl, NaCl$

2. Initially, all the sodium, sulfur and chlorine are present as $NaOH, SO_2$ and HCl (the 'primary' species),

3. Equations are written (R5 thru R9) expressing the formation of the other possible species ('secondary' species) from the primary species and equilibrium constants are evaluated for

31

these reactions from thermodynamic data available for the range of temperatures considered (*1000 – 1800 K*) as shown in Table 9,

4. Mass balance equations are written for the primary species, considering condensation of Na_2SO_4, Na_2CO_3 and $NaCl$ (the amounts of majority species are considered so large that they essentially remain constant) as shown in Equations (25), (26) and (27),

5. Equilibrium and mass balance equations are simultaneously solved with the constraint that the amounts of Na_2SO_4, Na_2CO_3 and $NaCl$ in the gas cannot exceed the saturated vapor pressure of the individual compounds calculated from thermodynamic data at the temperature of calculation.

Table 9: Chemical reactions and equilibrium constants used in waste gas equilibrium calculations [16]

	Chemical reaction equations and expressions for equilibrium constants	Equilibrium constant at temperature *(K)*					
		1000	1200	1300	1400	1500	1800
1	$NaOH(g) + HCl(g) \rightarrow NaCl(g) + H_2O(g)$ --(R6)						
	$K_1 = \dfrac{n_{NaCl}n_{H_2O}}{n_{NaOH}n_{HCl}}$	1.05×10^6	9.38×10^4	3.72×10^4	1.65×10^4	8.28×10^3	1.64×10^3
2	$2NaOH(g) + CO_2(g) \rightarrow Na_2CO_3(g) + H_2O(g)$ --(R7)						
	$K_2 = \dfrac{n_{Na_2CO_3}n_{H_2O}(n)}{(n_{NaOH})^2 n_{CO_2}}$	1.02×10^4	3.52×10^1	4.90×10^0	9.77×10^{-1}	2.51×10^{-1}	1.28×10^{-2}
3	$2NaOH(g) + SO_2(g) + \frac{1}{2}O_2(g) \rightarrow Na_2SO_4(g) + H_2O(g)$ --(R8)						
	$K_3 = \dfrac{n_{Na_2SO_4}n_{H_2O}(n)^{1/2}}{(n_{NaOH})^2 n_{SO_2}(n_{O_2})^{1/2}}$	1.77×10^{14}	2.84×10^9	5.62×10^7	1.64×10^6	8.93×10^4	1.19×10^2
4	$NaOH(g) + \frac{1}{4}O_2(g) \rightarrow NaO(g) + \frac{1}{2}H_2O(g)$ ---(R9)						
	$K_4 = \dfrac{n_{NaO}(n_{H_2O})^{1/2}(n)^{-(1/2)}}{n_{NaOH}n_{O_2}^{1/4}}$	7.88×10^{-8}	2.66×10^{-6}	1.03×10^{-5}	3.28×10^{-5}	8.98×10^{-5}	9.47×10^{-4}
5	$SO_2(g) + \frac{1}{2}O_2(g) \rightarrow SO_3(g)$ --(R10)						
	$K_5 = \dfrac{n_{SO_3}(n)^{1/2}}{n_{SO_2}(n_{O_2})^{1/2}}$	1.82×10^0	2.59×10^{-1}	1.23×10^{-1}	6.52×10^{-2}	3.80×10^{-2}	1.06×10^{-2}

$$q_{NaOH} = n_{NaOH} + n_{NaCl} + 2n_{Na_2SO_4} + 2n_{Na_2CO_3} + D_{NaCl} + 2D_{Na_2SO_4} + 2D_{Na_2CO_3} \quad \text{----------------(25)}$$

$$q_{SO_2} = n_{SO_2} + n_{SO_3} + n_{Na_2SO_4} + D_{Na_2SO_4} \quad \text{--(26)}$$

$$q_{HCl} = n_{HCl} + n_{NaCl} + D_{NaCl} \quad \text{--(27)}$$

where:

n_i --Equilibrium amount of species i in system,

q_j ---Total number of moles of 'primary' species j in system initially,

(n) --Total number of moles in system at equilibrium, and

D_k --Equilibrium amount of species k condensed

Table 10: Expressions for vapor pressure and vapor pressure values from thermodynamic data at various temperatures [16]

Specie	Expression for vapor pressure	Vapor pressure *(atm)* at temperature *(K)*					
		1000	1200	1300	1400	1500	1800
$NaOH$	$\log P = \dfrac{-7.520}{T} + 4.55$	$1.07\text{x}10^{-3}$	$1.92\text{x}10^{-2}$	$5.82\text{x}10^{-2}$	$1.51\text{x}10^{-1}$	$3.44\text{x}10^{-1}$	$2.35\text{x}10^{0}$
$NaCl$	$\log P = \dfrac{-11.530}{T} - 3.48\log T + 17.89$	$6.74\text{x}10^{-5}$	$3.69\text{x}10^{-3}$	$1.53\text{x}10^{-2}$	$8.49\text{x}10^{-2}$	$1.41\text{x}10^{-1}$	$1.43\text{x}10^{0}$
Na_2SO_4	$\log P = \dfrac{-1.554 \, x \, 10^4}{T} + 5.86$	$2.09\text{x}10^{-10}$	$8.32\text{x}10^{-8}$	$8.13\text{x}10^{-7}$	$5.74\text{x}10^{-6}$	$3.16\text{x}10^{-5}$	$1.70\text{x}10^{-3}$
Na_2CO_3	$\log P = \dfrac{-1.15 \, x \, 10^4}{T} + 3.96$	$2.88\text{x}10^{-8}$	$2.40\text{x}10^{-6}$	$1.29\text{x}10^{-5}$	$5.56\text{x}10^{-5}$	$1.95\text{x}10^{-4}$	$3.71\text{x}10^{-3}$

The results of equilibrium partial pressure of the chemical species in a sample exhaust gas of composition as shown in Table C2 are given in Figure 10 (taken from Reference [16]).
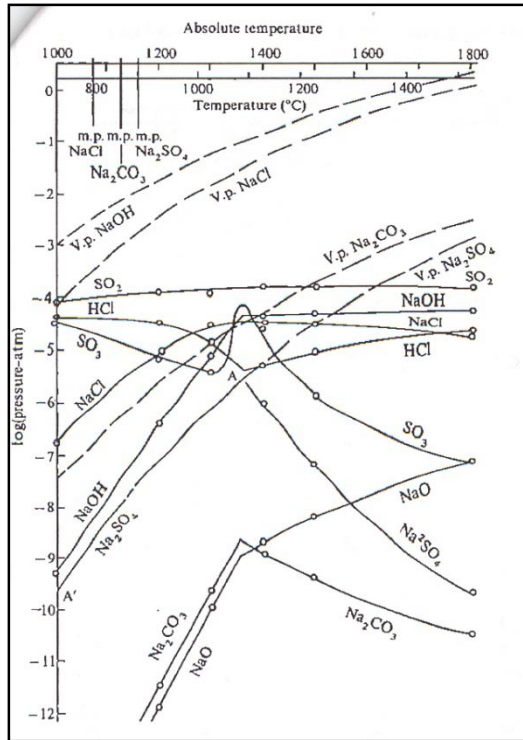
Figure 10: Equilibrium pressure of materials in the exhaust gas from a gas-fired glass furnace [16]. Solid lines represent the variation of pressure with temperature of the indicated species, and dotted lines indicate the variation of vapor pressure with temperature of the pure compound.

Figure 11 (from Reference [16]) shows the change in distribution of the available sodium among different compounds with changes in temperatures.
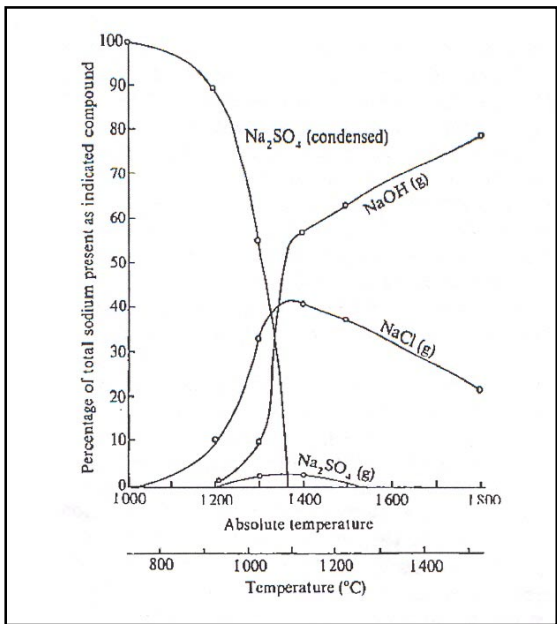
Figure 11: Distribution of sodium between different compounds in the waste gas from a gas-fired flat glass furnace as function of temperature [16]

34

From Figure 10 and Figure 11 [16], the following can be observed:

1. At the highest temperature (1800 K), virtually all of the sodium is present as either $NaOH$ (79%) or $NaCl$ (21%).

2. As the gas cools, both Na_2SO_4 and Na_2CO_3 are formed increasingly by chemical reactions (R8) and (R7) respectively.

3. At 1400 K, Na_2SO_4 accounts for only 2.4% of sodium present (see Figure 11).

4. At 1300 K, the gas is saturated with Na_2SO_4 (see Figure 10). Further cooling gives rise to condensation of Na_2SO_4 and the vapor pressure of Na_2SO_4 follows the curve $A - A'$ (see Figure 10) and correspondingly, increasing amounts of Na_2SO_4 condense, as can be seen from Figure 11. By 1200 K, about 90% of the sodium has condensed as Na_2SO_4 and at 1000 K, this reaches virtually 100%.

5. As can be seen from Figure 11, condensation of Na_2SO_4 causes a reduction in the total amount of sodium in the gas phase, and thus causes a reduction in the $NaOH$ and Na_2CO_3 concentrations. $NaCl$ concentration also falls, although at a much more gradual rate than that of $NaOH$.

6. The condensation of Na_2SO_4 from the exhaust gas as it is cooled, is due to 2 factors:

   a. Increasing stability of Na_2SO_4 molecule in the gas, and

   b. The fact that among the compounds of sodium, Na_2SO_4 has the lowest saturation vapor pressure at a given temperature (as can be seen from the dotted lines in Figure 10).

The Kirkbride model [16] (published in 1979) thus provided a basis for calculating the condensation of sodium in the form of its compounds at different temperatures of the exhaust gas as it cools down. The subsequent research works since about models concerning deposition and condensation products from exhaust gases of glass furnaces (for instance, [12], [18], [17] and [3]) have cited the Kirkbride model [16] as a reference for chemical changes that take place in flue gases from glass furnaces during cooling. The next sub-section (4.1.2) describes the more advanced models that were developed during the period 1986-1989 by researchers at the TNO institute of Applied Physics at Delft, Netherlands.

4.1.2. Beerkens et al. Model

Reference [12] details a model that was developed (by R.G.C Beerkens as part of his doctoral research) and used to predict the condensation products from flue gases of a soda-lime glass furnace. References [18] and [17] are research papers published with Beerkens as the primary author, and Reference [3] was co-authored by Beerkens. The relevant observations from these four references are consolidated and presented in this sub-section.

Reference [18] describes findings from experiments conducted using simulated flue gases (on a laboratory scale) from glass furnaces compared to results from a theoretical model. According to the authors, "solid or liquid alkali sulfates are the main compounds formed during the cooling of alkali-rich and sulfur-rich flue gases". Condensation can occur in two ways – (a) increasing super-saturation of salt vapors as the temperature drops leads to condensation in the bulk gas, resulting in the formation of small particles, *0.05 – 10 μm* in diameter, and (b) condensation due to presence of relatively cold surfaces in the exhaust gas flow, leading to deposition of liquid or solid salts on these surfaces. A thermodynamic model for predicting the condensation products from exhaust gases of glass furnaces was published in Reference [16], although it was not validated against experimental data. Reference [18] explains research that was carried out to compare experimental data from simulated glass furnace exhaust gases to results of calculations based on thermodynamics.

In theory, deposition of compounds results in a decrease in their concentration along the direction of exhaust flow. However, deposition of salts accounts for *5-10%* [18] of the salt content in flue gases. Due to this reason, the model presented in Reference [16] did not take into account the decreasing concentration of compounds in the exhaust gas due to deposition. In Reference [18], experimental and theoretical studies were carried out with the six flue gas compositions as listed in Table C5 in Appendix C. Calculations were made in Reference [18] to estimate the influence of changing concentrations of compounds in the exhaust gases (due to condensation of those compounds) on further condensation. Also, a reaction scheme was constructed (as shown in Table 11) in which all possible compounds were included and calculations were done at various temperatures to determine the equilibrium composition of exhaust gases, with the constraint that the vapor pressure for the individual substance cannot exceed the saturation vapor pressure at the temperature of calculation. Hence, condensing products will have their vapor pressures equal to saturation vapor pressure at a given temperature.

Gas *I* (with sodium, chlorine and sulfur) (see Table C5 in Appendix C) resembled the composition of a typical soda-lime glass furnace flue gas mentioned in Reference [16] (see Table C2 in Appendix C). Thermodynamic calculations show that only Na_2SO_4 was expected to condense from this gas, which was in agreement with the experimental results from Reference [18]. However, a temperature difference of about *100 K* between the dew points determined via thermodynamic calculations (*1320 K*) and experimental measurements (*1220 K*) was observed, and was thought to be the results of reaction and/or condensation kinetic limitations, although the exact reason for this difference was not known. Decreasing the oxygen concentration from *4.5%* to *2.25%* changed the dew point of sodium sulfate only by *5 K*.

Table 11: Gaseous and condensed compounds included in reaction scheme considered in Reference [18]

Gas number	Gaseous species	Condensed Species
I	CO_2, H_2O, O_2, N_2, Ar, $NaOH$, Na, $NaCl$, HCl, Na_2Cl_2, Na_2SO_4, $Na(OH)_2$, SO_2, SO_3, Na_2CO_3	$NaCl$, Na_2SO_4, Na_2CO_3
II	CO_2, H_2O, O_2, N_2, Ar, $NaOH$, Na, $NaCl$, HCl, Na_2Cl_2, Na_2SO_4, $Na(OH)_2$, SO_2, SO_3, Na_2CO_3, Mg, MgO, $MgOH$, $Mg(OH)_2$, $MgCl_2$, $MgCl$	$NaCl$, Na_2SO_4, Na_2CO_3, MgO, $MgCl_2$, $MgSO_4$
III	CO_2, H_2O, O_2, N_2, Ar, $NaOH$, Na, $NaCl$, HCl, Na_2Cl_2, Na_2SO_4, $Na(OH)_2$, SO_2, SO_3, Na_2CO_3, $Ca(OH)_2$, $CaCl_2$, $CaCl$	$NaCl$, Na_2SO_4, Na_2CO_3, CaO, $CaCl_2$, $CaSO_4$
IV	CO_2, H_2O, O_2, N_2, Ar, KOH, $(KOH)_2$, K, KF, K_2F_2, K_2CO_3, KBO_2, $K_2B_4O_7$, B_2O_3, BO_2, HBO_2, H_3BO_3, BF_3, SO_2, SO_3, SF_6, K_2SO_4	K_2SO_4, $K_2B_4O_7$, KBO_2, B_2O_3, KF
V	CO_2, H_2O, O_2, N_2, Ar, PbO, Pb_2O_2, Pb_3O_3, Pb_4O_4, Pb_5O_5, Pb_6O_6, Pb, Pb_2	PbO, Pb_3O_4, $Pb(OH)_2$, $PbCO_3$
VI	CO_2, H_2O, O_2, N_2, Ar, PbO, Pb_2O_2, Pb_3O_3, Pb_4O_4, Pb_5O_5, Pb_6O_6, Pb, Pb_2, $PbSO_4$, SO_2, SO_3	PbO, Pb_3O_4, $Pb(OH)_2$, $PbCO_3$, $PbSO_4$, $PbO.PbSO_4$, $2PbO.PbSO_4$, $3PbO.PbSO_4$, $4PbO.PbSO_4$

Gas *II* (with sodium, chlorine, sulfur and magnesium) differed from I in three ways: Mg was added, Na content was reduced by 50%, and S content was decreased to *27 ppm*. Three condensation products were determined from experimental measurements – above 940 K, only MgO was found. As the temperature decreases, increasing fractions of Na_2SO_4 were found, and below 890 K, $NaCl$ condensed. These results are shown in Figure 12, along with semi-quantitative estimation of the same compounds from experiments.

Gas *III* (with sodium, chlorine, sulfur and calcium) differed from gas II in one way: the Mg dopant was replaced by an equal amount (*33 ppm*) of Ca. As can be seen from the semi-quantitative estimation (a) in Figure 13, $CaSO_4$ and allied compounds were found from *800 – 1150 K*. Comparable amounts of Na_2SO_4 was also found in the same temperature range, and $NaCl$ was found below *950 K*. There is marked variation of experimental results (see Figure 13(a)) compared to theoretical calculations (see Figure 13 (b)) in this case: According to the theoretical calculations, considerable amounts of condensed CaO should have been observed above 850 K, contradictory to what was observed from experiments. This was thought to be because even though CaO is formed, the particles were so fine that the deposition on the platinum surface used for the experiments was probably negligible. Also, below 950 K, the formation of Na_2SO_4 was inhibited bythe condensation of $NaCl$, according the theory and experiments.
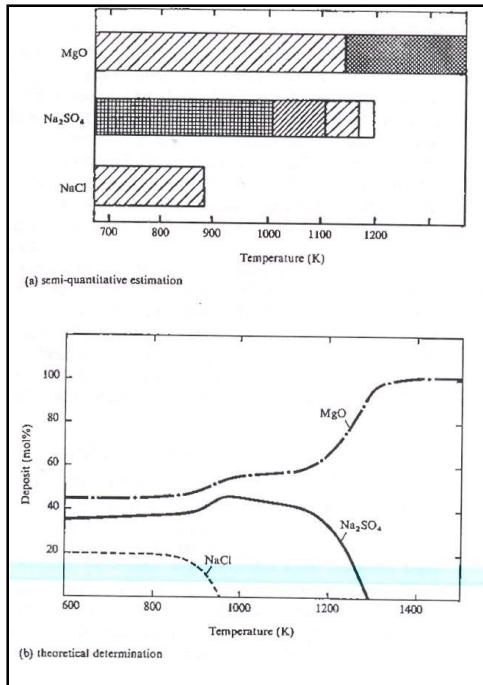
Figure 12: Distribution of deposition compounds in samples from gas *II* vs. temperature [18]
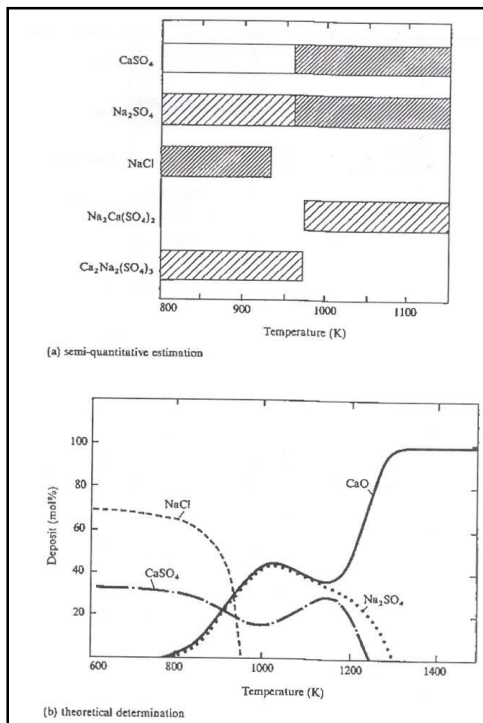
Figure 13: Distribution of deposition compounds in samples from gas III vs. temperature [18]

Research outlined in Reference [18] thus gave insight into the reliability of a thermodynamic equilibrium model for predicting chemical changes in exhaust gases from glass furnaces. However, discrepancies were found between experiments and calculations using the model, which was thought to be due to the model not taking into account the kinetic limitation aspects that might have affected the dew point temperatures predicted by the model. The theoretical model was thus found out to be suitable for predicting the nature of condensation products, but predictions of deposition rates could not be made directly and accurately with this model.

Reference [17] gives a new mathematical model developed by R.G.C. Beerkens and H. de Waal, which describes the processes involved in the deposition of different compounds in flue gas channels. The motivation for the development of this model was the fact that for regenerator construction and heat exchanger function, it is important to determine the influence of flue gas composition and velocity on deposition rates of different compounds. Also, the previous mathematical model was not capable of predicting deposition rates of different compounds directly, and this was another improvement made with this model [17]. According to the authors, deposition of compounds in flue gas channels takes place by two processes: (a) condensation of salt compounds or metal oxides on the relatively cold channel surfaces, and (b) deposition of fine particles already present in the flue gas, formed by condensation reactions. The former process is predominant at higher exhaust temperatures (> *800 K*), and the latter is important at temperatures below *800 K* (*527°C*). Deposition process (a) is schematically shown in Figure 14, reproduced from Reference [17].
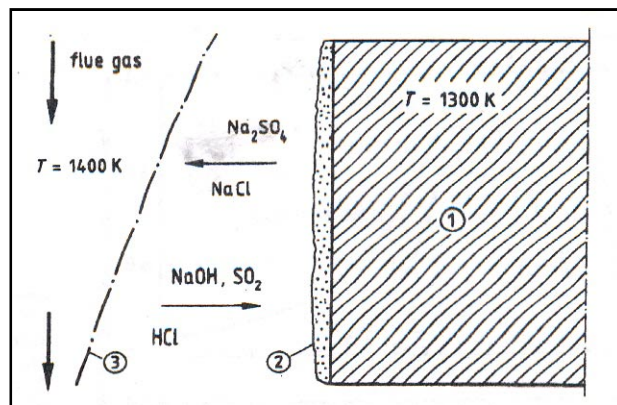
Figure 14: Schematic representation of deposition process in regenerator of a soda-lime glass furnace. 1: regenerator brick, 2: deposition, 3: boundary layer [17]

The chemical composition of the flue gas is calculated on a thermodynamic basis. Since the gas temperature is generally higher than the surface temperature by *30 − 50 K*, the composition of the exhaust gas in the boundary layer (region (3) in Figure 14) is considered different from that of the bulk phase. This concentration gradient leads to a diffusion of gaseous salt components of the bulk gas towards the relatively cool surfaces.

The method used to determine deposition rates from flue gases is based on Chemically Frozen Boundary Layer (CFBL) theory. This model consists of four assumptions:

1. The main flow of exhaust gases is in thermodynamic equilibrium,

2. The flue gas phase in the boundary layer is also in thermodynamic equilibrium,

3. No chemical reactions occur in the boundary layer (chemically frozen), and

4. The net diffusion rates of the gaseous components determine the condensation/deposition rates of those compounds at the surface.

The most important gaseous components for the deposition process in a flue gas sample from a soda-lime glass furnace are $NaOH$, Na, $NaCl$, Na_2SO_4, HCl, SO_2, SO_3, N_2, NO_x, O_2, H_2O and CO_2. By a thermodynamic calculation procedure, local flue gas compositions were calculated for different temperatures of the gas. The flue gas composition at the surface was also determined by thermodynamic equilibrium calculations including the determination of the composition of the condensed material at the surface. These calculations were executed iteratively combined with mass transport equations governing the diffusion of the gas molecules through the boundary layer. For example, the diffusion equation of $NaOH$ molecules is given in Equation (28) [17]:

$$j_{NaOH} = \frac{1}{M_{NaOH}} \cdot \frac{Sh_{NaOH}}{L} \cdot D_{NaOH} \cdot F_s(NaOH) \cdot \rho \cdot \left((w^m_{NaOH} - w^s_{NaOH}) + \frac{\tau_{NaOH}}{F_s(NaOH)} \cdot w^s_{NaOH} \right) \quad --- \quad (28)$$

where:

j_i --Molar flux *(mol/m².s)*,

M_i ---Molar mass *(kg/mol)*,

$Sh_i = \dfrac{k_i . L}{D_i}$ --Sherwood number *(.)*,

k_i --Mass transfer coefficient *(m/s)*,

D_i ---Diffusivity *(m²/s)*,

τ_i --Thermophoretic parameter *(.)*,

$F_s(i)$ ---------------------------------Correction parameter for thermophoretic diffusion *(.)*,

w_i --Mass fraction *(.)*,

L --Characteristic length *(m)*,

ρ ---Density of flue gas in main stream *(kg/m³)*,

Subscripts:

i ---Of specie '*I*',

Superscripts:

s ---At surface location (in gaseous phase),

m --In main stream of gas flow (in gaseous phase)

Thus, deposition rates are calculated as equal to the diffusion rates of the particular specie. For the case of Na_2SO_4 deposition only, a constraint is applied such that the net molar transport rate of sodium has to be twice that of sulfur.

This model was verified by determination of experimental deposition rates of chemical compounds in a simulated flue gas channel. Figure 15 shows such an experimental determination of deposition rate of Na_2SO_4 compared to deposition rates predicted by the mathematical model at different surface temperatures. The general observation from Figure 15 is that the theoretically calculated values of dew point of Na_2SO_4 (temperature below which deposition of Na_2SO_4 starts to occur - ~1400K from 'theoretical' curve as opposed to ~1300K from 'experimental' curve) are higher than the experimentally observed value of the same. However, between 900 and 1300 K, model-predicted trends in deposition rates follow the general shape of trends observed from experiments.
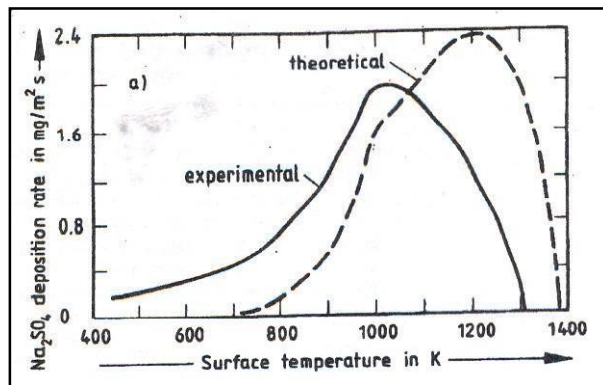
Figure 15: Experimental and theoretical deposition rates of Na_2SO_4 from simulated flue gases [17]

This mathematical model was used to predict the deposition rates of Na_2SO_4 associated with a regenerator of a soda-lime glass furnace. For the base case (curve A_1 in Figure 16), the maximum deposition rate was observed in the mid-section of the regenerator where the temperature was 1310 K. For the base situation, it was also calculated that 89% of the totally formed Na_2SO_4 was transported by the flue gases from the regenerator exit, and approximately 11% was deposited on the regenerator bricks.
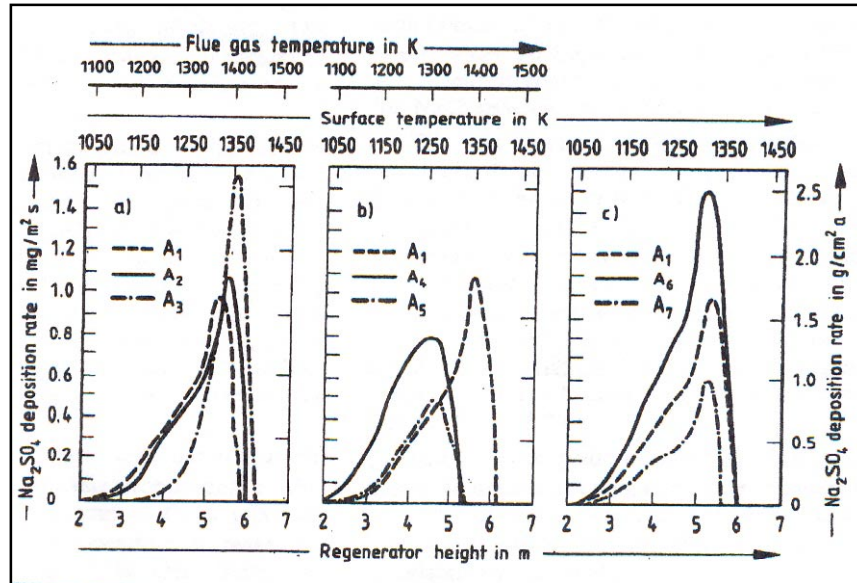
Figure 16: Calculated Na_2SO_4 deposition rate as a function of the regenerator height for a soda-lime glass furnace [17]. A_1 = base, A_2 = with doubled sulfur concentration in flue gas, A_3 = without chloride, A_4 = with reduced sulfur and increased chlorine concentration, A_5 = with reduced sodium concentration, A_6 = with doubled flue gas velocity, A_7 = with reduced temperature difference between gas and brick surface (25 K instead of 50 K)

This model [17] was also used for prediction of condensation products from a sodium borosilicate glass furnace. The important conclusion from the analysis of results obtained from experiments and thermodynamic calculations was that the mathematical model based on CFBL theory approach could be successfully applied to study the fouling in regenerators of industrial glass furnaces. The model is applicable for deposition of gaseous components condensing on relatively cold surfaces.

Reference [3] details another research effort whose purpose was "to obtain an understanding of the fouling and corrosion processes of secondary heat exchangers". The simulation model used in this research was derived from that used in Reference [17], and has been used to predict the deposition rates and the nature of deposits as a function of temperature and location on the heat exchanger tube. The model explained in Reference [3] was validated by conducting experiments to measure deposition rates as functions of:

1. Angular distance of location of interest from the upstream stagnation point of a cylinder in cross-flow (simulating a single heat exchanger tube exposed on the outer surface to the exhaust gas, and hence fouling occurs externally),

2. Tube surface temperature, and

3. Diameters of different size particles of Na_2SO_4 dust.

These results are shown in Figures 17, 18 and 19 respectively.

Figure 17 (reproduced from Reference [3]) shows a comparison of the theoretical and experimental values of deposition rates (measured in *mg/m².min*) of the particulate matter as function of the angle

from the upstream stagnation point of the heat exchanger tube, showing a maximum deposition rate of about *20 mg/m².min* at the upstream stagnation point. The experimentally measured values show good agreement with the model predictions.
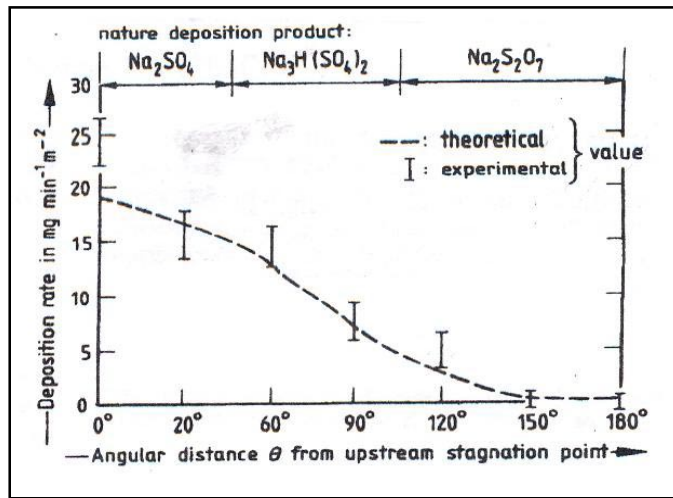
Figure 17: Experimental and theoretical deposition rates as functions of the angular distance from the upstream stagnation point of the heat exchanger tube. The tube surface temperatures are at the upstream and downstream stagnation points are 582 and 550 K respectively [3]

Figure 18 shows the dependence of deposition rate of Na_2SO_4 at the upstream stagnation point of the heat exchanger tube on the tube surface temperature. There is good agreement between the experimental and theoretical values except in the temperature range of *520 - 550 K*. This was thought to be due to the agglomeration of sodium bisulfate particles formed in this temperature range leading to larger particle sizes of diffusing dust particles, leading to higher experimentally observed deposition rates in this temperature range than expected from the calculations.
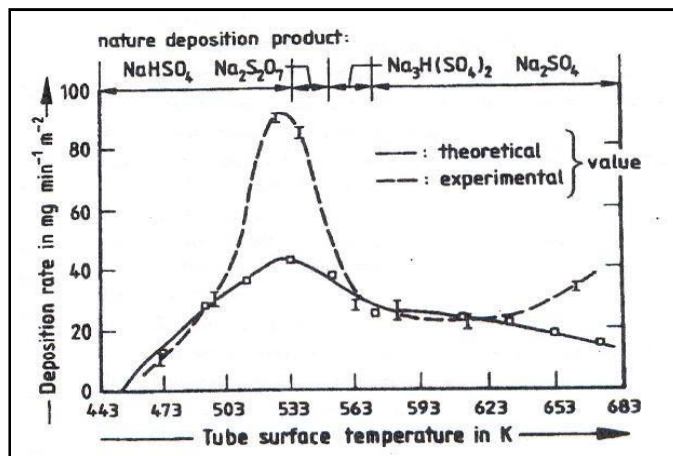
Figure 18: Experimentally and theoretically derived deposition rates at the upstream stagnation point of a cylindrical tube as function of tube surface temperature [3]

Figure 19 shows the dependence of calculated deposition rates of 3 different particle diameters on tube surface temperature. As can be observed, the deposition rates for large particles (*0.24 μm* dia.) are greater than that for smaller particles (*0.12* and *0.06 μm* dia.).
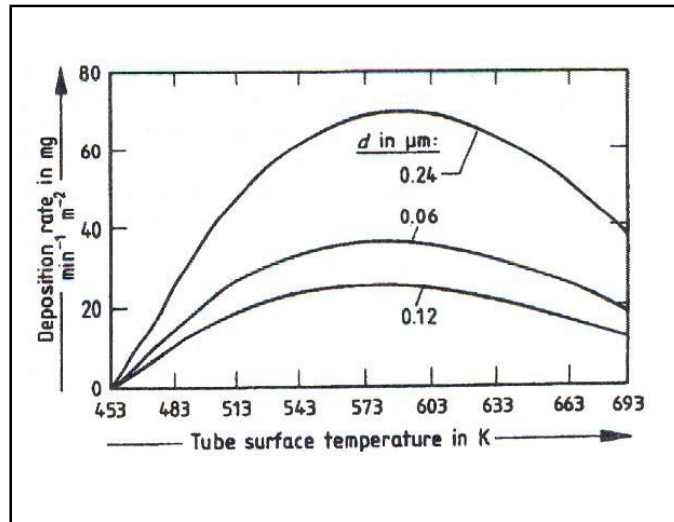
Figure 19: Theoretical deposition rate as function of tube surface temperature for Na$_2$SO$_4$ dust particles with different diameters [3]

The important conclusion from the research outlined in Reference [3] is that "the degree of fouling of heat exchanger tubes depends strongly upon the location and temperature of the tube surface". Maximum fouling occurs at the upstream stagnation point of the tube. Also, maximum fouling was found to be occurring between *520* and *550 K* tube surface temperatures. Also, size of the dust particles formed was an important parameter in the model calculations, and therefore, accurate measurements of particle size distributions, according to the authors, will improve the applicability of the deposition model.

4.1.3. Important Findings from Model Studies [16], [18], [17] and [3] Concerning Na_2SO_4 Formation of Particulate Matter on Heat Pipe External Surfaces

From studies that were described in sub-sections 4.1.1 and 4.1.2, the following are the important findings particularly relevant for the formation of Na_2SO_4 particulate matter:

1. Surface temperature of the heat pipe is an important factor which influences the deposition rate of particles. From Reference [3], maximum deposition rates of Na_2SO_4 were observed for a cylindrical heat exchanger tube at tube surface temperature range of 520-550 K. From reference [17], maximum deposition rates of Na_2SO_4 were calculated on a regenerator brick surface to be occurring at surface temperature of about 1310 K. This difference may be due to the differences in the approaches used in the two models.

2. Angular position of the location of deposition is another important parameter affecting Na_2SO_4 deposition rates. Maximum Na_2SO_4 deposition rate was observed at the upstream stagnation

44

point, i.e., in the case of the heat pipe, along the uppermost part of the curved surface area of the heat pipe. Figure 20 shows an end view of the heat pipe, indicating the expected region of maximum deposition rate.
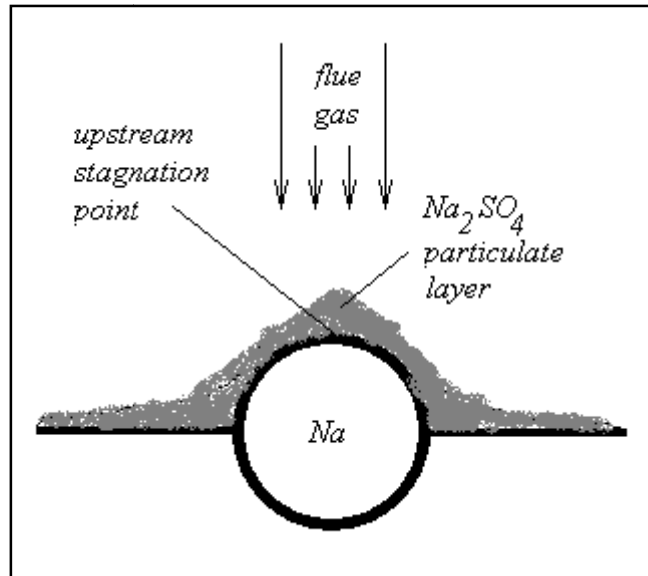
Figure 20: Schematic representation of the 'fouled' heat pipe showing upstream stagnation point

3. Diameter of the particles formed may be another important factor that affects the formation rates, as is indicated model studies from Reference [3]. This might be another measurement that should be done for the exhaust gas from the flue duct of the oxy-fuel furnace at PPG's Meadville plant that can be helpful in determining if the planned position of the heat pipe within the flue duct is optimal.

In the event that the placement of the heat pipe is constrained, in other words, if the particulate formation rate on the heat pipe is virtually unchangeable, the next best solution to the problem of reduction in heat transfer effectiveness of the heat pipe is periodic cleaning of the heat pipe external surfaces.

Sodium sulfate particulate matter can be cleaned by primarily mechanical cleaning methods, primarily because it is a weakly adhering deposit. On-line cleaning methods are preferred, since the TEG need not be removed and re-installed each time a cleaning is required. Since the heat pipe geometry is simple (3.5 in. diameter tube with two longitudinal fins) and the surfaces to be cleaned are on the upper half of the heat pipe, both contact and non-contact cleaning methods can be considered, although the high temperature (500-700°C) of the flue gases limits the applicability of contact-type cleaning methods.

In order to renew the heat transfer performance of heat exchangers, a variety of cleaning methods are used in the industry. All cleaning methods can be broadly classified into two categories: Off-line and On-line. The next two sub-sections (4.2 and 4.3) describe the various common cleaning methods in the off-line and on-line categories respectively.

4.2. Off-Line Cleaning Methods of Fouled Heat Exchanger Surfaces

Off-line methods are usually performed when the heat exchanger performance deteriorates beyond a specified limit, and involve taking the device out of operation for cleaning. Steinhagen [14] and Bott [13] have a variety of off-line cleaning methods listed. They can be broadly classified into chemical and mechanical methods.

4.2.1. Chemical Methods

Chemical methods are frequently used for cleaning internal surfaces of heat exchangers. They have a number of advantages compared to mechanical cleaning methods [14, 13], such as:

1. They are relatively quick,

2. Surfaces do not experience mechanical damage,

3. Chemical solutions reach otherwise inaccessible areas,

4. They are less labor-intensive than mechanical cleaning, and

5. Cleaning can be performed in situ.

Most of the chemical cleaning methods consist of five distinct processes, each being monitored for good results before proceeding to the next method. They are:

1. Alkaline clean,

2. Rinses,

3. Acidic clean,

4. Rinses, and

5. Passivation.

References [14] and [13] give details about different cleaning agents and typical deposits removed using chemical cleaning, although sodium sulfate is not one of the deposits mentioned (in Table 4 on page 34 of Reference [14] and Table C5 in Appendix C).

4.2.2. Mechanical Methods

These methods involve dismantling of the whole apparatus and cleaning using pressurized steam (steam-blasting) or water (hydro-blasting). Sand can be added to the cleaning water to improve the cleaning efficiency. Rigid lancing and flexible lancing are also popular methods used to clean the internal surfaces of heat exchanger tubes. Various methods of cleaning external surfaces are also described in Reference [14], such as high and ultra high pressure pumps, cleaning nozzles, turbojets, push and pull nozzles and rotorjets. Automatic mechanical cleaning method for external surfaces with high-pressure water seems to be a method of interest for the cleaning of the TEG. This cleaning takes place without any additives, and is effective.

4.3. On-Line Cleaning Methods for Fouled Heat Exchanger Surfaces

These cleaning methods are performed continuously and/or periodically to renew the heat exchanger heat transfer performance, as opposed to off-line methods. Again, they can be classified into chemical and mechanical methods.

4.3.1. Chemical Methods

Particulate fouling in heat exchangers is usually mitigated via on-line chemical means by the addition of surfactants or dispersants [14] or by the injection of chemical solutions called 'dosing' [13]. This is especially applicable for internal tubes of heat exchangers where a liquid medium is used to transfer heat. By reducing the surface tension, large particles can break down into smaller particles, which are carried away by the heat exchanger liquid itself. Table C5 in Appendix C [13] gives some chemical cleaning agents used in the industry.

4.3.2. Mechanical Methods

Various on-line mechanical particulate fouling mitigation methods have been developed, based on the following mechanisms:

1. Short-time overheating of the heat transfer surfaces (different thermal expansion of tubes and tube deposits may cause cracking of the deposit, and the cracked deposit falls off, and is deposited on the bottom, or carried away by the circulating fluid),

2. Mechanical vibration of heat transfer surfaces,

3. Acoustic vibration of heat transfer surfaces,

4. Increased shear stress at fluid deposit interface, and

5. Reduced adhesion of deposits.

A number of techniques are available (Reference [13]) for reducing the effects of fouling, some of which are mentioned below:

1. Circulation of sponge rubber balls,

2. Brush and Cage systems,

3. Air or gas injection,

4. Magnetic devices,

5. Soot blowers,

6. Sonic technology,

7. Water washing,

8. Shot cleaning,

9. Galvanic protection, and

10. Use of Inserts.

In liquid-flow type heat exchangers, reversal of flow direction in conjunction with a short-time increase of flow velocity is sometimes used as a method of cleaning out weakly adhering deposits.

4.4. Feasible Cleaning Methods for Cleaning Heat Pipe Surfaces Periodically

Appendix A gives a list of companies mentioned in Reference [14] that are in the business of providing heat exchanger cleaning services and devices/products/equipments. Hydro-blasting/Steam-blasting and Sootblower technologies [14] seem to be promising ways of cleaning the heat pipe external surfaces periodically and with relative ease of operation. In particular, the Sootblower technology seems to be most promising since in Reference [14], it is also mentioned that "Cleaning systems are installed with proper results in regenerative gas/air heaters" (Reference [14] page 280 – "Clyde Bergemann Cleaning Technology for Heat Exchanger", Stephan Simon & Richard Zachay, Clyde Bergemann, D-Wesel, Germany). The following sub-section gives an overview of sootblower technology as described in Reference [14].

4.4.1. Sootblower Technology

Sootblower technology basically relies on the kinetic energy of a blowing jet which is generated in a venturi nozzle from pressurized gas, to perform cleaning of heat exchanger surfaces from particulate deposits. Air, water and steam are used as blowing media. It is also mentioned that in order to meet each individual cleaning requirement basic design features have to be considered, such as:

• Selecting the right sootblower type,

• Economic arrangement of sootblowers,

• Selection of the required nozzle geometry,

• Choosing the proper blowing pressure, and

• Operating support.

Sootblowers of different types have been developed for different applications, such as:

Long retractable blower (for superheater area), helical blower (for economizer with smooth tube), wall blower (for furnace area – steam and water-operated), rotating element blower (for heat exchanger with smooth tubes), rake blower (for economizer with fin tubes), Water cannon™ (for furnace area,

hopper, other furnace chambers), lance-type water blower (for furnace area and other applications), and sootblowers for special applications.

The blowing medium can be steam, air or water. For the heat pipe, since thermal shock will be an important criterion to be considered, and also since the cleaning method is envisioned to be an on-line method, air at similar temperatures (as the heat pipe surface temperatures) is a feasible option. For this, re-circulated and filtered flue gas may be used with sootblowers.

4.4.2. Gears and Vibrators (Rapping Device)

Rapping gears and vibrators can be used for cleaning in case of heating surface coatings that are thick slagging [14]. Cleaning in this case is caused by the vibration process acting on the heating surface. In case of the heat pipe, this method has the advantage of being installed on-line and also not introducing any thermal shock to the system. The effectiveness of this technique, however, depends on the nature of the deposit itself, and the precariousness of the heat pipe system installation. This is another method that should be considered an alternative to direct contact cleaning methods. Clyde Bergemann Inc. (one of the contacts listed in Appendix A) seems to be knowledgeable of this procedure.

5. Proposed Experiments for Determining How to Control Sodium Sulfate Particulate Formation on the Heat Pipe or to Clean the Heat Pipe

This section outlines a plan for experiments that are to be conducted at the PPG plant at Meadville, PA in order to:

1. Measure and determine the variables that affect the rate of formation of Na_2SO_4 particulate layer on the heat pipe, and thereby determine the optimal location of the heat pipe in the flue duct,

2. Monitor the decrease in heat transfer effectiveness of the heat pipe in converting the available thermal energy to electrical energy (via the TEG module) as a function of duration of operation, and

3. Use the monitoring technique to test the level of recovery of heat transfer effectiveness of the heat pipe due to cleaning the heat pipe using two cleaning methods.

In order to understand the formation of Na_2SO_4 particulate formation rate, the theoretical and experimental results from research work that has been conducted on laboratory scale (as discussed in section 4.1 and its sub-sections in this report) will be used. According to Reference [3], the most important parameter that affects the rate of deposition of Na_2SO_4 particulate is the surface temperature of the heat pipe. From information supplied by PPG, the parameters that are being measured currently are:

1. The voltage (V) across the TEG and electric current (I) drawn from the TEG as time-history variables,

2. The heat pipe surface metal temperatures $(T_1, T_2, T_3, T_4, T_5)$ at the locations as indicated in Figure 21.

The temperatures currently being monitored will be sufficient to determine the temperature distribution on the external surface of the heat pipe. In addition to this information, it will also be useful to know the flue gas temperature in the vicinity of the heat pipe and also the flue gas temperature as the gas passes through the downcomer from the furnace. Figure 22 shows the additional thermocouple locations that can be used to determine the temperature change of the flue gas. This information will be useful to compare with Figure 11 from Reference [16], which gives the distribution of the total sodium in exhaust gas from a gas-fired flat glass furnace (which is the same as that in PPG plant in Meadville, PA – although it is not clear whether the one mentioned in Reference [16] is an oxy-fuel type furnace) as a function of gas temperature. This will give an indication of what the relative deposition of sodium would be in the exhaust gas as Na_2SO_4 particulate for different positions of the heat pipe in the flue duct.
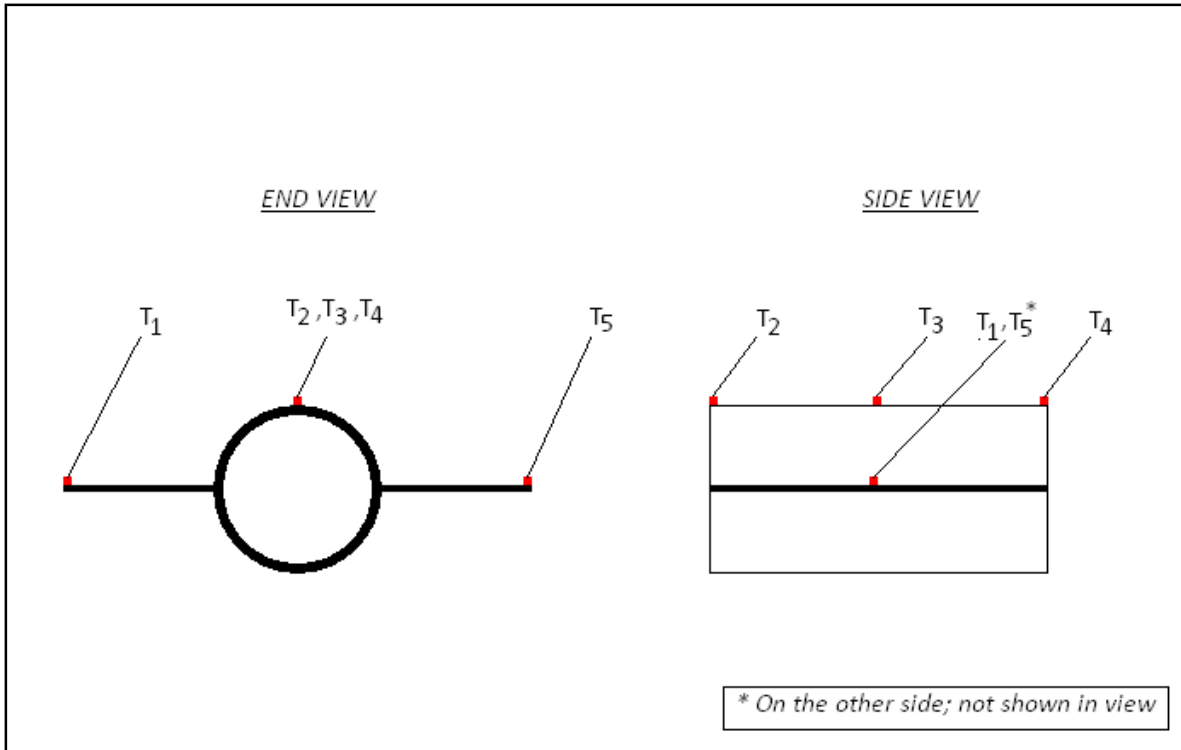
Figure 21: Schematic representation of thermocouple layout on heat pipe to measure surface temperatures
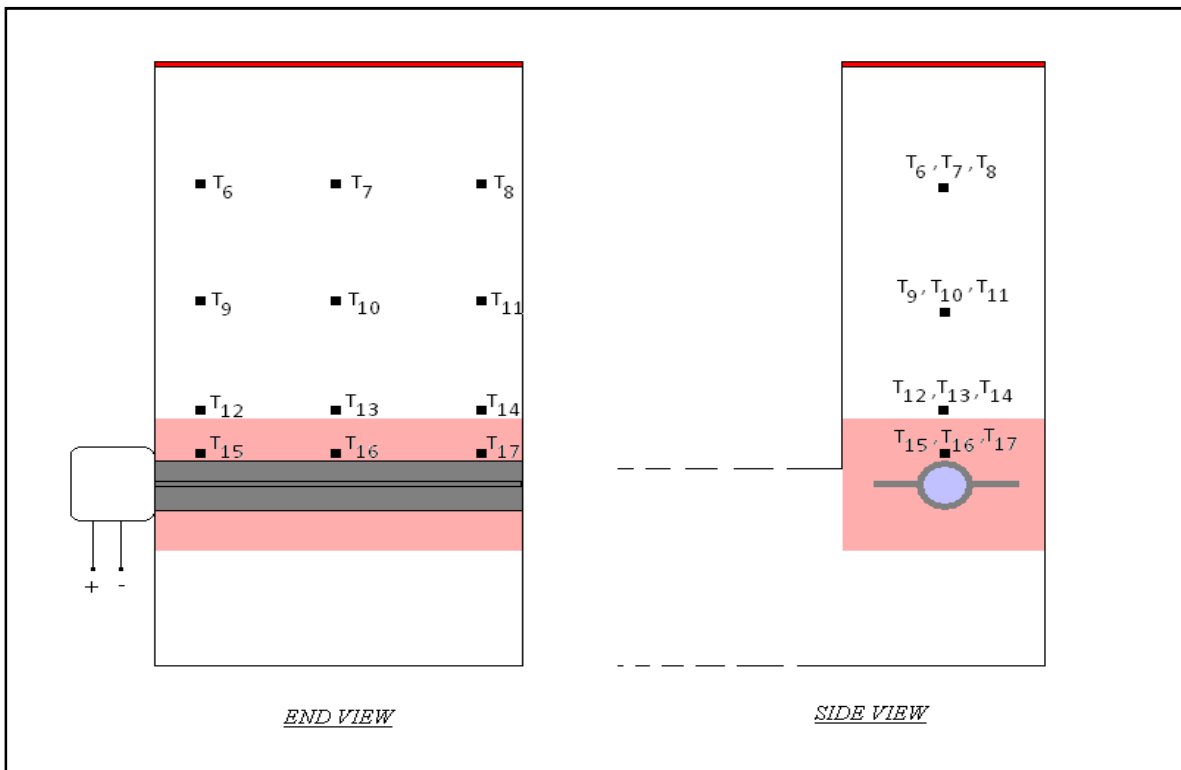
Figure 22: Schematic representation of thermocouple layout in the downcomer to measure flue gas temperatures

Another important factor affecting the deposition rate on a cylindrical tube is the angular distance from the upstream stagnation point (refer Figure 17 and Figure 20). According to Reference [3], maximum deposition rate of Na_2SO_4 was observed at the upstream stagnation point (as shown in Figure 17). Accordingly, a schematic representation of the 'fouled' heat pipe with an expected particulate deposition profile is shown in Figure 20. This can be challenging to measure, but is possible by measurements of thickness of the Na_2SO_4 deposit layer at various angular distance locations (as schematically shown in Figure 23) at regular intervals of time by taking the device off-line.
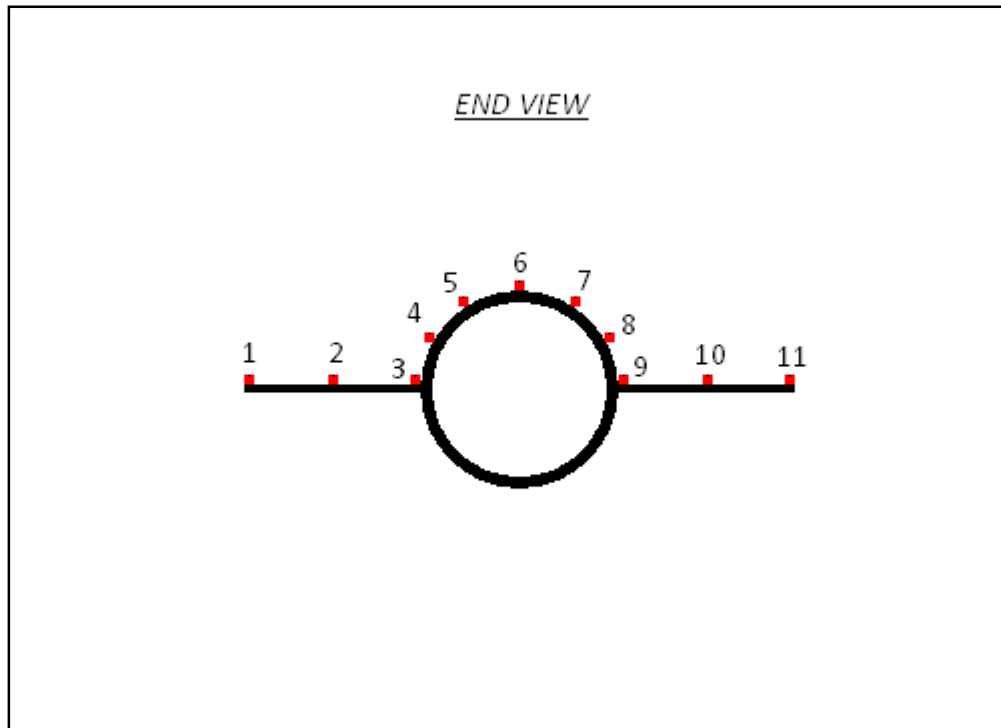
Figure 23: Schematic representation of locations on the heat pipe to assess the effect of angular distance from the upstream stagnation point (location '6') on Na_2SO_4 deposition rate

The third and perhaps the least investigated factor that affects the particulate deposition rate is the individual particulate sizes, as shown in Figure 19 and as mentioned in the conclusions drawn by Reference [3]. The deposition rates in Figure 19 were derived from the mathematical model; hence they are the theoretical values of depostion rates of particles of different diameters. Published data on the particulate size distribution measured from two furnaces melting flint glass and amber glass respectively is shown in reproduced from Reference [4]. According to Reference [4], particles in the flue gases from these furnaces were between 0.05 and 0.5 μm. Referring to Figure 19, if the particle size distribution of the Na_2SO_4 formed from the flue gases in the oxy-fuel furnace at the PPG plant in Meadville, PA is measured from flue gas samples, the deposition rates (as predicted by the mathematical model by Mutsaers et al. [3]) can be predicted for the different particle diameters, and integrated to get the total deposition rate. In Reference [4], a sampling train with Teflon filters was used to collect the particulate matter and electron photomicrographs were used for determining the particle size distribution from the collected samples. Various techniques such as Scanning Electron Microscopy (SEM), Doppler Laser Scattering (DLS), Laser Diffraction, X-Ray Sedimentation, Centrifugal Sedimentation, Electrical Zone

Sensing etc. are used for determining the particle size distributions. Further investigation needs to be done to find out what method will be best suited for the situation at hand, that is, high temperature exhaust gas contanining particulate matter that is mainly comprised of inorganic salts.
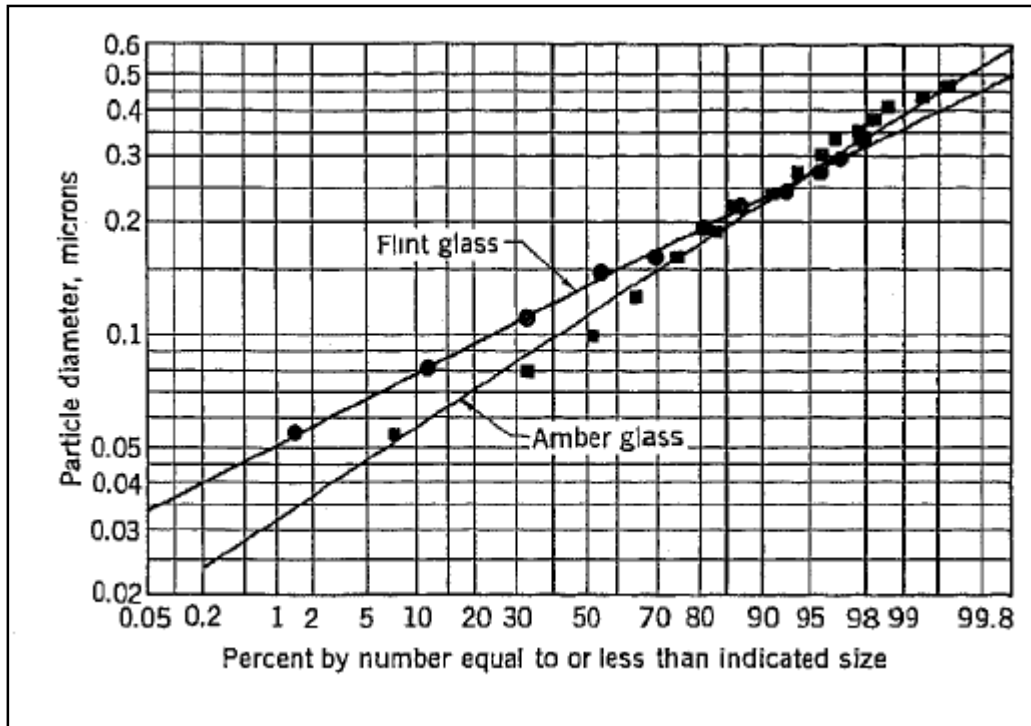
Figure 24: Particle size distribution of effluents from two glass furnaces [4]

From Equation (11) in section 3.2 of this report, the variables affecting convection heat transfer rate from the heat pipe to the exhaust gas (the direction of convection heat transfer rate is from the heat pipe to the flue gas as confirmed with PPG - see Reference [23]) are:

1. $\bar{h}$　　-　　the convection heat transfer coefficient,

2. A_{up+dn} -　　total surface area of heat pipe outer surface,

3. T_g　　-　　absolute gas temperature, and

4. T_s　　-　　absolute surface temperature.

Note that T_s may not be equal to $T_{m,o}$ the temperature of the outer metal surface of the heat pipe (which is being measured at the PPG plant as T_1, T_2, T_3, T_4 and T_5 - see Figure 21), especially when a particulate layer of Na_2SO_4 is present on the heat pipe. Measuring T_s may be difficult; a better method of estimating T_s from $T_{m,o}$ will be to measure the thermal conductivity (from laboratory scale experiments) of the Na_2SO_4 particulate layer and then calculate T_s (Figure 8) using measured heat flux $\left(\dot{Q}_{net}\right)$ through the particulate layer, measured values of metal outer surface temperature ($T_{m,o}$ in Figure 8) and flue gas temperature (T_g in Figure 8), and measured particulate layer thickness $\left(w_{dep}\right)$. The absolute gas temperature T_g may be obtained as the average of T_{15}, T_{16} and T_{17} (see Figure 22).

The change in radiation heat transfer rate can be monitored by knowing the absorptivity $\left(\alpha_s^{loaded}\right)$ of the Na_2SO_4 particulate layer and the surface temperature $\left(T_s^{loaded}\right)$ when the heat pipe surface is covered with Na_2SO_4 particulate layer. According to Reference [23], the absorptivity of the special coating $\left(\alpha_s^{clean}\right)$ on the heat pipe upper surface is 0.94; hence, from Equation (6) in of this report, radiation heat transfer rates can be computed at any instant of time as:

$$\dot{Q}_{rad}^{clean} = A_s F_{fs} \sigma \alpha_s^{clean} \left(\left(T_f\right)^4 - \left(T_s^{clean}\right)^4\right) \quad \text{--} \quad (6a)$$

and

$$\dot{Q}_{rad}^{loaded} = A_s F_{fs} \sigma \alpha_s^{loaded} \left(\left(T_f\right)^4 - \left(T_s^{loaded}\right)^4\right) \quad\quad (6b)$$

Note that in Equation (6a), $T_s^{clean} = T_{m,o}$ whereas in Equation (6b), $T_s^{loaded} \neq T_{m,o}$ but T_s as estimated from Equation () by the previously discussed method (page 48 of this report) could be used for T_s^{loaded}. But the major difference between $\dot{Q}_{rad}^{clean}$ and $\dot{Q}_{rad}^{loaded}$ is due to α_s^{clean} (**0.94**, according to Reference [23]) being much greater than α_s^{loaded} (From Table 7, α for a white $(BaSO_4)$ coating with polyvinyl alcohol is **0.06**, according to Reference [9]). Also, since the heat transfer into the heat pipe is entirely due to radiation (the convection is from the heat pipe to the flue gas, according to Equation (6) and from information about gas and heat pipe surface temperatures in Reference [23]), and since the working fluid (sodium) in the heat pipe is at a constant temperature (649°C from Reference [23]) and pressure (6.89 kPa - absolute), this variation will dictate the change in the power output $\dot{W}_{out}$ while the heat pipe is in operation.

In order to monitor the heat transfer effectiveness of the heat pipe, the power output $\left(\dot{W}_{out} = V \; x \; I\right)$ from the TEG module is being monitored at the PPG plant as function of time of operation. The decrease in heat transfer effectiveness of the heat pipe will be manifested as a decrease in $\dot{W}_{out}$ over time. Reference [13] has some techniques listed for assessing heat exchanger performance through acquisition of plant data. One of the assessment techniques is monitoring mean fouling resistance versus days on stream, and the expected trend for fouling-prone heat exchangers is an increase in mean fouling resistance. This, however, is equivalent to monitoring the power output from the TEG in the case of the heat pipe.

This monitoring technique can be used for assessing the effectiveness of different cleaning methods as well. In order to do this, one needs to know:

1. $\dot{W}_{out,initial}$ - i.e., power output initially, when the heat pipe is 'clean'

2. $\dot{W}_{out,before}$ - i.e., power output before cleaning using one of the cleaning methods being tested out, and

3. $\dot{W}_{out,after}$ - i.e., power output after cleaning is completed.

Then, from the definition of effectiveness, an effectiveness value of the particular cleaning method (η_i) can be defined as:

$$\eta_i = \frac{\dot{W}_{out,after} - \dot{W}_{out,before}}{\dot{W}_{out,initial} - \dot{W}_{out,after}} \qquad \text{--} \qquad (29)$$

Effectiveness of different cleaning methods can thus be compared using this technique.

Therefore, from the planned experiments, the variables that need to be measured or calculated for monitoring degradation of heat pipe performance and assessing effectiveness of different cleaning methods are:

1. Heat pipe outer surface temperatures (T_1 thru T_5 - already being measured),

2. Flue gas temperatures (T_6 thru T_{17}),

3. Particulate layer outer surface temperatures (need to determine whether there is a direct way to measure; could be estimated from particulate layer thermal conductivity and particulate layer thickness measurements),

4. Particulate deposit layer thermal conductivity (k_{dep}) and absorptivity (α_{dep}),

5. Voltage across TEG module (V) and current drawn from the TEG module (I) (already being measured),

6. Particulate deposition rate $(\dot{m}_{dep})$ and corresponding particulate layer thicknesses (w_{dep}) as functions of the heat pipe outer surface temperature (T_s), angular distance from the upstream stagnation point (θ) and particulate diameters (d_p), and

7. Particulate size distribution (n_p) of the Na_2SO_4 deposit layer as functions of particulate diameters (d_p). These might also be functions of the heat pipe surface temperatures, so that accordingly, different samples may be taken at different heat pipe surface temperatures and analyzed for particulate size distribution.

Experiments at the PPG plant can be designed according to the data that needs to be collected as listed above and conducted. Cleaning methods that are potential candidates for cleaning the heat pipe periodically need to be tested for their individual effectiveness and feasibility. Currently, two cleaning methods seem to be potential candidates for testing (as given in section 4.4 of this report); they are:

1. Sootblower® technology, and

2. Rapping device

These methods need to be studied more closely with regard to applicability to cleaning the heat pipe periodically. After the experiments are conducted, data regarding the effectiveness of cleaning methods tested out will be studied and decisions made thereof as to which cleaning method should be used for periodically restoring the performance of the heat pipe.

Currently, there are three companies that have knowledge about online cleaning methods for external cylindrical surfaces; they are:

1. *Clyde Bergemann, Inc.*,

2. *j&w Reinigungssysteme GmbH*, and

3. *Tube Tech International Ltd.*

The contact details for these companies are listed in [Appendix A](#) of this report. Visits to these companies to discuss the problem and possible solutions would be helpful to determine the best method for cleaning the heat pipe.

6. Summary

A detailed study of the literature regarding the heat transfer processes taking place in a heat pipe placed in the exhaust flue duct of a oxy-fuel type natural gas-fired flat glass furnace and the changes occurring to the heat pipe as a result of particulate deposition on the outer surfaces has been conducted. Existing literature on the subject were used to draw conclusions from the research effort as applied to the heat pipe. From the study, the following points are to be noted:

1. The rate of deposition of particulate matter (which consists mainly of sodium sulfate - Na_2SO_4) is probably the single factor that affects the rate of degradation of the heat pipe performance. This deposition rate is in turn a function of the gas temperature at/near the heat pipe (T_g), the heat pipe outer surface temperature (T_s), the angular distance of the location on the heat pipe from the upstream stagnation point (θ) and the individual diameter of the particle being deposited (d_p).

2. Heat transfer from the furnace to the heat pipe occurs via thermal radiation. Convection heat transfer consistently occurs from the heat pipe to the flue gas. The majority of the degradation in heat pipe performance occurs due to the change in thermal radiation absorptivity of the heat pipe surface when the surface, initially at an absorptivity of **0.94**, becomes covered with particulate deposit layer, which probably has an absorptivity of around **0.06** (as suggested by normal-total absorptivity values for solar radiation of a white barium sulfate coating, although the value of absorptivity of Na_2SO_4 and thermal conductivity of Na_2SO_4 have not been found in the literature available).

3. Online mechanical cleaning methods seem to be most suited for cleaning the heat pipe periodically, given the nature of the particulate deposit and the heat pipe setup. Specifically, the **Sootblower® technology** and **Rapping device** (explained in section 4.4 of this report) seem to be the two most promising cleaning methods for the heat pipe.

4. The effectiveness of each cleaning method planned to be tested on the heat pipe can be determined by monitoring certain variables at various time instances during operation of the heat pipe as mentioned in section 5 of this report.

References

1. "Electronic Code of Federal Regulations (e-CFR) Title 40: Protection of Environment - Part 60 - Standards of Performance for New Stationary Sources - Subpart CC - Standards of Performance for Glass Manufacturing Plants"

2. "Sodium Sulfate: Handbook of Deposits, Processing and Use", Donald E Garrett, Academic Press, 2001.

3. "Fouling of Heat Exchanger Surfaces by Dust Particles From Flue Gases of Glass Furnaces", Peter L.M.Mutsaers, R G C Beerkens and Henk de Waal, TNO Institute of Applied Physics, Delft (NL) – Glastech. Ber. 62 (1989) No. 8 pp 266-273

4. "The Composition of Gases Evolved from Glass Furnaces", Stockham J D, Journal of the Air Pollution Control Association Vol. 21 Issue 11, 1971, pp 713-715

5. "Solubilities of Inorganic and Metal Organic Compounds", Linke, W.F.; A. Seidell, 4th edition, Van Nostrand (1965).

6. "Fundamentals of Heat and Mass Transfer", F.P.Incropera and D.P.Dewitt, John Wiley and Sons, 5th Edition, 2001

7. http://www.monarchserver.com/TableofEmissivity.pdf, Online resource, Accessed last on 03/14/2008.

8. "Thermophysical Properties of Matter Vol. 2 – Thermal Conductivity – Nonmetallic Solids", Y.S. Touloukian, R.W.Powell, C.Y.Ho and P.G.Klemens, IFI/Plenum, New York, 1970-1979

9. "Thermal Radiation Heat Transfer", Robert Siegel and John R. Howell, Hemisphere Publishing Corporation, Third edition, 1992

10. "NIST Chemistry Webbook", Online Resource, Accessed on 01/05/2008

11. "The Heat of Hydration of Sodium Sulfate. Low Temperature Heat Capacity and Entropy of Sodium Sulfate Decahydrate", G Brodale and W F Giauque, Journal of the American Chemical Society 80: 2042–2044, 1958

12. "Deposits and Condensation from Flue Gases in Glass Furnaces", R G C Beerkens, University of Technology Eindhoven (The Netherlands) PhD thesis, 1986.

13. "Fouling of Heat Exchangers", T.R.Bott, Elsevier, 1995

14. "Heat Exchanger Fouling: Mitigation and Cleaning Techniques", Hans Muller-Steinhagen, IChemE, 2000

15. "Fundamentals of Engineering Thermodynamics", M.J.Moran and H.N.Shapiro, Wiley, 5th Edition, 2003

16. "The Chemical Changes Occurring during the Cooling of Hot Gases from Flat Glass Furnaces", Kirkbride B J, Glass Technology 20 no. 5, pp 174-180, 1979

17. "Simulation of the Condensation and Deposition Processes in Regenerators of Glass Furnaces", Ruud G.C.Beerkens and Henk de Waal, TNO Institute of Applied Physics, Delft (NL) – Glastech. Ber. 61 (1988) No. 2 pp 36-42

18. "Experimental and Thermodynamic Characterization of Deposition and Condensation Products from Exhaust Gases of Glass Furnaces", Beerkens R G C, Waal H de, Glass Technology 28 no. 6, pp 246-251, 1987

19. "Modification of Deposit Formation in Glass Furnace Heat Recovery", Hempel et al. - United States Patent No. 4,561,873 Dec. 31, 1985

20. "Fouling of Heat Exchangers: New Approaches to Solve an Old Problem", Steinhagen, Malayeri, and Watkinson, Heat Transfer Engineering, 2005

21. "SO_2 emissions and sulphur balances of soda lime glass melting furnaces", Report of the International Commission on Glass (ICG) Technical Committee 13 "Environment", Ruud G.C.Beerkens and Hans van Limpt (TNO Institute of Applied Physics, Eindhoven , Netherlands), Ulrich Kircher (Huttentechnische Vereinigung der Deutschen Glasindustrie (HVG), Frankfurt/M. (Germany)), Bianca Maria Scalet (Stazione Sperimentale del Vetro, Murano-Venice (Italy)), Andreas Kasper (Sekurit Saint-Gobain Deutschland GmbH & Co. KG, Herzogenrath (Germany)), Guy van Marcke (Glaverbal SA, Jumet (Belgium)), Guy Tackels (Saint-Gobain Conceptions Verrieres, Aubervilliers (France)), George Delhopital (BSN Emballage, Villeurbanne (France)), Charlotte Masy (Insitut National du Verre, Charleroi (Belgium)) – Glastech. Ber. Glass Sci. Technol. 72 (1999) No. 10 pp 303-314

22. "Economic Comparison of Emission Control Systems for Glass Manufacturing Furnaces with Heat Recovery", Antonio C Caputo and Pacifico M Pelagagge, Department of Energetics, Faculty of Engineering, University of L'Aquila, Monteluco, L'Aquila, Italy, Journal of Air & Waste Management Association, 51, pp 1009-1020, 2001

23. "Re: A few questions related to the heat pipe problem", Private (e-mail) communication with PPG, dated 03/21/2008.

Appendix A: Sample Letter and Write-up to Companies that Provide Heat Exchanger Fouling Treatment Equipment/Services

A.1. Letter Body

This letter is regarding a potential problem that a company manufacturing flat glass is faced with, which is in relation to fouling of the heat transfer surfaces of a heat recovery equipment (a heat pipe) that the company plans to install in one of their glass furnace exhaust flue ducts. Please provide description of potential cleaning equipment that might be useful for maintaining the heat transfer effectiveness of the heat pipe at the earliest possible. Attached with this message is a problem description document that you may use as input to providing us information on a suitable cleaning method.

A.2. Problem Description

A Thermo-Electric Generator (TEG) is planned to be used on an experimental basis for heat recovery of exhaust gas from a furnace as part of a research project for DOE (U.S. Dept. of Energy). The heat pipe is approximately 3.5 inches in diameter and 12.3 feet long. Figure A1 shows a sketch of the approximate dimension of the exhaust flue, with the planned location and orientation of the heat pipe, and Figure A2 shows a schematic representation of the heat pipe.
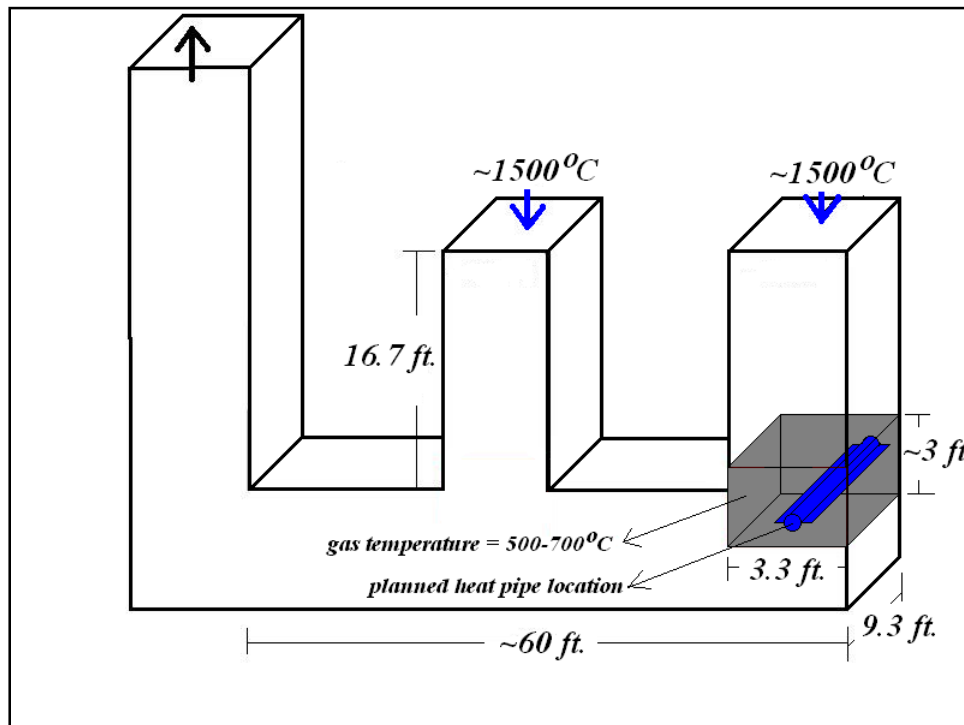
Figure A1: Schematic representation of the furnace exhaust flue

Heat energy from a natural gas-fired furnace above the exhaust flue is transferred to the TEG by a liquid metal working fluid inside the heat pipe and converted to electricity by the TEG. The operational temperature of the exhaust gas in the region where the TEG is intended to be placed is approximately

500 to 700°C and the pressure is slightly below atmospheric pressure. The heat pipe is placed in the direction normal to the plane of the page, at an angle (~10°) to the horizontal. As can be seen from Figure A2, the heat pipe also has two lateral fins to enhance the heat transfer from the exhaust gas. The primary mode of heat transfer will likely be radiation from the furnace directly above the heat pipe.
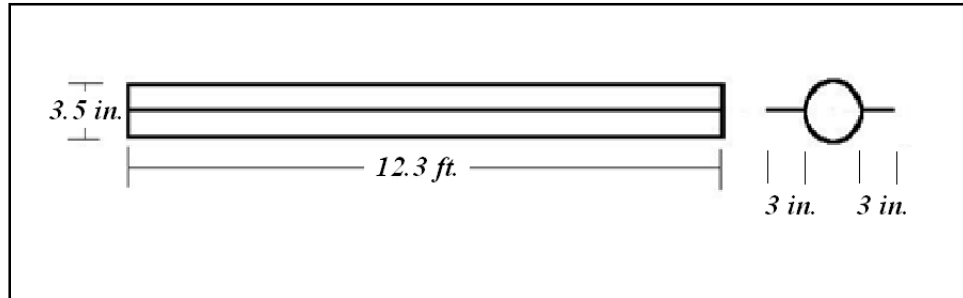
Figure A2: Schematic representation of the heat pipe

One of the problems anticipated with the implementation of this project, however, is the formation of a layer of particulate from the exhaust gas passing over the heat pipe and the resultant loss in heat transfer efficiency of the heat pipe. This is because the powdery particulate layer is mostly an inorganic salt, which is a poor conductor of heat. In order to minimize the loss of heat transfer efficiency, it is intended to clean the surfaces of the heat pipe, particularly the upper surfaces where particulate formation rate is maximum.

Towards this, a variety of cleaning methods are being evaluated to determine the optimal method. A good cleaning method will:

1. be simple to setup,
2. be relatively inexpensive (i.e., uses a readily available and inexpensive cleaning medium like high-pressure steam or air),
3. be able to be carried out relatively easily (i.e., no removal of the heat pipe is intended), and
4. be effective (i.e., able to revive the heat transfer efficiency of the heat pipe as close to the original or 'clean' value as possible).

All feasible methods of cleaning the heat pipe will be reviewed.

Our question is: what method of cleaning the TEG do you recommend? Do you sell commercial equipment suitable for this or would it need to be specially designed?

A.3. List of Companies That Provide Heat Exchanger Cleaning Services / Products / Equipment [14]

1	Conco Systems, Inc.	530 Jones Street Verona, PA 15147 USA Tel: 412-828-1166 Fax: 412-826-8255 E-mail: info@concosystems.com
2	Tube Tech International Ltd.	Unit 14 Rawreth Industrial Estate Rawreth Lane, Rayleigh, Essex, SS6 9RL (Great Britain) Tel: +44 (0) 870-24-14-999 Fax: +44 (0) 870-24-34-999 Website: www.tubetech.com E-mail: info@tubetech.com
3	URACA GmbH + Co. KG	Postfach 1260. D-72563 Bad Urach, Germany Tel: (07125) 133-0 Fax: (07125) 133-202 Website: www.uraca.com
4	Hammelmann Maschinenfabrik GmbH	Zum Sundern 13-21, D-59302 Oelde, Germany Tel: +492522/760 Fax: +492522/76444 Website: www.hammelmann.de E-mail: mail@hammelmann.de
5	j&w Reinigungssysteme GmbH	D-44866 Bochum, Germany Tel: +49-2327-9834-0 Fax: +49-2327-9834-17 Website: www.jw-gmbh.de E-mail: info@jw-gmbh.de
6	Balcke-Durr Energietechnik GmbH (BDT Engineering)	P.O.Box 1240 40832 Ratingen, Germany Tel: +49 (0) 2102 / 855-0 Fax: +49 (0) 2102 / 855-494

7	WOMA Apparatebau GmbH	Werthauser Str. 77-79
		D-47226 Duisburg
		P.O.Box 141820 D-47208 Duisburg
		Tel: +49 2065 / 304-0
		Fax: +49 2065 / 304-200
		Website: www.woma.de
		E-mail: info@woma.de
8	Clyde Bergemann, Inc.	4015 Presidential Parkway
		Atlanta, GA - 30340-3707
		Tel: 770-557-3600
		Fax: 770-557-3651
		Website: www.clydebergemann.com
		E-mail: asd@clydebergmann.com

Appendix B: List of Sources Used for Writing This Report

B.1. A List of Journals of Interest (Updated last on 12/20/2007)

No.	Title	Type	Years available at MTU library	Keywords used
J1	Journal of the American Chemical Society	Journal	1879-2007	Sodium Sulfate, Recuperator fouling, Particulate fouling
J2	Environmental Science and Technology	Journal	1967-2007	Particulate fouling, Recuperator fouling
J3	Journal of the Air & Waste Management Association	Journal	1998-2007	Sodium Sulfate, Recuperator fouling
J4	Journal of Chemical & Engineering Data	Journal	1956-2007	Sodium Sulfate
J5	Chemical Engineering Journal	Journal	1997-2007	Sodium Sulfate, Recuperator fouling
J6	Environmental Sciences & Pollution Management	Journal	Online	Heat exchanger fouling
J7	Environmental Protection Agency – Standards – Information Services	Standards – gov. docs	Online (e-CFR database)	Glass manufacturing
J8	Glastech. Ber. (Glass Science & Technology)	Book (elsevier) Glastechnische Berichte [German - Reports on Glass Technology]	No prints online; thru Inter-Library Loan on specific papers	(individual papers requested)
J9	Glass Technology	Journal	1998-2007	Sodium Sulfate, Heat exchanger fouling

No.	Title	Type	Years available at MTU library	Keywords used
J10	American Ceramic Society Bulletin	Magazine	Online, needs registration	Sodium Sulfate, Recuperator fouling
J11	Steklo i Keramika (Russian - Glass and Ceramics)	Journal	Online; in Russian (1956-2007)	Sodium Sulfate, Heat exchanger fouling
J12	American Glass Review	Journal	1997-1999	Sodium Sulfate, Heat exchanger fouling
J13	International Glass Review	Journal	2003-2005	Sodium Sulfate
J14	Glass Physics and Chemistry	Journal	2000-2007	Sodium Sulfate, Heat exchanger fouling
J15	Glass	Magazine	1997-2007	Sodium Sulfate, Heat exchanger fouling
J16	International Journal of Environmental Science & Technology	Journal	Online	Sodium Sulfate, Heat exchanger fouling
J17	United States Patent and Trademark Office	Database	Online (1976-present available as full-text)	Recuperator, Sodium Sulfate
J18	Journal of Heat Recovery Systems	Journal	Inter-Library Loan from MTU library	Sodium Sulfate
J19	Heat Transfer Engineering	Journal	Online (1979-present available in full-text)	Heat exchanger fouling, Recuperator fouling

B.2. A List of Books & Papers (Updated last on 02/11/2008)

No.	Title and Description	Type	Significance (scale of 1 to 10, 1 - low, 10-high)	Source
P1	"Fouling of heat exchanger surfaces by dust particles from flue gases of glass furnaces", Peter L.M.Mutsaers, Ruud G.C. Beerkens and Henk de Wall, TNO Institute of Applied Physics, Delft (NL) – Glastech. Ber. 62 (1989) Nr. 8 pp 266-273	Paper	8	J8
P2	"Simulation of the condensation and deposition processes in regenerators of glass furnaces", Ruud G.C.Beerkens and Henk de Waal, TNO Institute of Applied Physics, Delft (NL) – Glastech. Ber. 61 (1988) Nr.2 pp 36-42	Paper	5	J8
P3	"SO2 emissions and sulphur balances of soda lime glass melting furnaces", Report of the International Commission on Glass (ICG) Technical Committee 13 "Environment", Ruud G.C.Beerkens and Hans van Limpt (TNO Institute of Applied Physics, Eindhoven , Netherlands), Ulrich Kircher (Huttentechnische Vereinigung der Deutschen Glasindustrie (HVG), Frankfurt/M. (Germany)), Bianca Maria Scalet (Stazione Sperimentale del Vetro, Murano-Venice (Italy)), Andreas Kasper (Sekurit Saint-Gobain Deutschland GmbH & Co. KG, Herzogenrath (Germany)), Guy van Marcke (Glaverbal SA, Jumet (Belgium)), Guy Tackels (Saint-Gobain Conceptions Verrieres, Aubervilliers (France)), George Delhopital (BSN Emballage, Villeurbanne (France)), Charlotte Masy (Insitut National du Verre, Charleroi (Belgium)) – Glastech. Ber. Glass Sci. Technol. 72 (1999) No. 10 pp 303-314	Paper	6	J8
P4	"Sampling regenerator carryover", T.S.Busby and W.M.Sengelow, British Glass Industry Research Association, Sheffield – Glass Technology Vol. 19 No. 3 June 1978 pp 47-53	Paper	2	J9
P5	"Modification of deposit formation in glass furnace heat recovery", Hempel et al. - United States Patent No. 4,561,873 Dec. 31, 1985 (5 pages)	Paper	6	J17, PPG
P6	"Heat generator", Richard J.Monro – United States Patent No. 4,444,128 Apr. 24, 1984 (7 pages)	Paper	3	J17, PPG

No.	Title and Description	Type	Significance (scale of 1 to 10, 1 - low, 10-high)	Source
P7	"Steam generator using waste heat from glass furnace", Banfi et al. – United States Patent No. 4,362,129 Dec. 7, 1982 (4 pages)	Paper	1	J17, PPG
P8	"A waste heat recovery boiler on a glass-melting furnace", J.A. Nycz and D.T.Sturgill – The Glass Industry (magazine), June 1980 pp 12-16 and 43 (also Glass Problems Conference Paper)	Paper	2	PPG
P9	"Using waste gas heat from a glass furnace in a waste heat boiler", M.Ya. Khinkis, S.V. Levitin, L.G. Gol'denberg, V.Ya. Polyak and L.I. Zingman – Experimental Design Office for Power-Engineering Processes in the Chemical Industry (OKB, ETKh-IM) and Moscow K.I. Kalinin Cut Glass Factory. Translated from Steklo I Keramika, No. 1, pp. 15-19, January, 1968.	Paper	2	J11
P10	"Utilization of the heat from waste gases of the glass-making furnace", M.D. Shapiro, A.I. Tyurin and Yu.V. Lashenkov - Plant Experience – Kalininskii Glass Factory. Translated from Steklo I Keramika, No. 11, pp. 24-25, November, 1980.	Paper	2	J11
P11	"TCF technology for oxy-fuel glass-melting: Heye glas experience", H. Kobayashi, K.T. Wu, G.B. Tuson and F. Dumoulin (Praxair Inc., Danbury, Conn.) and H.P.Kiewall (Heye International GmbH, Obernkirchen, Germany) - Part 2 of a 2-part series – American Ceramic Society Bulletin, Vol. 84, No. 3, March 2005 pp. 24-27.	Paper	2	J10
P12	"Sources of emissions, chemistry of flue gases & emission reduction", Hans van Limpt and Ruud Beerkens (TNO Institute of Applied Physics, Delft (NL)) (78 pages)	Pres.	4	PPG
P13	"Sodium Sulfate: Handbook of Deposits, Processing and Use", Donald E Garrett	Book	5	Purchased through Amazon
P14	"The Heat of Hydration of Sodium Sulfate. Low Temperature Heat Capacity and Entropy of Sodium Sulfate Decahydrate", G Brodale and W F Giauque, Journal of the American Chemical Society 80: 2042–2044, 1958	Paper	5	J1

No.	Title and Description	Type	Significance (scale of 1 to 10, 1 - low, 10- high)	Source
P15	"Economic Comparison of Emission Control Systems for Glass Manufacturing Furnaces with Heat Recovery", Antonio C Caputo and Pacifico M Pelagagge, Department of Energetics, Faculty of Engineering, University of L'Aquila, Monteluco, L'Aquila, Italy, Journal of Air & Waste Management Association, 51, pp 1009-1020, 2001	Paper	5	J3
P16	"The Composition of Gases Evolved from Glass Furnaces", Stockham J D, Journal of Air Pollution Control Association, 21 no. 11, pp 713-715, 1971	Paper	6	P1
P17	"Heat Exchangers for Secondary Heat Recovery from Glass Plants", Webb R L, Marchiori D, Durbin R E et al., Journal of Heat Recovery Systems 4 no. 2 pp 77-85, 1984	Paper	3	P1
P18	"The Chemical Changes Occurring during the Cooling of Hot Gases from Flat Glass Furnaces", Kirkbride B J, Glass Technology 20 no. 5, pp 174-180, 1979	Paper	7	P1
P19	"Deposits and Condensation from Flue Gases in Glass Furnaces", Beerkens R G C, Univ. of Technology Eindhoven (The Netherlands), thesis 1986	Thesis	7	P1
P20	"Experimental and Thermodynamic Characterization of Deposition and Condensation Products from Exhaust Gases of Glass Furnaces", Beerkens R G C, Waal H de, Glass Technology 28 no. 6, pp 246-251, 1987	Paper	5	P2
P21	"Heat Exchanger Fouling: Mitigation and Cleaning Techniques", Hans Muller-Steinhagen, IChemE, 2000	Book	8	Internet
P22	Electronic Code of Federal Regulations (e-CFR) Title 40: Protection of Environment - Part 60 - Standards of Performance for New Stationary Sources - Subpart CC - Standards of Performance for Glass Manufacturing Plants	online database article	6	J7
P23	Fouling Science and Technology, NATO Advanced Study Institute on Advances in Fouling Science and Technology, 1987 (Alvor, Portugal)	Book	7	Internet
P24	"Fouling of Heat Exchangers: New Approaches to Solve an Old Problem", Steinhagen, Malayeri, and Watkinson, Heat Transfer Engineering, 2005	Paper	6	Internet

No.	Title and Description	Type	Significance (scale of 1 to 10, 1 - low, 10-high)	Source
P25	"Solubilities of Inorganic and Metal Organic Compounds", Linke, W.F.; A. Seidell, 4th edition, Van Nostrand (1965).	Book	4	P1
P26	"NIST Chemistry Webbook", Online Resource, Last accessed on 02/01/2008	Database	4	Internet
P27	"Fouling of Heat Exchangers", T.R.Bott, Elsevier, 1995	Book	4	Internet
P28	"Fundamentals of Engineering Thermodynamics", M.J.Moran and H.N.Shapiro, Wiley 5th Edition, 2003	Book	4	MTU library
P29	"Fundamentals of Heat and Mass Transfer", F.P.Incropera and D.P.Dewitt, John Wiley and Sons, 5th edition, 2001	Book	5	MTU library

Appendix C: Additional Figures and Tables Containing Properties of Sodium Sulfate Deposit

Table C1: Various Properties of Sodium Sulfate Minerals [1]

Table 7.13
Various Properties of Sodium Sulfate Minerals

Mineral	Molecular weight[a]	% Na_2SO_4	Density (g/cc)	Hardness (mohs)	Crystal structure
Thenardite (Na_2SO_4)	142.0431	100.000	2.66–2.70	2.5–3	Orthorhombic pyramidal
Mirabilite ($Na_2SO_4 \cdot 10H_2O$)	322.1959	44.086	1.46–1.49	1.5–2	Monoclinic prismatic
Glauberite ($Na_2SO_4 \cdot CaSO_4$)	278.1847	51.061	2.7–2.85	2.5–3	Monoclinic prismatic
Burkeite ($2Na_2SO_4 \cdot Na_2CO_3$)	390.0747	72.829	—	—	Orthorhombic
Astrakanite ($Na_2SO_4 \cdot MgSO_4 \cdot 4H_2O$)	334.4729	42.468	2.20–2.28	2.5–3.2	Orthorhombic (monoclinic)
Vanthofite ($3Na_2SO_4 \cdot MgSO_4$)	546.4980	77.975	2.69–2.85	3.5	Monoclinic prismatic
Loewite ($Na_2SO_4 \cdot MgSO_4 \cdot 2.5H_2O$)	307.4499	46.200	2.37–2.42	2.5–3.5	Rhombohedral triagonal
Hanksite ($9Na_2SO_4 \cdot 2Na_2CO_3 \cdot KCl$)	1564.9161	81.691	2.56	3–3.5	Hexagonal
Glaserite ($Na_2SO_4 \cdot 3K_2SO_4$)	664.8237	21.366	2.64–2.70	2.5–3.5	Rhombohedral (hexagonal)

Index of refraction (average of faces): Thenardite 1.477; mirabilite 1.396; glauberite 1.528; burkeite 1.477; astrakanite 1.487; loeweite 1.481; hanksite 1.471; glaserite 1.491.

Table C2: Composition of waste gas from a flat-glass furnace [16]

Component	*Volume %*
H_2O	13.3
CO_2	8.6
O_2	5.2
N_2	72.7
SO_2	1.6×10^{-2}
Total Na (as NaOH)	8.3×10^{-3}
Total Cl (as HCl)	4.0×10^{-3}

Table C5: Flue gas compositions for experiments in Reference [18]

Specie	Gas number					
	I	*II*	*III*	*IV*	*V*	*VI*
Major species – *(% vol.)*						
O_2	4.5	4.5	4.5	2.0	4.5	4.5
N_2	72.7	72.7	72.7	72.2	72.7	72.7
H_2O	13.0	13.0	13.0	15.0	13.0	13.0
CO_2	9.0	9.0	9.0	10.0	9.0	9.0
Ar	0.8	0.8	0.8	0.8	0.8	0.8
Dopants – *(ppm)*						
Na	125	66	66	-	-	-
K	-	-	-	60	-	-
Ca	-	-	33	-	-	-
Mg	-	33	-	-	-	-
Pb	-	-	-	-	40	40
B	-	-	-	96	-	-
S	240	27	27	150	-	30
Cl	62.5	66	66	-	-	-
F	-	-	-	60	-	-

Table C6: Some chemical cleaning agents (reproduced from [13])

Foulant	Chemical cleaning agent	Comments
Iron oxides	Inhibited hydrofluoric, hydrochloric, citric or sulphamic acid, EDTA	Inhibited hydrofluoric acid is by far the most effective agent but cannot be used if deposits contain more than 1% *w/v* calcium
Calcium or Magnesium scale	Inhibited Hydrochloric acid, EDTA	As for iron oxides
Oils or light greases	(a) Sodium hydroxide, carbonate or tri-sodium phosphate with or without detergents or (b) Solvent – water emulsions, e.g. kerosene - water	Alkalis are also used for the removal of biological deposits Useful for non-ferrous systems which may be attacked by alkalis
Heavy organic deposits, e.g. tars, polymers	Chlorinated or aromatic solvents followed by jet washing	Trichloroethylene and perchloroethylene are non-flammable
Coke/carbon	Alkaline solutions of potassium permanganate or steam/air decoking	Steam/air decoking is used on furnace tubes where coke is removed by controlled burning

Appendix D: Parametric Equations Demonstrating Change in Heat Transfer Rates to the Heat Pipe due to Na₂SO₄ Particulate Formation

Here, the mean gas temperature T_g is assumed as *600°C = 873.15 K*.

Case I – Heat pipe surface is clean (no deposit)

From air properties table in Reference [6], at $T_g = 600°C$,

ϑ = 97.986 x 10⁻⁶ m²/s, --(D1)

Pr = 0.7181, --(D2)

Pr_s = $Pr(T_s)$, --(D3)

k = 60.7 x 10⁻³ W/m.K --(D4)

For solving Equation (12), we also need to know Reynold's number Re_D at $(T = T_g)$.

$Re_D = \frac{vD}{\vartheta}$ --(D5)

v = 5 ft/s, (information supplied by PPG) --(D6)

D = 3.5 inch (information supplied by PPG) --(D7)

So,

Re_D = (5.0 x 0.3048) x (3.5 x 0.0254) / (97.986 x 10⁻⁶)

       = **1382.7** ---(D8)

From Table 8 in Reference [6],

C = 0.26, and --(D9)

m = 0.6 ---(D10)

for $1000 < Re_D < 2 \times 10^5$

and

$n \qquad = 0.37$ for $Pr \leq 10$ --(D11)

Solving Equation (12),

$\overline{Nu}_D \quad = (0.26)(1382.7)^{0.6}(0.7181)^{0.37}(0.7181/Pr_s)^{0.25}$

$\qquad\qquad = 16.2272/Pr_s^{0.25}$ --(D12)

From Equation (13),

$\overline{h} = \overline{Nu}_D \dfrac{k}{D} \qquad = 16.2272/Pr_s^{0.25}$ x $((60.7 \times 10^{-3})/(3.5 \times 0.0254))$

$\qquad\qquad\qquad = 11.0798/Pr_s^{0.25}$ W/m².K --(D13)

$A_s = \dfrac{\pi DL}{2} + 2w_{fin}L$

$\qquad = (3.14159$ x $(3.5$ x $0.0254)$ x $(9.3$ x $0.3048)/2) + (2$ x $(3$ x $0.0254)$ x $(9.3$ x $0.3048))$

$\qquad = 1.2237$ m² --(D14)

Solving Equation (11),

$\dot{Q}_{conv} = \overline{h}A_s(T_g - T_s)$

$\qquad\qquad = 11.0798/Pr_s^{0.25}$ x 1.2237 x $(873.15 - T_s)$ --(D15)

Since Equation (D15) is now expressed as a function of T_s only, convection heat transfer rates can be plotted versus surface temperatures, as shown in Figure D1.

From Equation (6),

$\dot{Q}_{rad} = A_s F_{fs} \sigma \alpha_s (T_f^4 - T_s^4)$

Here,

$A_s \qquad = 1.2237$ m² --(D16)

$F_{fs} \qquad = 0.0236$ (from calculations as shown by Equation (7) and using the simplified configuration as shown in Figure 7), --(D17)

$\sigma \qquad = 5.67 \times 10^{-8}$ W/m².K⁴, --(D18)

$\alpha_s \qquad =$ variable, ---(D19)

$T_f \qquad = 1500°C = 1773.15$ K (information supplied by PPG) --(D20)

Solving Equation (6),

$$\dot{Q}_{rad} = 1.2237 \times 0.0236 \times (5.67 \times 10^{-8}) \times \alpha_s \times (1773.15^4 - T_s^4) \text{-----------------------------------(D21)}$$

Figure D1 shows plots of $\dot{Q}_{conv}(T_s)$ and $\dot{Q}_{rad}(\alpha_s, T_s)$ versus T_s, for various values of α_s ($\alpha_s = 1, 0.9, 0.5, 0.1 \text{ and } 0.01$). The negative value of $\dot{Q}_{conv}$ at $T_s = 700°C$ indicates that when $T_g > T_s$, heat is convected away from the heat pipe.
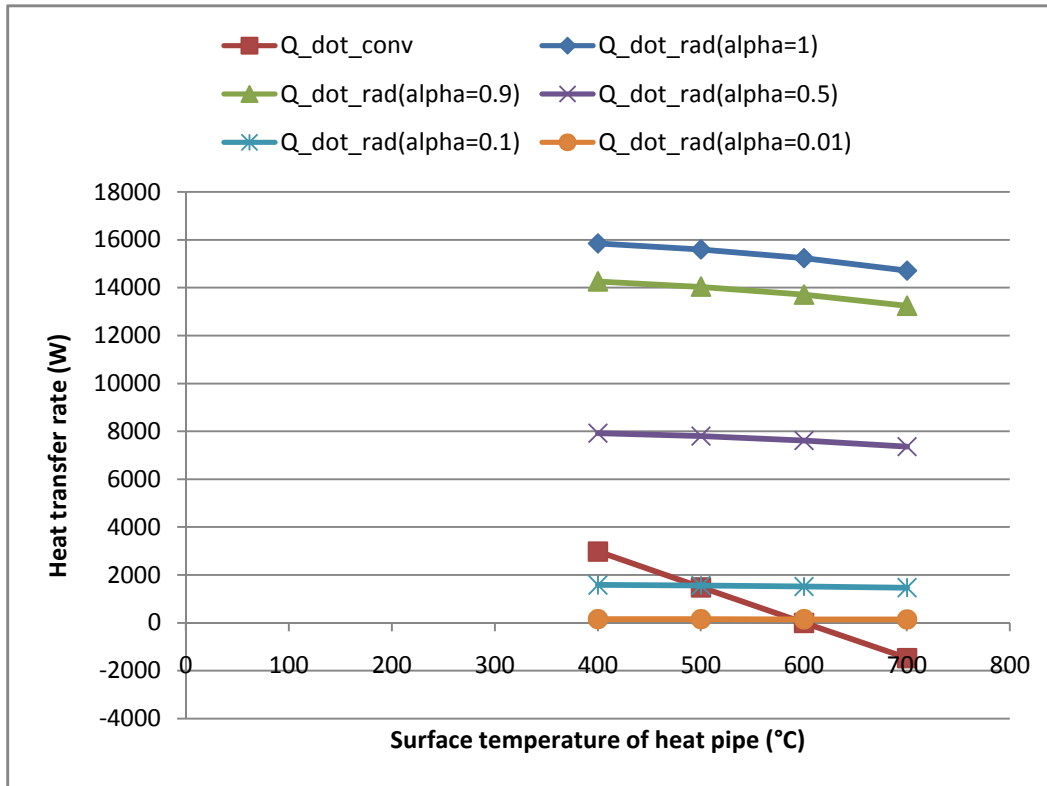
Figure D1: Heat transfer rates via convection and radiation for various values of surface absorptivity (α_s) versus surface temperatures (T_s) [Since $T_s > T_g$, convection heat transfer is negative.]

Case II – Na₂SO₄ deposit of thickness $\left(w_{dep}\right)$ is formed on the heat pipe surface

In order to calculate the change in convection heat transfer rate, we can make use of Equations (16) and (17). From these 2 equations,

$$\bar{h} = \frac{1}{R_{conv}} \text{ ---(D22)}$$

So, convection thermal resistance when the heat pipe is clean can be found out from Equation (D13) as:

$$R_{conv}^{(1)} = \frac{1}{\bar{h}} = \frac{Pr_s^{0.25}}{11.0798}$$ --(D23)

Now, the additional thermal resistance due to the particulate layer can be added on to the right-hand side of (D23) to get the new convection thermal resistance as:

$$R_{conv}^{(2)} = R_{conv}^{(1)} + \frac{w_{dep}}{k_{dep}}$$ --(D24)

From Equations (10) and (D24), the convection heat transfer rate can now be calculated as:

$$\dot{Q}'_{conv} = \frac{1}{R_{conv}^{(2)}} A_s (T_g - T'_s) = \frac{1}{R_{conv}^{(1)} + \frac{w_{dep}}{k_{dep}}} A_s (T_g - T'_s)$$ ---(D25)

Note that $T'_s \neq T_s$ and also k_{dep} is also a function of T_s. The change in convection heat transfer rate $\left(\Delta \dot{Q}_{conv} = \dot{Q}'_{conv} - \dot{Q}_{conv} \right)$ is a function of w_{dep}, k_{dep}, T_s and T'_s for a given value of T_g.

Radiation heat transfer rate to the system also changes, due to $\dot{Q}_{rad} = \dot{Q}_{rad}(\alpha_s, T_s)$. Equation (D21) can be used to calculate $\dot{Q}_{rad}$ with $\alpha_s = \alpha_{dep}$.

From Equation (D21),

$$\dot{Q}'_{rad} = A_s F_{fs} \sigma \alpha_{dep} (T_f^4 - T'^4_s)$$ ---(D26)

From Equations (6) and (D26),

$$\Delta \dot{Q}_{rad} = \dot{Q}'_{rad} - \dot{Q}_{rad} = A_s F_{fs} \sigma \left[\alpha_s (T_f^4 - T'^4_s) - \alpha_{dep} (T_f^4 - T_s^4) \right]$$ --------------------------------------(D27)

From Equation (D27), the important variables that determine $\Delta \dot{Q}_{rad}$ are α_s, α_{dep}, T_s and T'_s, for a given value of T_f and a given setup, as represented in Figure 6.

Also, from Equation (6), the radiation thermal resistances when the heat pipe is 'clean' and when there is a Na$_2$SO$_4$ deposit layer are:

$$R_{rad} = \frac{1}{h_{rad}} = \frac{1}{F_{fs} \sigma \alpha_s \left(T_f^2 + T_s^2 \right) (T_f + T_s)}$$ --(D28)

and

$$R'_{rad} = \frac{1}{h'_{rad}} = \frac{1}{F_{fs} \sigma \alpha_{dep} \left(T_f^2 + T'^2_s \right) (T_f + T'_s)}$$ --(D29)

Appendix E: Responses to Enquiry Letter (in Appendix A) from Potential Suppliers of Heat Exchanger Fouling Control Equipment

----

Gentlemen

Tube Tech International Ltd posses every tube / pipeline cleaning method available worldwide. That is, we are aware of every conceivable alternative that you will have knowledge of and its limitations. This should save you re-inventing the wheel.

We have over 12 solutions to clean this tube that will be robust and cost effective.
If you wish me to list all the alternatives I am happy to do so or even discuss via tel conference. (try 1600 uk time Monday afternoon)

To this end I recommend the Rotaflex. Graham will provide a proposal if you wish once you have completed a Tube Tech questionnaire

Kind regards

Mike

Mike Watson

Technical Director

Tube Tech International Ltd

"Failure is not an option"

www.tubetech.com